UNIVERSITÀ DEGLI STUDI DI PADOVA

UNIVERSITÀ DEGLI STUDI DI PADOVA

DIPARTIMENTO DI INGEGNERIA INDUSTRIALE

Corso di Laurea Magistrale in Ingegneria Meccanica

OPTICAL INVESTIGATION OF THE IN-CYLINDER FLOW OF A NATURAL GAS LARGE BORE DUAL FUEL ENGINE

Studente

Daniel Battorti

Mat. 1130362

Relatore

Prof. Giovanna Cavazzini

Università degli Studi di Padova

Correlatori

M.Sc. Markus Mühlthaler

Technical University of Munich

Prof. Georg Wachtmeister

Technical University of Munich

A.A. 2017/2018

UNIVERSITÀ DEGLI STUDI DI PADOVA

UNIVERSITÀ DEGLI STUDI DI PADOVA

DIPARTIMENTO DI INGEGNERIA INDUSTRIALE

Corso di Laurea Magistrale in Ingegneria Meccanica

OPTICAL INVESTIGATION OF THE IN-CYLINDER FLOW OF A NATURAL GAS LARGE BORE DUAL FUEL ENGINE

Studente

Daniel Battorti

Mat. 1130362

Relatore

Prof. Giovanna Cavazzini

Università degli Studi di Padova

Correlatori

M.Sc. Markus Mühlthaler

Technical University of Munich

Prof. Georg Wachtmeister

Technical University of Munich

A.A. 2017/2018

Optical Investigation of the In-Cylinder Flow of a Natural Gas Large Bore Dual Fuel Engine

Master's Thesis

Scientific work to obtain the degree
M.Sc.
at the Department of Mechanical Engineering at the Technical University of Munich.

Advised by Markus Mühlthaler, M.Sc.
Univ.-Prof. Dr.-Ing. Georg Wachtmeister
Chair of Internal Combustion Engines

Presented by Daniel Battorti, B.Sc.
Matriculation number: 03699228

Finished by Munich, March 30, 2018

Optische Untersuchung der Zylinderinnenströmung an einem Erdgas Dual Fuel Motor

Masterarbeit

Wissenschaftliche Arbeit zur Erlangung des Grades
M.Sc.
an der Fakultät für Maschinenwesen der Technischen Universität München.

Betreut von	Markus Mühlthaler, M.Sc.
	Univ.-Prof. Dr.-Ing. Georg Wachtmeister
	Lehrstuhl für Verbrennungskraftmaschinen
Eingereicht von	Daniel Battorti, B.Sc.
	Matrikelnummer: 03699228
Eingereicht am	München, den 30.03.2018

Chair of Internal Combustion Engines
Technical University of Munich
Prof. Dr.-Ing. G. Wachtmeister

Mr. Daniel Battorti
Matr.-Nr.: 3699228

Experimental Master's Thesis

Optical Investigation of the In-Cylinder Flow of a Natural Gas Large Bore Dual Fuel Engine

Problem definition:

With the introduction of the national emission legislation IMO Tier III in 2016, especially NOx-emission limits in coastal areas are reduced. To counter that, the development of dual fuel operation is enhanced. Instead of relying on the diesel principle alone, a secondary, gaseous fuel (methane, LPG) is ignited by a diesel pilot as in a lean, gasoline engine. Positively, a diminishment of NOx-emissions can be achieved. However, the disadvantages of a gasoline engine, e.g. of abnormal combustion, are introduced. In order to increase the overall efficiency, the engines operate at the frontier of stability, with the danger of running into the knock limit.

Within the European research project HERCULES 2 (HIGHER EFFICIENCY, REDUCED EMISSIONS, INCREASED RELIABILITY AND LIFETIME, ENGINES FOR SHIPS) a large bore dual fuel single cylinder research engine is built up with an industrial partner. The test rig is to be designed as optically accessible as possible. The optical access grants the application of LIF and PIV measurements, thus enabling a three-dimensional recording of the in-cylinder mixture distribution and flow-fields. These enable the identification of areas within the combustion chamber at risk for knocking with high spatial and temporal resolution. With increased knowledge of the injection, ignition, combustion and emission formation by use of alternative fuels, future generations of propulsion systems can be designed in a more efficient manner.

The goal of this master's thesis is the testing of Particle Image Velocimetry (PIV) on the institute's single cylinder, large bore dual fuel engine. Essential for successful application is the generation of a continuous and constant seeding density of the introduced particles. Therefore, an overview of different seeding materials followed by a characterization and the usability for different operating regimes in internal combustion engines is required. Based on the theoretical selection, the final setup for the experiments is deduced. At the test-rig, the in-cylinder flow is characterized.

In summary, the following items are part of the thesis:

- Familiarization with the Particle Image Velocimetry theory and working principle of the applied measurement equipment
- Investigation, characterization and selection of promising seeding substances
- Comparison of different post-processing routines with the goal of an automated approach
- Testing of the final setup at the optical accessible single cylinder research engine

Turnaround times: October 3, 2017 – April 3, 2018

Munich, October 9, 2017

Advisor: M. Mühlthaler, M.Sc.

Student: D. Battorti

Lehrstuhl für Verbrennungskraftmaschinen
Technische Universität München
Prof. Dr.-Ing. G. Wachtmeister

Herr Daniel Battorti
Matr.-Nr.: 3699228

Experimentelle Masterarbeit

Optische Untersuchung der Zylinderinnenströmung an einem Erdgas Dual Fuel Motor

Aufgabenstellung:

Mit der Einführung der nationalen Abgasgesetzgebung Tier III ab 2016 werden vor allem in Küstennahen Gebieten die NOx Emissionsgrenzwerte für Schiffe erheblich reduziert. Um dem zu begegnen, werden vermehrt Dual Fuel Brennverfahren entwickelt und eingesetzt. Dabei können in einem rein Dieselmotorisch betriebenen Aggregat zusätzlich gasförmige Kraftstoffe (Methan, LPG) mit einem Dieselpilotstrahl in einem Ottomotorisch mageren Brennverfahren entzündet werden. Durch den Wechsel des Brennverfahrens werden vor allem die NOx Emissionen reduziert und die entsprechenden Grenzwerte eingehalten. Durch die Verwendung eines Ottomotorischen Brennverfahrens werden aber auch die Nachteile, insbesondere einer anormalen Verbrennung, in Kauf genommen. Um die Effizienz der Dual Fuel Motoren zu steigern müssen diese auch weit im Grenzbereich betrieben werden, in dem eine erhöhte Klopfgefahr besteht.

Im Rahmen eines europäischen Forschungsprojektes Hercules 2 (HIGHER EFFICIENCY, REDUCED EMISSIONS, INCREASED RELIABILITY AND LIFETIME, ENGINES FOR SHIPS) wird deshalb in Kooperation mit Forschungspartnern ein optisch maximal zugänglicher Groß-Dual Fuel Einzylinder-Motor aufgebaut. Mit entsprechender Messtechnik ausgerüstet, wird dieser genutzt, um die Ladungszusammensetzung im Brennraum dreidimensional zu erfassen und so potentielle klopfgefährdete Bereiche identifizieren zu können. Ziel des Forschungsprojektes ist damit das Wissen über die Vorgänge der Einspritzung, Zündung, Verbrennung und Emissionsentstehung bei Verwendung alternativer Kraftstoffe im Dual Fuel Betrieb für künftige effizientere Schiffsantriebsgenerationen zu schaffen.
Ziel Ihrer Bachelorarbeit ist die Erprobung der PIV-Messtechnik an einem Vorversuchsaufbau. Wesentlich dabei ist die Kontinuität einer ausreichenden Seedingdichte. Dabei sollen von Ihnen verschiedene Seedingmaterialien untersucht und ihre Eignung hinsichtlich der Anwendung im Verbrennungsmotor charakterisiert werden. Mit dem finalen Setting werden Untersuchungen der Zylinderinnenströmung am volloptisch zugänglichen Versuchsmotor des LVK durchgeführt.

Folgende Arbeitsinhalte sind Gegenstand Ihrer Aufgabe:

- Einarbeitung in die Thematik Particle Image Velocimetry (PIV) und verwendete Messtechnik
- Untersuchung, Charakterisierung und Auswahl geeigneter Seedingsubstanzen
- Vergleich verschiedener Methoden des Postprocessings mit dem Ziel einer automatisierten Auswertung
- Erprobung der Technik an einem optisch zugänglichen Versuchsmotor

Der Kandidat verpflichtet sich, die Arbeit selbständig durchzuführen und die von ihm verwendeten wissenschaftlichen Hilfsmittel anzugeben.

Die eingereichte Arbeit verbleibt als Prüfungsunterlage im Eigentum des Lehrstuhls und wird Dritten nicht zugänglich gemacht.

Bearbeitungszeitraum: 03.10.2017 – 03.04.2018

München, den 09.10.2017

Betreuer: M. Mühlthaler, M.Sc. Bearbeiter: D. Battorti

To my mom and my dad

Always by my side

A mia mamma e mio papà

Sempre al mio fianco

Contents

List of Figures

List of Tables

Nomenclature

α	Aperture angle
Δt	Time between the two frames
$\dot{m}$	Mass flow rate
λ	Wavelength
μ_f	Dynamic fluid viscosity
ω_s	Angular velocity
ϕ	Correction function of τ_p that takes into account the dynamics of the particle
ρ_f	Fluid density
ρ_p	Particle material density
τ_p	Relaxation time
a	Acceleration
d_p	Particle diameter
I_t	Intensity field
M_0	Scale of the detection system
R_s	Cross correlation
T	Temperature
t	Time
v_f	Fluid kinematic viscosity
v_{px}	Velocity component x
v_{pz}	Velocity component y
v_s	Particles slip velocity
τ_Δ	Turn-over time scale of small eddies
τ_e	Engine time scale
τ_s	Mean swirl turn-over time scale
τ_t	Turbulent turn-over time scale

Acronyms

PIV	Particle Image Velocitmetry
CAD	Crank Angle Degree
TDC	Top Dead Center
BDC	Bottom Dead Center
CCD	Charge Coupled Device
CMOS	Complementary Metal-Oxide Semiconductor
ICE	Internal Combustion Engine
BEV	Battery Electric Device
EU	European Union
CO2	Carbon Dioxide
HDV	Heavy Dutz Vehicles
CFD	Computational Fluid Dynamics
3D	Three Dimensional
GDI	Gasoline Direct Injection
CR	Compression Ratio
2D2C	Two Dimensions Two Components
3D3C	Three Dimensions Three Components
POD	Proper Orthogonal Decomposition
YAG	Yttrium Aluminum Garnet
QE	Quantum Efficiency
HFSB	Helium Filled Soap Bubbles
DEHS	Di Ethyl Hexyl Sebacat
GB	Gigabyte
RGB	Red Green Blue
GUI	Graphical User Interface
SN	Swirl Number

1 Introduction

Since its invention, the internal combustion engine (ICE) has aroused a lot of interest in the world. The first engine was successfully created in the 1859 by Étienne Lenoir [59] and, in 1876, Nikolaus Otto [44] created the first modern petrol engine. Only in 1892 the diesel cycle was proposed by Rudolf Diesel, but the high pressures and temperatures didn't permit an easy realization thus, in subsequent years, there were a succession of tests in order to obtain a working diesel engine until, in 1897 at MAN in Augsburg, Diesel realized the first successful engine test [38]. In 1885 first car was invented by Karl Benz, but only in 1908 the cars became accessible for the common people with the Model T by Ford Motor Company. The car created the mobility concept and nowadays, it is a basic human need for freedom and independence.
The basis of this mobility was in the past and it is still today the internal combustion engine. The internal combustion engine is thus an essential foundation on which the mobility and economy of our society today are based. This inevitably raises the question of what mobility will look like in the future. It seems clear that the desire for individual mobility will remain unchanged in the future. How these vehicles will be driven in the future, is one of the focal point in modern research because fossil fuels are not unlimited and the air pollution continues to grow, in particular in the urban area [11, 58]. The main question is: could the internal combustion engine be centre of human mobility in the future? And more, could the alternative vehicle as battery-electric vehicles being discussed as internal combustion engines substitutes? Indeed as known, nowadays the major opponent for the combustion engine are the electric cars or even called Battery electric vehicles (BEV). The electric car, compared with a combustion one, has lower running cost, less moving parts like radiators, injection and exhaust system, only one moving part (rotor) etc. but it has many disadvantages like duration batteries, charging infrastructure, autonomy, price and more. Thus, the countries are applying new rules for BEV owner as reserved parking spaces, no car tax, discounts on the BEV price and more.
The current market forecasts are different: there are who expect that in the 2035, the whole market will be electric, other like AVL's forecast, suggests that only around 2% of vehicles registered in China in 2020 will have electric propulsion [12]. The reasons why electric vehicles are so slowly established in the market are manifold, one for all is the ecological Sustainability. If it only takes into consideration the kilometer emission, the electric cars emit around about 50 % less the than diesel cars [9], but if it takes into consideration battery life, battery autonomy and the market segment, it is clear how the BEVs have a big gap from the ICEVs. Indeed, the BEVs are actually made for private vehicles, but regarding the big transports, the electric vehicle is not taken into consideration not even in the near future.
Cars are responsible for around 12% of total EU emissions of carbon dioxide (CO2), the main greenhouse gas. This is the official figure published from the European Commission responsible of Climate change field. Then, if the Trucks emission contribute (around 6 %) is added to cars contribute, the carbon dioxide emission reaches 18%. For this reason, more and more strict rules are imposed on the builders. This legislation is the landmark of the EU's strategy

to improve the fuel economy of cars sold on the European market. The rules are divided according to the kind of vehicle:

- Cars: The average emissions level of a new car sold in 2016 was 118.1 grams of CO2 per kilometre (g CO2/km). Since monitoring started under current legislation in 2010, emissions have decreased by 22 g CO2/km (16%). By 2021, phased in from 2020, the fleet average to be achieved by all new cars is 95 grams of CO2 per kilometre. This means a fuel consumption of around 4.1 l/100 km of petrol or 3.6 l/100 km of diesel.
- Vans: The law requires that new vans registered in the EU do not emit more than an average of 175 grams of CO2 per kilometre by 2017. For 2020, the target is 147 grams of CO2 per kilometre – 19% less than the 2012 average. This target corresponds to around 5.5 l/100 km of diesel.
- Heavy-Duty Vehicles (HDV): the on-road commercial transport is and will remain fundamental for the international economy. Currently there is not legislation for the HDV but some forecast indicate that, without policy action, emissions from them increasing by up to 10% until 2030. Anyway, the fuel rising price and the upcoming legislation, pushed the manufacturers to increase the engine efficiency. In fact, during 2018, the Commission will propose new legislation on CO2 emission standards for HDVs.

Furthermore, the European commission invites the builders to respect the CO2 limit emission imposing penalty payments for excess emission for each g/km of exceeding. More, the UE set up a "Super Credits" of additional incentives to produce vehicles with extremely low emissions (below 50g/km). Thus, all the major builders are investing a big part of their income in research and development. For example, in Germany, the automotive industry invested 34 billion euro in the 2016 and 39 billion euro in the 2017 (twice as much as ten years ago). The German automotive industry invests more than any other sector in research and development. The major topics for the future range from the advancement of classic powertrains and alternative fuels, the roll-out of electric mobility and the digital revolution in vehicles, right up to self-driving cars.

1.1 Dual fuel engine

Dual fuel are vehicles that can use two different fuel types to run. As soon as it hears dual fuel cars, comes to the mind petrol cars that can switch their mode use of operation in GPL/methane mode (Bi-fuel vehicle), but these are only one part of dual fuel vehicles. Indeed, dual fuel in the diesel engine, is also used to get better efficiency but, differently from the previous case, it needs to use both fuels in the same time. Indeed, a diesel engine does not have spark plugs with the consequent that it needs always a supply of Diesel in order to get the mixture ignition. Normally, in a dual fuel engine, the gas bulk (natural gas and air) is mixed before entering in the combustion chamber by a common mixer (before the turbocharger if it is present). The advantages of dual fuel respect to normal diesel engine are:

- sustainable development
- energy conservation
- environmental preservation

1.2 Particle Image Velocimetry (PIV)

Basically, Particle Image Velocimetry (PIV) is an easy and intuitive method to study the velocity and the direction of a fluid: it's enough to observe how a little pieces of wood float in a river to understand its direction and velocity. However, in this case, it's possible to get only a rough estimate of velocity and motion behind the surface. To improve the investigation method it is necessary to get better visualization techniques. The first that used this method was Ludwig Prandtl in the beginning of 19th century. He did the first experiment to try to study the water flow in a tunnel created by himself, adding particles in the fluids in order to visualize the flow direction. Obviously, technologies and equipment in the 19th century were not enough evolve to allow to get precise data like flow velocity, flow direction and vorticity [41]. With the technology developing, it was possible to improve optical technique, and in the 80s there was the first computer experiment. In that years, the time required to set up the entire measurements system was a week. Nowadays, the rapid development of software and hardware, allows to get GigaByte of data for each measurement and process them in few minutes. Furthermore, it's possible to do a stereo analysis in order to get the complete 3D flow thanks to use of two cameras [43]. Nowadays, PIV is used in very different areas, one of these is the Internal combustion engine. Mixture formation and combustion process are the main aspects to study in order to reduce the fuel consumption and, consequently, the exhaust noxious emissions. The mixture formation derived by many variables as intake system design, piston shape and combustion chamber. PIV allows to study the air flow inside the combustion chamber and it is coming day by day a useful tool to research and analyze new components in order to improve the combustion efficiency. Further, PIV can used jointly with CFD (Computational Fluid Dynamics) optimization techniques in order to reduce the developing time. In fact, the evaluation done by CFD is based on a optimization loop and normally are require 4 or 5 iteration to get satisfying results. This means that are necessary some days to reach the target design. PIV helps to validate the CFD simulation results by a direct measurements and thus it helps to rise the quality of CFD-simulation methods.

2 Thesis's focus

The internal combustion engine is one of the most studied power system in the world and it has created more energy in the human history. Every day the researchers study new methods to improve the engine efficiency. To make it possible, are necessary new technologies for feedback estimation. One of these methods is Particle Image Velocimetry, a non-intrusive optical method for flow investigation. In this thesis will be explain the principal tasks of the PIV and how to apply it to measure the internal flow of a natural gas large bore dual fuel engine. Applying the PIV in an internal combustion engine leads many problems and to use an adequate instruments system and it is necessary a scrupulous and careful data analysis to avoid evaluation errors. They will be explained the main problems in PIV as seeding materials, camera/laser timing, seeding generator and particle motion and how face up to them. Moreover, will be taken into consideration the possibility to use an alternative way for data elaboration by a MATLAB toolbox and it will be explained its way of working and the results will be compared with the results get from $DaVis$8.4.0, a commercial software suite. Finally, some different particles types will be used in the experiments and the flow results will be shown and discussed.
The thesis is developed in different parts but together connected by a logical thread. In Figure 1 is shown how the thesis is structured.

2.1 Motivation

Every year, new emission laws impose the reduction of engine harmful emissions. This push the researchers to study and adopt new elaborated engine components. The formation of harmful pollutants is directly correlated by fuel's spray formation, fuel–air mixing processes, and consequently the combustion. Expand and improve the techniques to study the internal flow is thus very important. PIV helps the researcher to get a lot of information about the flow state in every section and condition in the combustion chamber. The main problems to study an engine with this method is the necessity to have an optical engine and an adequate seeding material that can withstand temperatures reached during the compression and the combustion. In this way, it has been tried to find the best solution in order to allow the flow investigation during the entire engine cycle.

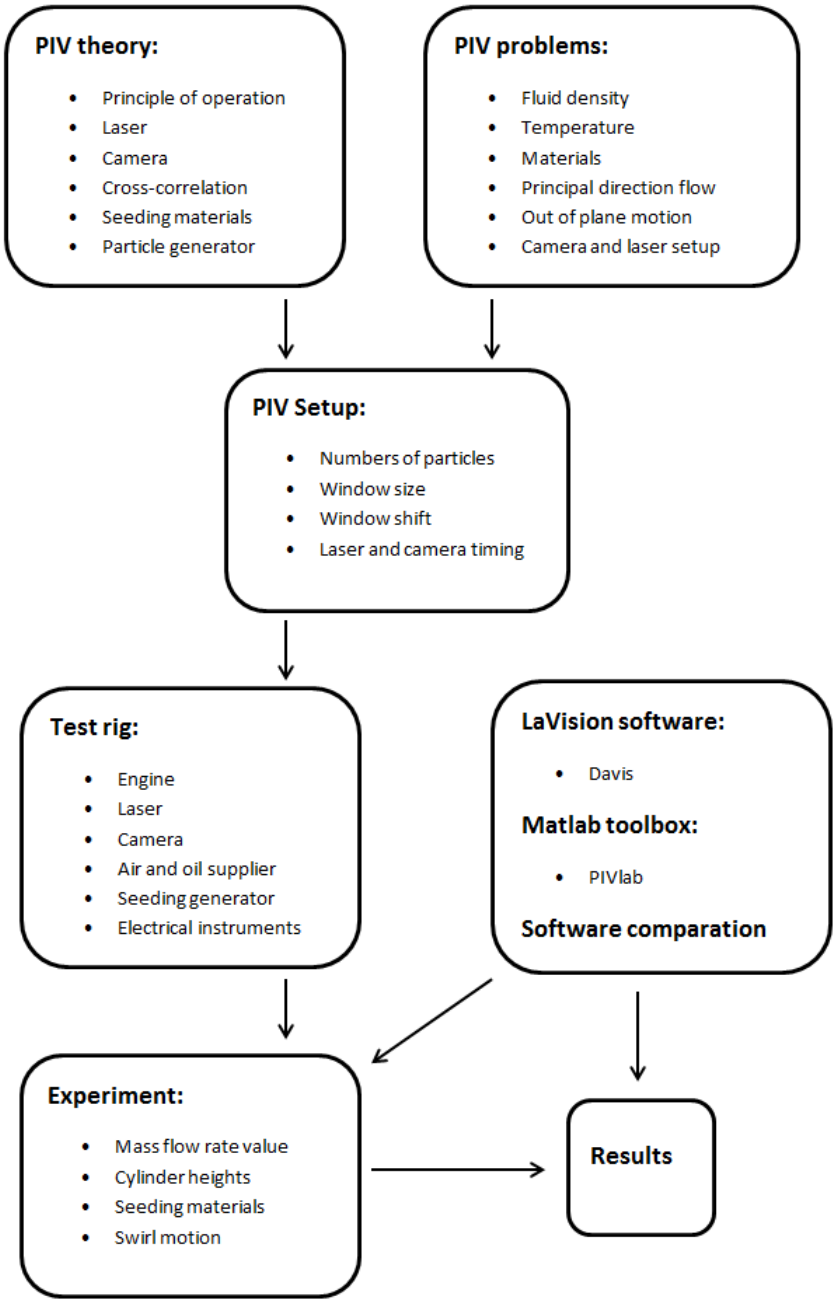

Figure 1: Thesis's flowchard.

3 State of the art

The development of Particle Image Velocimetry has begun around the 1980. Initial, it was used only in laboratory, but year by year, it has been applied effectively in industrial research. The development of PIV has increased thanks to the improvement of computer and vision system that becoming every day more and more powerful, thus expanding drastically the range of possible applications over the years. PIV is successful applied in many different field, from biology to applications in the space shuttle, from cold environments to hot chamber. This is the best PIV property, it adapts to every condition. In particular, PIV could be utilized to analyze the internal flow in a combustion engine to measure various flow characteristics as turbulence properties, cycle-to-cycle variations, injection and ignition, flow behaviour during the intake and exhaust stroke, tumble and swirl motion formation, etc. Applying PIV in a combustion chamber is a challenge for the researchers due to high temperature, high pressure, viscosity changes and velocity gradients. All these features lead researchers to continuous compromises in order to get good results. One of the most critical aspects is the seeding material selection. In the years, the researchers have continued to research and change the seeding material in order to improve the experiments. At first, they used materials as silicon oil [4, 39] and water droplets [20], however they were not suitable because of high temperature that let them evaporate. Thus, solid tracers as graphite [14, 58] and molybdenum disulfide [56] have been used because they are more resistant. Nowadays PIV is a method to verify the influence of some engine parameters as intake and exhaust pressure, valves lift timing or for testing new components. Thus, PIV and CFD are parallels methods to analyze the flow and often they are used in combination to fit the results. Some recent examples of PIV application in engines are now examined.

In 1997 A. Melling [36], studied the size specifications for suitable tracer particles for PIV, particularly with respect to their flow tracking capability. The choice of optimal diameter for seeding particles is a compromise between particles response in the fluid, requiring small diameters, and a high signal-to-noise ratio, necessitating large diameters. It has been explained that to ensure acceptable flow tracking demand particle diameters of about $1\mu m$ or smaller in typical turbulent or high speed gas flows. For high quality PIV records a scattering particle concentration of about 15 particles per interrogation volume is necessary. Types of particles which have been used in recent years in gases and liquids are reported as well as their refractive index m, density ρ, particle diameter dp, the type of laser and the width w and the thickness t of the light sheet.

In 2012 T. Hadad et al. [17], examined the influence of seeding particles parameters on the mean and turbulent flow properties, measured in Eulerian and Lagrangian frameworks, using PIV. It has been possible demonstrated that at higher Reynolds numbers, the influence of the parameters was more pronounced compared to the low Reynolds number case and that seeding particles affects the results in some manner, however the concentration had no unambiguous influence.

In 2016, the Addepalli S. Krishna et al. [23], used the PIV and computational

fluid dynamics (CFD) to analyze a two-stroke gasoline direct injection (GDI) engine in order to evaluate the effect due to the variation of engine parameters like engine speed and compression ratio (CR), with the purpose to design a fuel efficient two-stroke engines. The optical access, into the in-cylinder region, allows to use the PIV method. In this case, they have been used PIV in order to get detailed information on the in-cylinder flow fields in IC engines to validate the results obtained from CFD simulations. The relative low temperatures reached in the experiment, allow to use di-ethyl-hexyl-sebacate as seeding material. The results obtained show that there is a good agreement between CFD and PIV.
In 2016, the Jean Rabault et al. [42], it is been done a study using PIV (planar and stereoscopic) in a diesel engine. They have noted that there is some clear flow differences at high and low valve lifts with distinct change in the swirl intensity. Their main target was to get information about the swirl and tumble motion during the valves lift. For this purpose, swirl number and tumble number were measured for valves lifts ranging from 1 to 15 mm. They have studied the contribution from each valve separately and the two valves together with the result that the flow obtained from two valves strongly interact. Finally, a complete 3D3C (3-dimensions 3-components) reconstruction of the mean flow was obtained and the stability in time of the swirling structure obtained by tracking the instantaneous swirl center position in each crankshaft angle.
In 2006, the Cosadia I et al. [8], it has been evaluated the cyclic variations of the swirling flow in a diesel engine. They have considered the flow in the middle of the compression phase in order to analyze the instantaneous velocity fields. Then, the circulation data are decomposed by using the Proper Orthogonal Decomposition (POD). Finally, they have studied the in-bowl flow at the end of the compression stroke. In this work it has been also evaluated the capacity of the seeding material to follow the velocity changes due to the piston and turbulent motion. In the middle of the compression phase, the fastest velocity measured is $v_m = 12m/s$ and the swirl motion is present and it exhibits a zero-velocity point (not located at the geometrical cylinder center). Indeed, the swirl center location is different from one plane to another because there are deformations and patchy in the mean velocity distribution. Thus, they have been taken into consideration the cycle-to-cycle variations of the flow structure, the parameters variation in a circle with center in the zero-velocity point, and the instantaneous velocity fields. The result is that the swirling flow varies very significantly from vortex type to annular type between two different cycles with the conclusion that the time for the turbulent transport of momentum is too short to enable a perfect swirl motion smoothing.
In 2015, the Kan Zha et al. [60], they have been analyzed the characterization of flow asymmetry during the compression stroke using swirl-plane PIV in a light-duty optical diesel engine, in particular they used a re-entrant piston bowl geometry. Three swirl-planes were chosen to quantify the flow asymmetry. Based on the averaged velocity results, the swirl center motion and the evolution of the swirl axis have been determined. With this test they understood that the evolution of swirl axis tilting is similar for various swirl ratios, this means that for the late-compression mean flow asymmetry, the details of intake flow are not of primary importance and that therefore the piston pip

might be responsible for it. Indeed, the late-compression swirl center is located closer to the intake valves when the measuring plane is farther away from the fire deck, while it is located closer to the exhaust valves in the same condition of measuring plane.

4 Theoretical Foundations

In this section will be explained the theoretical bases in order to have the fundamental concepts of PIV and the principal technologies related to it in order to have the basic concepts of this technique. It will be explained the main PIV features, operating principle and instrumentation for setting up the experiment.

4.1 Particle Image Velocimetry

Particle Image Velocimetry (PIV) is a method to measure the instantaneous flow fields. It allows to get resulting vectors which represent the instantaneous medium flow state in the measurement plane (conventional PIV) or in the three-dimensional state (stereo-PIV). PIV, thanks its non-invasive measurement, allows to calculate a large number of parameters as swirl number, velocity and flow turbulence making it very popular in the research field. It is based on measuring the displacement of a large number of particles, which have been adequately added to the flow, assuming that their velocity match the fluid velocity. A laser beam of $0,5 - 1mm$ [43], is formed by means of appropriate optics system in such a way that to have a quasi-two-dimensional light section. The laser illuminated the particles in the section plane into the flow by an optical access and, the perpendicular scatter light coming from the particles, is detected by a camera. In order to have the flow velocity is require the traveled particle distance and the time spent. The particles are flashed in a quick succession by two short laser pulses and the camera gets two particle images named frames. In order to determine the distance traveled by the particles between the two light pulses, the pictures are subdivided into interrogation windows. For each interrogation window is calculated the average particle shift between the two frames, getting the velocity with statistical methods (for example cross-correlation). It is assumed that all particles within one interrogation window have moved homogeneously between the two illuminations [43, 58]. With the particles displacement, in two plane directions, and the time between two laser pulses, it is then possible to calculate the two flow velocity components [1]:

$$v_{px} = \frac{\Delta x}{M_0 * \Delta t} \qquad v_{py} = \frac{\Delta y}{M_0 * \Delta t} \tag{1}$$

In which v_{px} and v_{py} are the velocity respectively in x and y, M_0 is the scale of the detection system and Δt is the time between the two frames.

In Figure 2 it is shown the operating scheme of a general PIV application. It is possible to observe that the images obtained from the camera are divided into interrogation windows. The calculator examines each interrogation windows and gets the result vector. With the modern devices is possible to capture and process more than 200 frames per minute [43, 58].

4.1.1 Tracer properties

Particle Image Velocimetry is based on measuring the particles velocity carried by the flow and for this it is an indirect measurement technique. The meaningfulness and accuracy of PIV therefore depends principally of the tracer

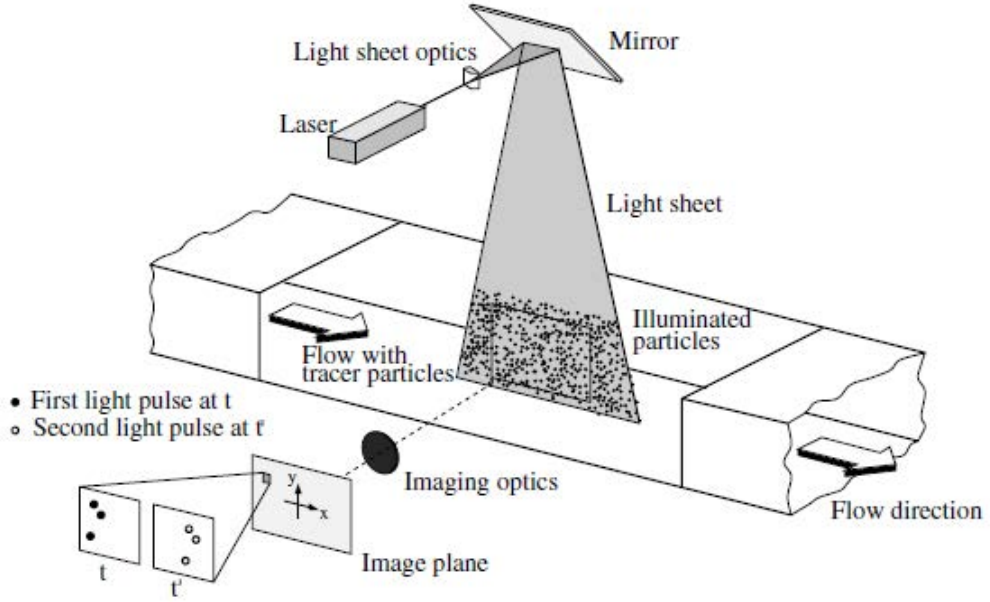

Figure 2: Operating scheme of a general PIV experiment [43].

properties. Selecting the tracer is always a compromise between elevated light scattered and capability to follow the flow variation. Indeed, large particle diameter allows elevated light reflection but they have difficulty to follow the flow velocity changes. The other way around, small particles are difficult to detect by the camera but they have high capacity to follow the flow. It should be mentioned that both the ability to follow the flow and to scatter the light have a quadratic dependency on the diameter of a spherical particle [1]. The particle slipping, during the flow acceleration, is the parameter to evaluate. It should be noted that a particle must always have a certain slip with respect to the fluid when a velocity change occurs, since, only in this way, the force which allows the particle to follow the acceleration can occur. It is possible to use a parameter to understand the time required from the particles to adapt its velocity to that of the flow. This parameter is called relaxation time τ_p [43]:

$$\tau_p = \frac{(\rho_p - \rho_f) * d_p^2}{18 * \rho_f * v_f * \phi} \tag{2}$$

In which ρ_p is the particle material density, ρ_f is the fluid density, d_p is the particle diameter, v_f is the fluid kinematic viscosity and ϕ stands for a correction function that takes into account the dynamics of the particle.
In a gas flow $\rho_p >> \rho_f$ thus, if it is hypothesized that the Reynolds numbers are small, it is possible to evaluate the particles slip velocity v_s in a fluid with constant acceleration a and with dynamic fluid viscosity μ_f [43]:

$$v_s = v_p - u_f = \frac{(\rho_p - \rho_f) * d_p^2 * a}{18 * \mu_f} \tag{3}$$

If the particle density is much greater than the fluid density, v_p follows an

exponential law [58]:

$$v_p(t) = (1 - \exp -\frac{t}{\tau_p})(u_f - v_p(t=0)) + v_p(t=0) \tag{4}$$

Imposing to the boundary conditions:

- $t = 0 \longrightarrow v_p(t=0)$
- $t = \infty \longrightarrow v_p(t) = u_f$

Finally, the relaxation time is given by [43]:

$$\tau_p = \frac{\rho_p * d_p^2}{18 * \mu_f} \tag{5}$$

In figure 3 it is possible to see the diameter influence in different flow velocity.

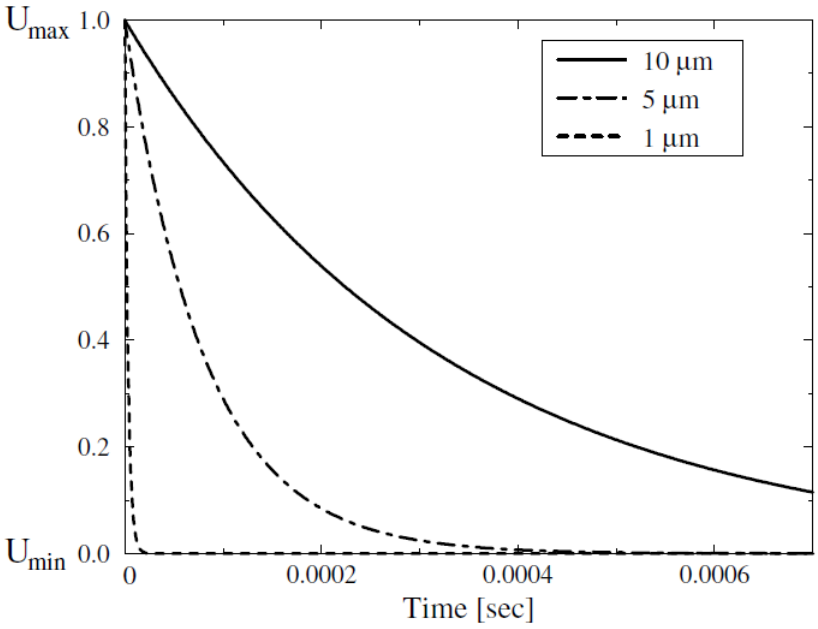

Figure 3: Time response of oil particles with different diameters in a decelerating air flow [43].

Due to the points mentioned here and other engine-specific limitations, the search for a suitable tracers to use in an engine is particularly difficult. This problem is discussed in detail in Section 5.

4.1.2 Cross-correlation

As already described, the purpose of PIV is to determine the distance traveled by a particle in a definite time. This particle shift is calculated automatically via a cross-correlation computer-based. The frames describe the three-dimensional flow state because the light sheet is not infinitely small to represent only a two-dimensional state. The frames are subdivided into interrogation windows and then they are transformed in two-dimensional. The scheme of this

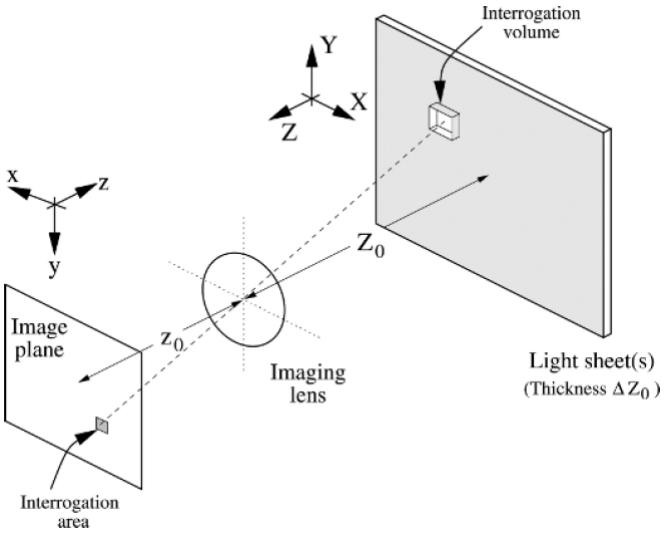

Figure 4: Geometric imaging scheme [43].

process is shown in Figure 4. Now, considering that the first interrogation is taken at time t and the second interrogation is taken at $t+\Delta t$ with respectively intensity field of $I_t(i,j)$ and $I_{t+\Delta t}(i+x, j+y)$, the cross-correlation $R_s(x,y)$ can be calculated with [3, 43, 58]:

$$R_s(x,y) = \sum_{i=-K}^{K} \sum_{i=-L}^{L} I_t(i,j) I_{t+\Delta t}(i+x, j+y) \tag{6}$$

Where i and j denote the position of the first interrogation window and x and y denote its displacement. If the intensity distributions of the images fit with each other, the value $R_s(x,y)$ is large, the other way around $R_s(x,y)$ is small and the measurement has a large uncertainty. When the results are calculated, the correlation peaks location defines the actual particle shift, Figure 5.

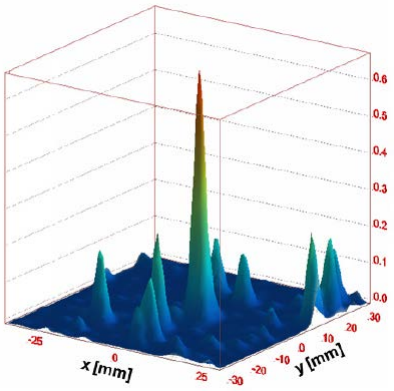

Figure 5: Correlation peak [58].

The random noise is represent by smaller peaks in the correlation plane. The ratio between the highest peak and the second highest peak is the signal-to-noise ratio also called *ratioQ*. The larger *ratioQ* the more reliable is the

particle displacement measurement [1]. As anticipated, it is necessary to adopt some countermeasures in order to have a big *ratioQ*:

- Number of particles in the interrogation window: more particles, better signal-to-noise ratio. In Figure6 it is possible to see the peak trend for different particles number in the interrogation window.

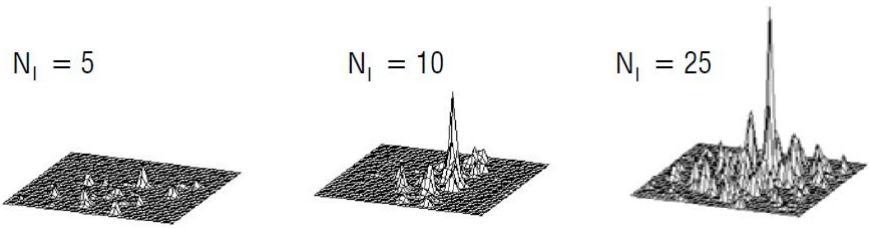

Figure 6: Different signal-to-noise ratio with different particles number [30].

- Particles displacement in x and y: it is necessary to impose a maximum particle displacement in the interrogation window. In Figure7, where F_I is the in-plane correlation factor (small F_0 means high loss of correlation), it is possible to see that the signal-to-noise ratio remains adequate for displacement minors of 1/4 of the window size [22].

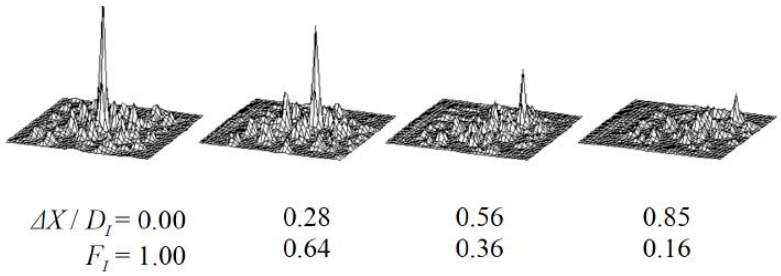

Figure 7: Different signal-to-noise ratio with different particles displacement [30].

- Out of plane displacement: it is necessary to impose a maximum particle displacement in the perpendicular plane. In Figure8, where Δ_z is the out of plane displacement and F_0 is the correlation factor, the *ratioQ* remains acceptable for displacement minors of 1/4 of light sheet thickness.

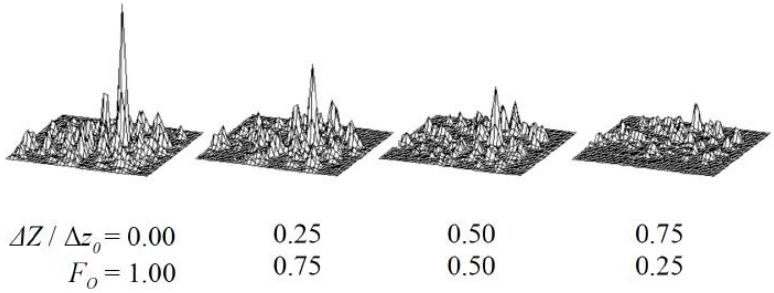

Figure 8: Different signal-to-noise ratio with different out of plane displacement [30].

- Influence of gradients: it is necessary to have a minimum particles dimension and small spatial gradients value. In Figure9, where a is the local displacement variation, D_I is the interrogation area size and d_τ is the particle image size, the $ratioQ$ remains acceptable using a $d_\tau = (2-4) * pixel - dimension$ and $a < 3 - 5\% D_I$ during the picture acquisition time.

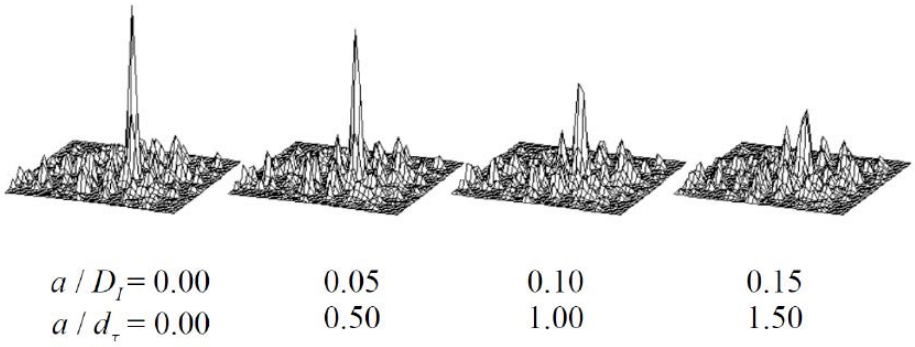

Figure 9: Different signal-to-noise ratio with different particle size and interrogation area size [30].

4.1.3 Particle image Velocimetry features

Will now be illustrated many features to consider about PIV [43]:

- Non-intrusive velocity measurements: the best advantages of PIV is its capacity to get information about the flow without alter the flow conditions. The non-intrusive capacity allows to apply this method in high-speed system or in boundary layers close to the wall.
- Indirect velocity measurement: the flow velocity is deducted from the tracer velocity.
- Whole field technique: PIV allows to detect all the field captured by the camera.
- Velocity lag: it is necessary to pay attention at the particles diameter in order to have small relaxation time.
- Duration of illumination pulse: the laser timing is a fundamental parameter that can influence the measurements results.
- Illumination: for application in gas flow, a high power light source is require due the small particle size, instead for application in liquid flow, larger particles can usually be used with the effect of better light scattered and consequently it is require less power light.
- Time delay between illumination pulses: the time delay between the illumination pulses must be long enough to determine the particles displacement, but it has to be short enough to avoid that the particles leaving the interrogation window between the two frames.

- Tracer particles distribution: homogeneous distribution of medium density is desired for PIV recording in order to obtain an optimal resolution.
- Density of tracer particle images: as described above, it is a important parameter that has to be evaluated.
- Number of components of the velocity vector: with one camera is possible to get information about two components ($\Delta x, \Delta y$). On the other hand it is possible studying the entire three dimensional flow using a couple of cameras.
- Spatial resolution: subdividing the picture in sub-windows allows to remove the velocity gradients in the results. The number of independent velocity vectors is directly connected to the interrogation window number (a vector for each interrogation window).

4.1.4 Problems in PIV

Will now be illustrated the mains problems to apply PIV in a particular field as studying the internal flow in a combustion chamber. All these problems have to be studied and solved before to improve the technique in the engine [1, 35, 43].

- Main direction of the flow: the flow direction changes in the four dimensions. This means that for establishing the flow direction in a determinate instant must be take into account some restrictions. It is necessary to impose an ideal time between the two laser pulses in order to determinate only the principal flow direction and neglecting the secondary flow direction. In particular, the particles motion in a determinate moment has not to be greater than 1/4 of the windows size (x and y directions) and 1/4 of the light sheet thickness (z direction).
- Mass flow rate: the flow velocity in the cylinder changes continuously. In particular, the velocity value in the central area is little, while the velocity value near the border is high (swirl motion). In this case is necessary a compromise because, more is the time between the pulses, major will be the move of slow particles, but information of fast field may be lost. On the other hand, the lower is the pulses time, the larger is the accuracy of the fast particles, but many information of the slow field is lost.
- Temperature and pressure: during the compression stroke, the pressure increase therefore temperature (fig. 29) and dynamic air viscosity (fig. 30) increase also. How will be possible to see in the chapter 5.1, Equation 5, the time necessary for a particles to follow the gas mixture decreasing from the bottom to the top dead center. Furthermore is necessary using particles that endure this environment.
- Particle density: the seeding density has not to be too poor in order to avoid particles deficiency in a interrogation window, but has not to be too rich to avoid wrong elaboration. The particles number for each interrogation window has to be from 10 to 20. After the closing of the intake port,

the number of the particles is determinate. During the compression, the particle density in the interrogation window increase. This involves the necessity to determinate the particles number before that the intake valve closing and it depends from the crankshaft angle studied Figure10.

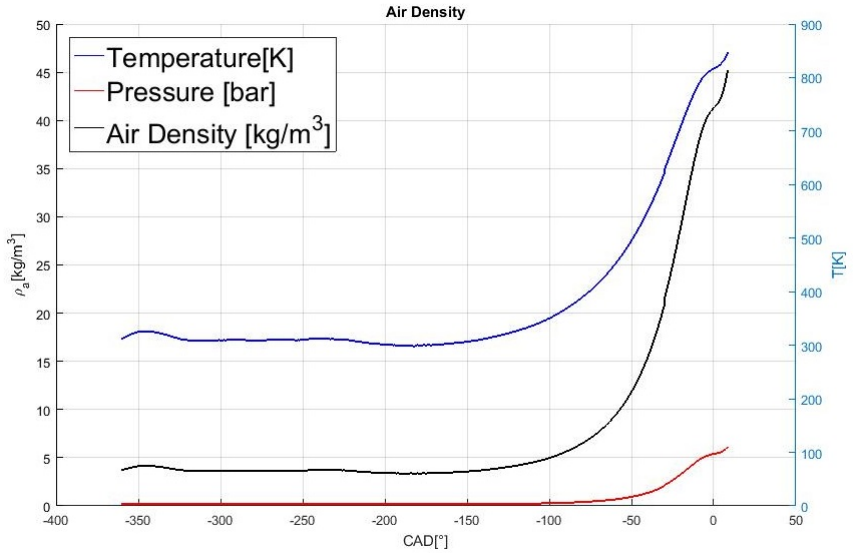

Figure 10: Air density evolution during the compression stroke.

- Reflections and disturbance: during the images acquisition, there are always some side effects due to the cylinder optical parts. Furthermore there are problems due to the background behind the cylinder. Is possible to add a matt finish in order to reduce the reflection. Then, is necessary to have an adequate pre-processing in order to delete the the background.

- Humidity: The humidity in the air involves a worst resolution. The effects of humidity can be reduced by the use of a compressor with a dehumidifier.

- Errors: the errors in the measurement is the combination of systematic and residual errors. Systematic errors could be generated by an inadequate statistical method as, for example, an inappropriate peak estimation. This trend of error is predictable and easy to remove. Residual errors are a measurement of uncertainty. A way to establish the repeatability errors is varying one parameter at a time for then evaluating and comparing the results.

- Optimization of Particle Image Diameter: there is an optimum particle image diameter in order that can reduce the measurement uncertainty. For a single exposure-double frame evaluation the best diameter is $d_\tau \approx 2pixel$, while for a double exposure-single frame is $d_\tau \approx 1.5pixel$. It is shows in Figure 11.

- Optimization of particle image shift: another parameter that influences the error in the PIV is the particle displacement in pixel length. In Figure 12 is shown the measurement uncertainty due the particle displacement. How it is possible to see, reducing the particle displacement the error

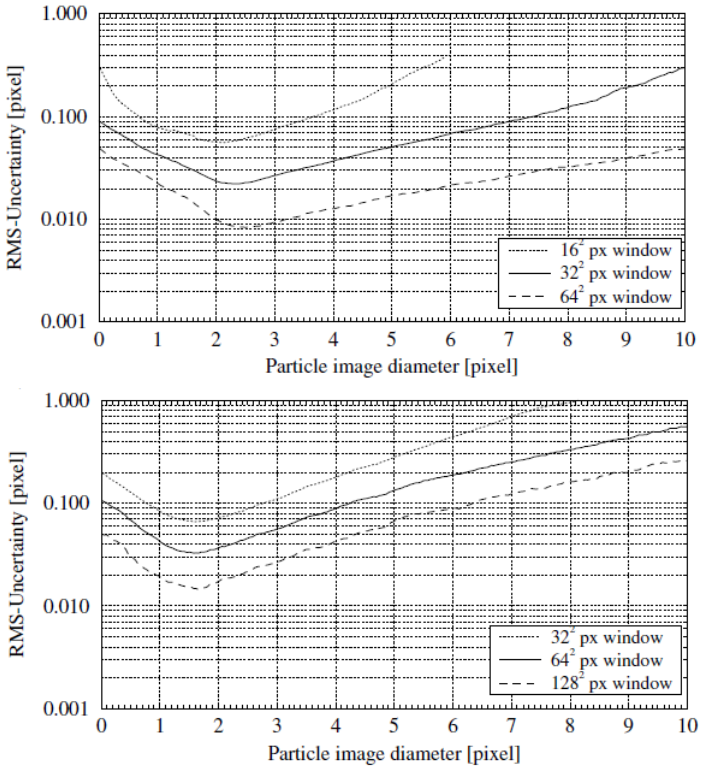

Figure 11: Random error in digital cross-correlation PIV evaluation [43].

decrease. Maintaining the same particle diameter and increasing the window size, the error is reduced. With small particle diameter is necessary using small windows size to avoid the errors increment, Figure12.

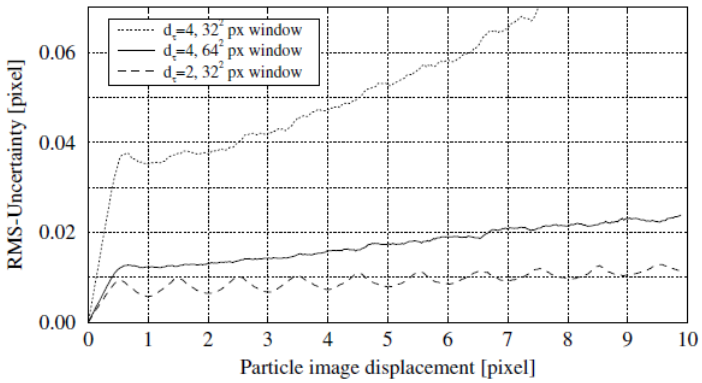

Figure 12: Measurement uncertainty due to the particle image displacement [43].

- Out of plane motion: the in-cylinder flow is obviously three-dimensional. This means that if it is studied a plane motion, there will be data losses due to the third velocity direction. Indeed, the particles that are illuminated in the first laser pulse could be going in a perpendicular direction and thus they won't illuminated in the second laser pulse. To avoid this setback there are three different solutions:
  1- The time between the two frame could be reduced, in this way less

particles go away from the laser sheet.
2- The light thickness could be raise in order to have bigger tolerance in the perpendicular motion plane (not even possible to apply).
3- The light sheet could be shifted in the direction of the flow between the two frame in order to follow the particles perpendicular motion.

- Effects of displacements gradients: not all the particles present in an interrogation window in the first frame will also be present in the same interrogation window in the second second frame, even if the interrogation window displacement is accounted for. If the interrogation windows does not have an offset, the displacement will be biased to a lower value because particles with small displacement will be present more frequently than those with higher displacement. Smaller interrogation windows can tolerate much higher displacement gradients, provided the particle image density is sufficiently high.

- Uncertainly of PIV near walls: the determination of the velocity profiles near walls is a very important task and a challenging problem in many fields of science and technology. The boundary layer strongly affects of velocity gradients. For the in-cylinder study, the velocity near the wall is not relevant and applying a mask during the image processing it is possible to exclude the wall uncertainly.

- Laser setup: the light has to illuminate all the perpendicular section of the cylinder compared to the camera position. Furthermore is necessary having a system to calibrate the direction and thickness of the laser. This is possible thank as particular lenses and control instruments. There is also the necessity to calibrate the two laser pulse in such way that they are perfectly synchronized.

- Camera setup: it is necessary to calibrate the camera focus before the data collection. Every time that a new cylinder height is analyzed it is necessary change the camera focus. Furthermore the camera timing as well as the laser need of a software to handle their operation.

- Tracer selection: the particles have to be large enough to achieve exposure levels that are at least 30-50 % of the saturation level of the image recording. The exposure is increased much more effectively by increasing particle diameter d_p than by increasing the laser energy. Is better increase the d_p of the particles than increase the laser energy (expensive energy for have the same reflection increment). But there is a limit for the dimension of the particles because they have to follow the air bulk with an error less than 1 % [43] .

- Glass clearing: the seeding materials used can scratch or dirty the cylinder glass. For this reason, it is often necessary turn off the engine and clearing the optical openings and using materials not hardness.

4.2 Laser

The term "LASER" means "Light Amplification by Simulated Emission of Radiation". The laser emits light spatially, coherently and temporally. A Laser systems are usually used in PIV to illuminate the particles in the flow. The laser is selected for two principal features [43, 58]:

- The monochromatic laser light is suitable with the spectral sensitivity of CCD and CMOS sensor.
- It is able to emit two short pulses of high energy in a short interval time.

In order to investigate high flow rates and to freeze the particle movement is require a short exposure time but this means that is necessary having a powerful lighting systems. The particles illumination must be very intense to ensure that enough light is scattered towards the camera in its short exposure time. As already mentioned, it is aggravated by the fact that the tracer particles dimension are very small and therefore they have a small area that reflects the light. In conventional PIV systems, with repetition rate of $10 - 30Hz$, almost exclusively Neodym-YAG solid-state lasers are used. This laser type emits light in the non-visible spectrum at a wavelength of $\lambda = 1064nm$, which is subsequently converted in the visible spectrum light with a wavelength of $\lambda = 532nm$. The beam is generated by Nd^{3+} ions. The Nd^{3+} ions are incorporated into YAG crystals (yttrium-aluminum-garnet). In this laser type the upper energy levels are continuous. In order to operate in triggered mode is necessary using a quality switch (Q-switch) in the laser cavity. The Q-switch functions is that to create a resonance at the most energetic point during the flash lamp cycle in such a way as to have the powerful laser pulse [43].
The ions are excited by the flashlamp light which pumps energy into the laser crystal in a broad spectrum. These flash lamps are powered by capacitors which can deliver a lot of energy in a short time at high voltages. The capacitors charging time significantly determines the laser repetition rate. The lasers are commonly referred to as so-called dual-cavity-Systems running. Two laser cavities independent of each other are combined and their laser beams are superimposed on one another via a system of mirrors [1]. This configuration allows to adjust the illumination time independently of the pulse strength.
Dual-cavity configuration could involves two problems:

- The two laser beams, even after they have been formed via a corresponding optics to a light section, still lie exactly above each other and thus illuminate the particles in the same way. If the two light sections are only slightly adjacent to each other, a correlation of the two particle images is not possible anymore.
- Different pulse intensities and different intensity distributions on the particle images. In particular, the laser with the more complex beam guidance, often from shot to shot, has significant intensity fluctuations and a more irregular intensity profile.

Both points can have a negative effect on the image correlation [58]. In Figure 13 is shown the laser system in Dual-cavity mode.

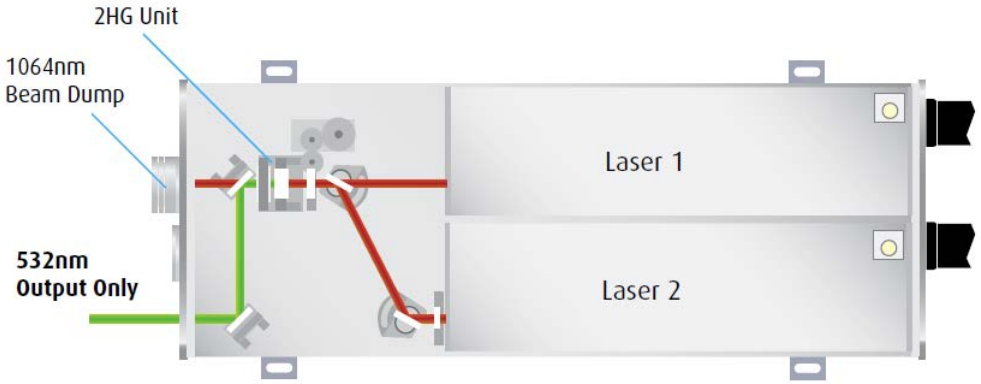

Figure 13: Scheme of Nano PIV laser [34].

4.2.1 Power supply

The power supply provides: the energy to the laser rod, system timing, synchronization controls, safety interlocks, master ON/OFF and key switch. The lamp trigger and the Q-switch driver are in the laser head [34].

4.2.2 Light sheet optics

The laser beam from the laser generator can't be used directly to light up the internal flow. It has to be directed and adapted in such a way that having a desired shape. More, for light source like Nd:YAG lasers, the optics system allows to direct the light sheet with six degrees of freedom ant to focus the light to an appropriate thickness.
The laser needs to be kept away from the experiment zone due to the space constraints. In the experiment, the laser output is lower left respect the cylinder, thus with a mirror system, the laser is moved until when the laser beam is perpendicularly respect the cylinder. Into the mirror system, the laser shape takes place thanks to two tools:

- Sheet Optics (Divergent) [31]: in this tool, different divergent lenses are used to adjust the light sheet dimension and refocusing. The divergent can be regulated by changing the aperture angle: the light sheet α is determined by the focal length f of the cylindrical lens and the beam diameter d by the relation $tan(\alpha/2) = (d/2f)$, Figure 14.

  In Figure 15 is possible to see how the divergent works. To adjust the light sheet thickness, it is necessary to change the distance of the two spherical lenses inside. If the lenses have a short distance between them the focal length is faraway otherwise, with a wide distance, the focal length is closer.

- Collimator optics [25]: The collimator optics, together with the sheet optics (divergent), produces a collimated light sheet. The sheet optics

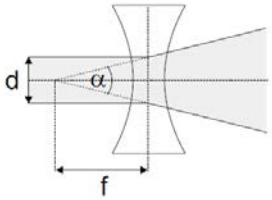

Figure 14: Aperture angle α [31].

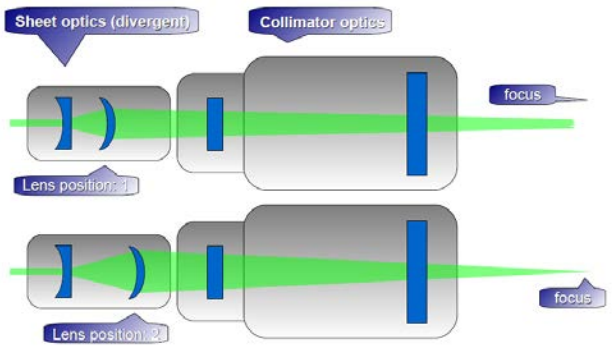

Figure 15: Focus length adjusting [25].

(divergent) has to be settled in front of the collimator optics. To obtain the desired light sheet shape, the sheet optics (divergent) has to be mounted in front of the collimator optics like in Figure 15.
In order to change the sheet height and expansion of the light sheet is necessary change the distance of the cylindrical lenses. There are 3 different possibilities to change the distance of the lenses inside the collimator:
- diverted light sheet (short distance)
- divergent light sheet (long distance)
- parallel light sheet (with a height of 50 mm).
The three different position are shown in Figure 16.

After the focus adjusting, sheet height and expansion of the light sheet is necessary correct the angular orientation. The regulation has to be done by rotating the first lens. Finally it is necessary aligns the lens onto the axis of the collimator (Figure 17).

4.2.3 Laser safety

The laser nano series belongs at CLASS4 laser device. It means that they are in the most dangerous category: they have the higher power beam and it may cause severe and permanent damage to eye and/or skin [18]. The laser may result dangerous not only from direct incidence of the beam on the eye, but even from reflections and diffused . This involves the necessity to wear protective eyewear with a sufficiently high optical capacity at the same wavelengths emitted by the laser. Several steps to minimize the danger posed by the laser [34]:

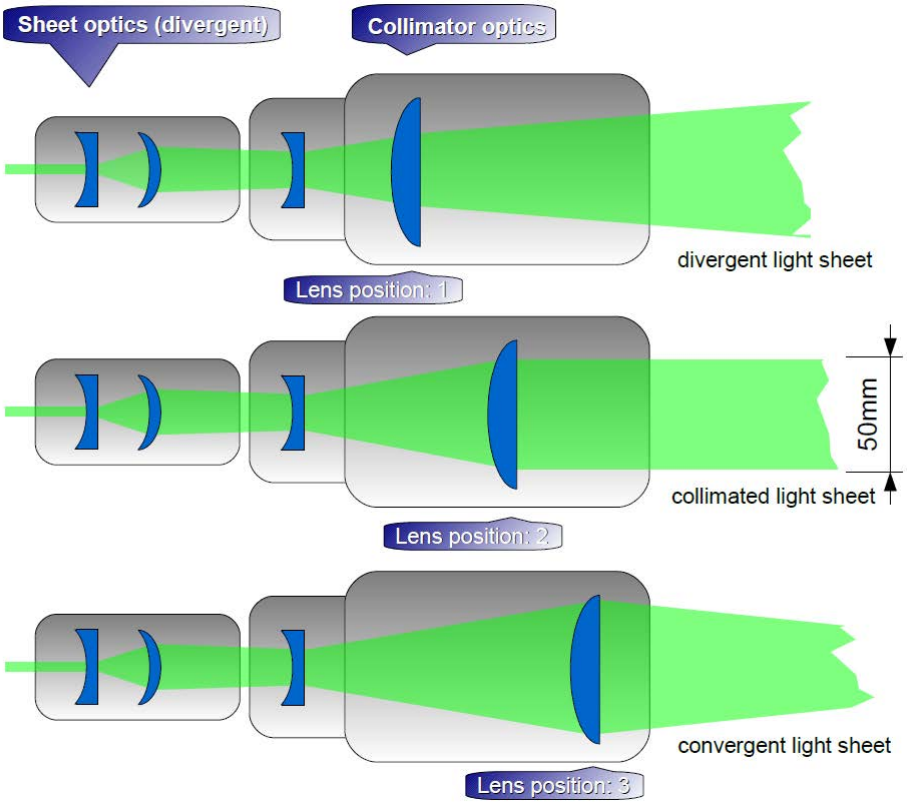

Figure 16: Sheet expansion adjusting [25].

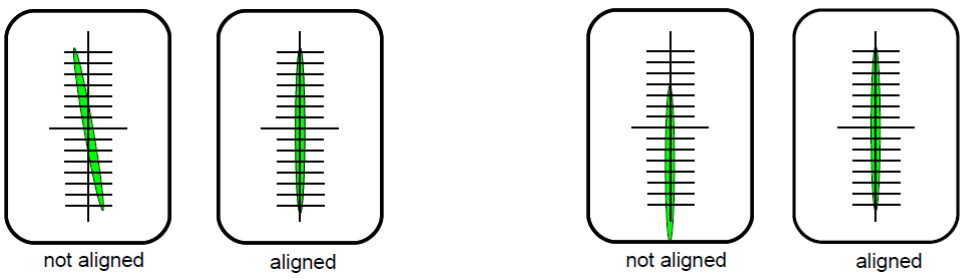

Figure 17: Light sheet alignment [25]. Left: Angular orientation; Right: Lateral adjustment.

- Not operate with the laser in a room where light can escape from windows or doors.
- Adequate and proper protective eyewear for all the people that may be exposed to radiation.
- Stop the laser whenever the output is not needed.
- Keep the room lights on in order to reduce the pupils areas.
- The laser head has to be in place when the laser runs. It's possible operate without cover only during the aligning operations.
- Never operate the laser with the cover removed from the power supply.
- Make sure that the laser is secured to a suitable table.
- Never watching the laser beam and its reflection directly even wearing protective eyewear.
- When it is possible, create a shield beam path in order to reduce the radiation spread in the room.
- Integrate an alarm system able to defuse the laser activity when the room doors are open.

4.3 Camera

The development in the electronic recording field is very rapid. The optical and electronic characteristics of sensors influence directly PIV. Indeed, have a good camera meaning good pictures and good picture meaning less errors in the rating. Typically there are two different camera based: CCD (charge coupled devices) and CMOS(Complementary Metal-Oxide Semiconductor) sensors.

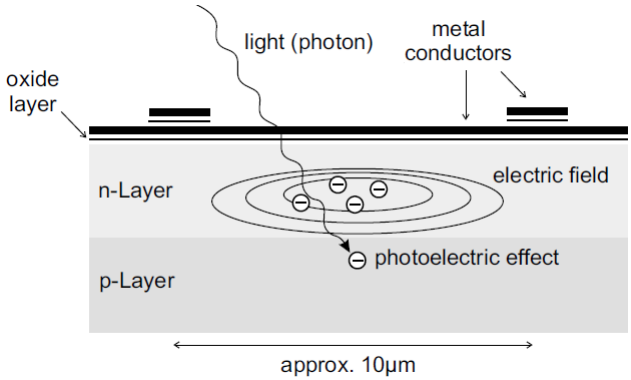

Figure 18: Model of CCD pixel [30].

- CCD sensors: CCD is a electronic sensor that convert light into electric charge (photons to electrons). The CCD sensors configuration clould be arranged in a rectangular array or in a line array. An individual CCD sensor is called pixel and normally there are $100 pixel/mm$ [43]. In Figure 18 it is possible to see how the sensor works. In a simple way, before

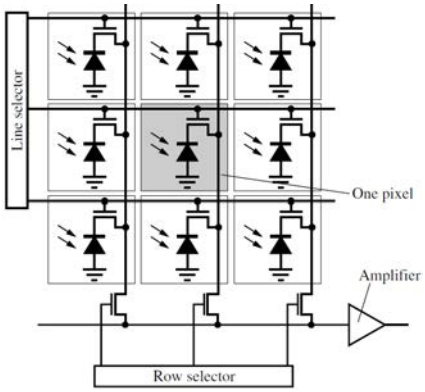

Figure 19: Model of a CMOS sensor [43].

to take a picture, the camera recharge the surface (metal conductors) of electrons. When the light (photon) hits the charge surface the electrons are agglomerated under the surface in proportion at the intensity of the light (more photon more electrons agglomerated). After the exposure, the camera counts how many electrons are agglomerated in each pixel and thus it count how many photons have hit the surface.

- CMOS sensors: Their main advantages are the high sensitivity, low noise [43], low temperature sensibility, low electrical energy consumption and superior capacity to resist at high energy due to the laser. In this case, each individual pixel contains an electronic circuit. This means that each pixel transforms directly the light in electrons. In Figure19 is shows an example of CMOS sensor.

4.3.1 CCD sensors

In this type of camera the photo-electrical effect convert photons to electric charge. During the exposure time a certain number of electrons are captured in each pixel. Having a larger number of pixel means better resolution. In Figure 20 is shown the sensor geometry. When the picture has read, the electrons are shifted vertically, row for row, in a special row that count one by one the electrons number for each pixel in that row. A charge-to-voltage converter, generates a voltage proportionally at the electrons number. In this way, it has been created the analogical signal [43]. The Figure 21 represents the readout procedure.

This method allow high reading velocity (few microseconds) and high image resolution. Furthermore, to increase the velocity for capturing two frames, it has been applied another solution: for each pixel is created a vertical masked in order to move the electrons in this area and then starting with the electrons counts. In this way, during the readout of the first frame, is possible to get another picture because the pixels are free [43]. The layout is shown in Figure 22. However, this method has a limitation or rather the time of second exposure. In detail, the time for the first exposure could be long as much it is necessary, but the second exposure can't because the readout time of the first frame. Then, before to start with the second readout, is necessary waiting

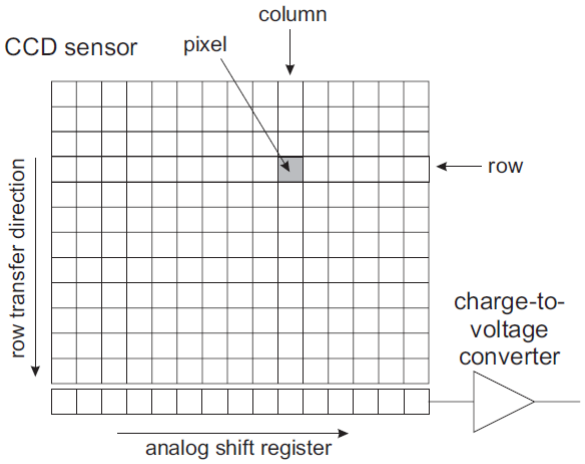

Figure 20: CCD sensor geometry [28].

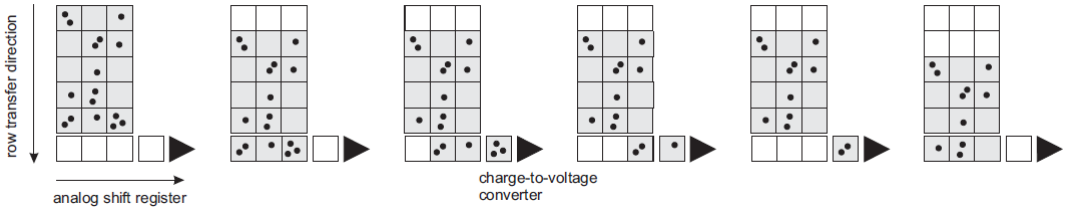

Figure 21: Readout sequence of CCD sensor [28].

until when the first data ended. Normally 100 milliseconds are necessary to process the first exposure, therefore the second exposure has to be minimum 100 milliseconds. This problem could be solved adding a band-pass filter on the camera lens, in this way only some wavelengths can pass and the exposure time is the laser flash time. The timing for a double frame recording is shown in Figure 23 The recording could be done either in Single frame, not helpful

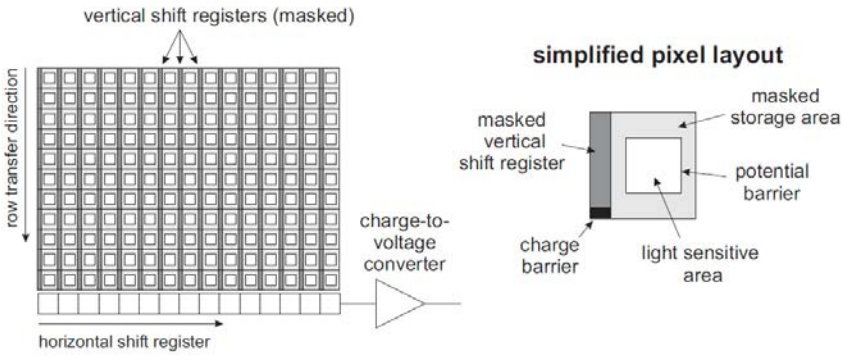

Figure 22: Progressive scan interline transfer CCD layout [28].

for the PIV recording, or in Double frame. The second method is used in PIV because it allows to get two different frames with a little delay between them 23. In order to reduce the quantity of light lost, micro lenses are used that directing the light into the pixel, Figure 24.

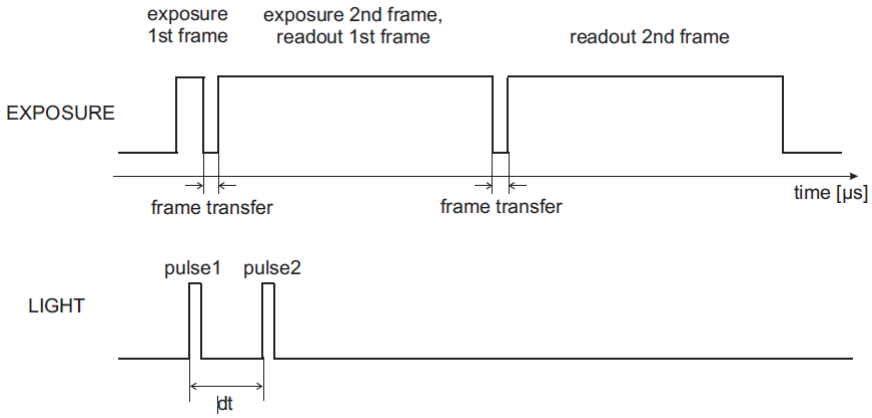

Figure 23: Timing scheme for a double frame recording [28].

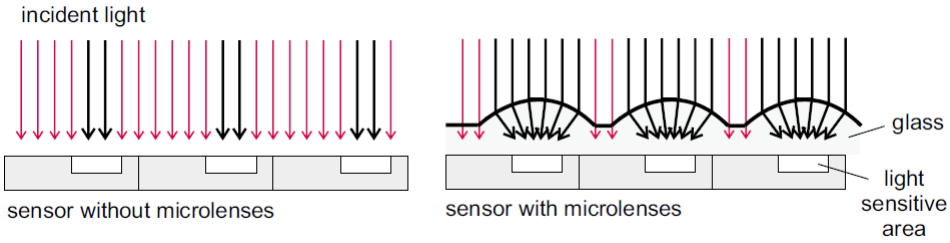

Figure 24: Microlenses [28].

During the experiment, two different camera have been used: $imagerproX2M$ and $sCMOS$ both from LaVision [28]. This cameras have a digital image output, a separate camera control unit and different image sensor that allow to get different spatial resolution and exposure time as mentioned before.

4.3.2 Spectral sensitivity

The ratio between the number of electrons in the pixel and the total number of incident photons gives the quantum efficiency QE or even called Pixel Sensitivity. It depends of a large number of factors as pixels dimensions, filter, lens and materials used. Normally, the camera sensors used silicon in the substrate that has a frequency employee of wavelength that means that the Sensitivity change based on the wavelength. As it is possible to see in Figure25, for the wavelength $532nm$, the sensitivity is 50% for the lens, 53% for the camera and 97% for the filter.

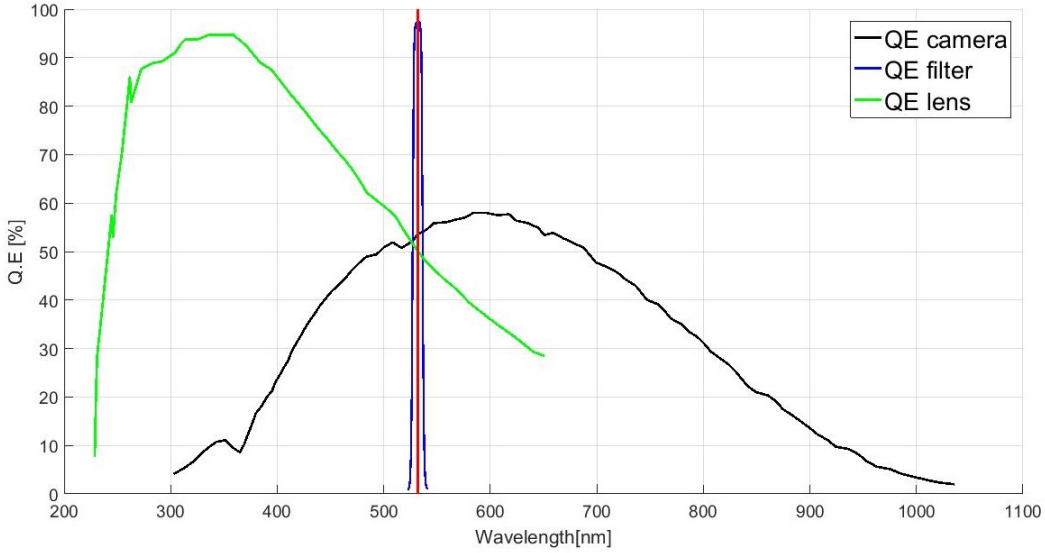

Figure 25: Quantum efficiency curves for CMOS camera,filter and lens used during the test [28].

4.3.3 Mirror

In order to visualize the internal flow is necessary an optical access in the piston and in the cylinder. These optical accesses allow to illuminate and photograph the internal cylinder area. In the case in which it is necessary studying the horizontal plane, the laser lights the particles by the cylinder access while the camera takes the pictures from the bottom of the cylinder, the other way around, if it is necessary studying the vertical plane, camera and laser will be inverted. To allow the positioning of the camera externally to the cylinder a mirror is collocate in a special piston section. In Figure26 is shown the engine view system. The laser beam (red line) illuminates the particles. The mirror (green) reflects the light scattered from the particles (blus line).

4.4 Seeding materials

As said above, the seeding materials is one of the most important parameter in PIV. A particular tracer feature in an application as an engine is the quantity of seeding added at the flow. Normally it must to be in a particular range in order to have a minimum quantity of particles to be allowed the cross correlation but

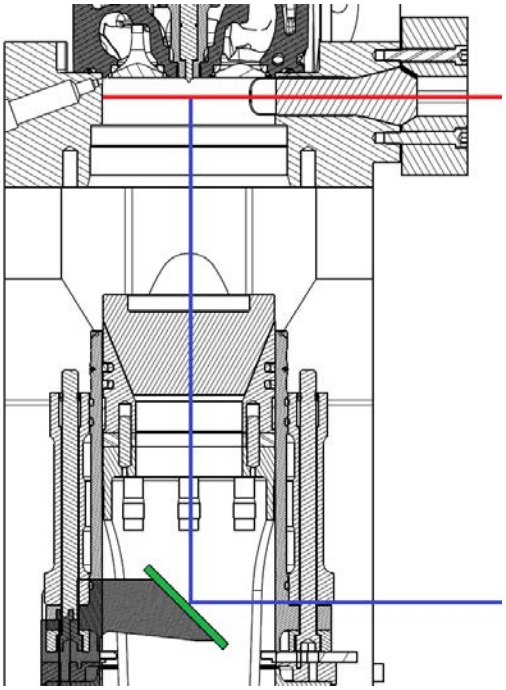

Figure 26: Large bore dual fuel engine: view system.

not much otherwise is not possible to apply the analysis. A good range is from 10 to 20 particles for each interrogation window [1]. In an open system it is easy to calculate and to apply, but in a close system as an engine is more difficult. Indeed, when the intake port is closed, is not possible to adjust the quantity of particles inside the cylinder anymore. Furthermore, during the compression curse, the particles density increase, in fact the volume inside the cylinder decrease by a factor employee at the compression-factor. This means that the number of particles necessary for the measurements change in according with the compression level. For example, for a measurement in the top dead center where the volume is the smaller, the particles quantity will be less that for a measurement in the bottom dead center where the volume is the biggest. The principals features required of the seeding material are [37, 43]:

- Follow the rapids flow variations.
- Being chemically stable.
- Easily accessible and at low cost.
- Environment friendly.
- Having adequate density.
- Having adequate reflective properties.
- Should not be abrasive.
- Withstand high temperatures.

In particular, the last point is essential for use PIV in an engine because if high temperature are reached. About seeding materials will be depth discussed in Chapter 5.

4.5 Seeding generator

The seeding generator is the element that allows to add and regulate the particles in the flow. Substantially they are divided into 2 categories: liquid seeding generator and solid seeding generator. When it is possible, the liquid seeding is preferred rather the solid seeding. This because supply a liquid tracer is easier than supply a solid tracer. An example of liquid generator is the oil seeding generator. It injects pressure air in an oil tank. In this way, the air generates bubbles that bring the oil in the empty part of the tank. Then by a pipe, the air with oil particles inside, is transported up to the work area. An illustration of this generator is shown in Figure 27.

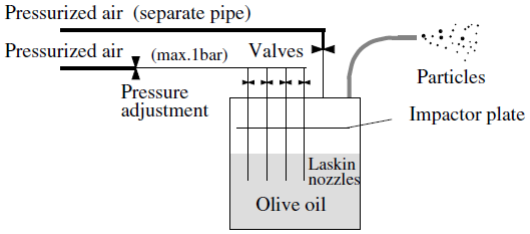

Figure 27: Oil generator scheme [43].

The solid generator works in the same way but the injected particles control is not easy as in the liquid generator. The solid generator scheme is shown in Figure 28. The seeding generator is equipped with two particular systems [25]:

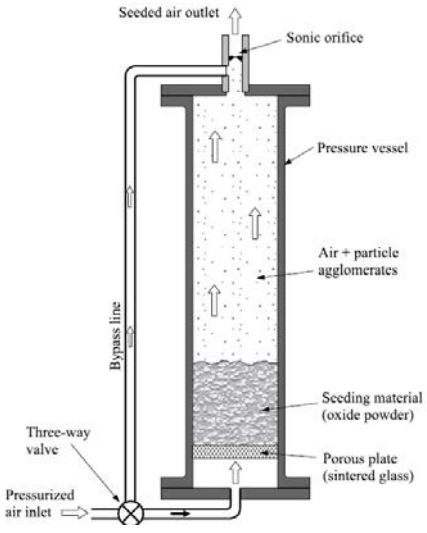

Figure 28: Solid generator scheme [43].

1. Sonic orifice: it creates turbulence that break up larger particles agglomerates.

2. Switchable by-pass line: it allows a constant air flow supply to the engine during the switch operations (when the seeding generator is turned on or off).

The main problem with this type of generator is the channels formation within the material powder inside the generator that could involve a reduction of tracer particles in the air flow.

5 Seeding materials

As anticipated in Chapter 4.4, the selection of the material to use in the experiment is of primary importance to get good results. Often, the final decision is a compromise between advantages and defects. For example, a material with a good refraction index leads the necessity to clear the optical section more frequently than a material with poor refraction, or again, a material with high temperature resistance is more dangerous for the glass part than a material with poor temperature resistance. In literature it has been used many different materials. A list of available materials and their maximum working temperature are shown in Table 1. Some of these materials are successfully applied in PIV, but the engine working conditions involve a drastic materials selection. High temperature and pressure subject the materials to high stress. Computing the increment of the isentropic temperature during the compression stroke, supposing that the inlet air is a 40°C, it is possible to still the temperature trend during the whole engine cycle Figure29. During the compression stroke, the

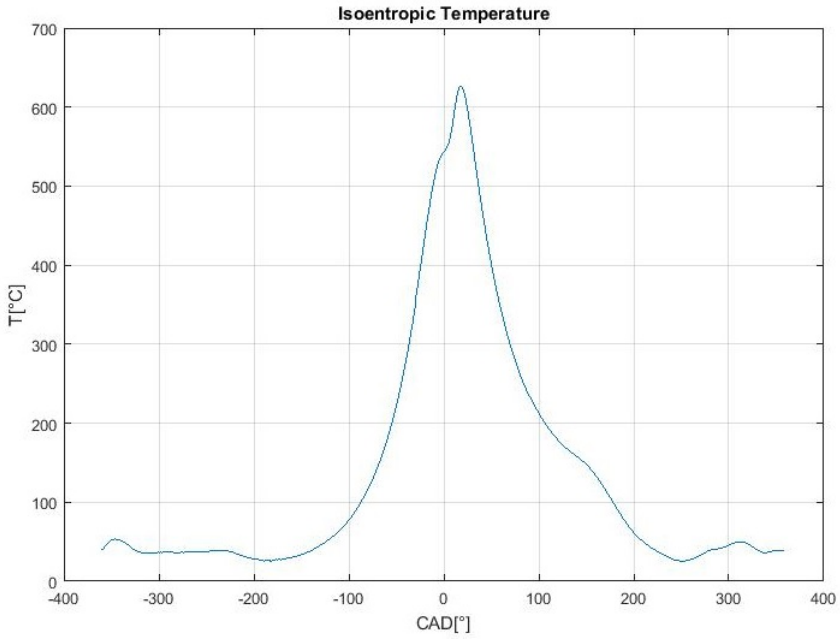

Figure 29: Isentropic temperature.

in-cylinder temperature reach around 550°C in the top dead center. it is clear that in this condition a liquid tracer evaporates with the result that the flow motion can not be studied. This involve the necessity to use solid tracers. Solid tracers allow to reach high temperature but with an different contraindications, or rather that the solid particles could breaking the glass surface and thus reducing the engine life and that the solid tracer supply it is difficult to control. A first materials evaluation could be done taking into account their maximum work temperature. In the table 1 are shown the maximum temperature for each material.

With the temperature list it is possible to exclude some materials. Thus the materials HFSB, DEHS, Polyamide particles, Plastic spheres, Natural oil, Silicon oil, Water, Acrylonitrile can be directly deemed unsuitable for the exper-

Material	Maximum temperature °C
Helium-filled soap bubbles HFSB [48]	< 100
Di-Ethyl-Hexyl-Sebacat DEHS ($C_{26}H_{50}O_4$) [10, 24]	260
Fumed Silica(Aerosil) [7, 49]	1800
Graphite (C) [14, 58]	450
Polyamide particles [46]	250
Glass hollow spheres [5]	$500 - 800$
Ceramic hollow spheres	1000
Plastic spheres [33]	240
Lycopodium [57]	460
Antracite coal	900
Solid soda lime glass	670
Natura Oil [16]	210
Silicon Oil [4, 39]	230
Water (H_2O) [20]	100
Sodium chloride ($NaCl$) [2]	810
Acrylonitrile (C_3H_3N) [55]	77
Aluminium oxide (Al_2O_3) [21]	2050
Magnesium oxide (MgO) [19]	2852
Titanium dioxide (Ti_2O) [6, 47, 50]	1855
Molybdenum disulphide (MoS_2) [56]	450
Boron nitride (BN) [40]	900
Zirconium oxide (ZrO_2) [40]	2715
Lead monoxide (PbO)	900
Molybdenum trioxide (MoO_3)	800
Calcium fluoride (CaF_2)	1400

Table 1: Maximum temperature of materials.

iments. Furthermore materials like Graphite, Lycopodium and Molybdenum disulphide can be used only in the first part of the compression stroke until when the temperature reach around 450°C and in non-fired conditions. Another selection method is the health risk. Indeed, the seeding materials have to be manipulated by hand and it may come into contact with skin or may be inhaled. For this reason, it is required a material a material non-hazardous. Thus, the material like Lead monoxide, Molybdenum trioxide and Calcium fluoride have to be excluded from the list because they are noxious or poisonous. The Zirconium oxide has been excluded from the list for its high price and hardness while the Antracite coal for its big size of particles. With the materials left are proposed others selection criteria.

5.1 Relaxation time

To understand the materials behavior inside the air flow is necessary analyzing their density and particles size. Indeed, the difference between flow density and particles density may caused a velocity lag and thus a results error. Indeed, as mentioned in Chapter 4.1.1, to check the materials compatibility is necessary to evaluate the relaxation time with the following equation [43]:

$$\tau_p = \frac{\rho_p * d_p^2}{18 * \mu_f} \tag{7}$$

Thus, it is necessary to know the particles diameter $[m]$ (supposing that the particles are spherical), the particles density $[kg/m^3]$ and finally the air dynamics viscosity μ_f $[kg/m * s]$. The air dynamics viscosity μ_f is based on temperature Figure30. How it will be possible to see then, it is not necessary

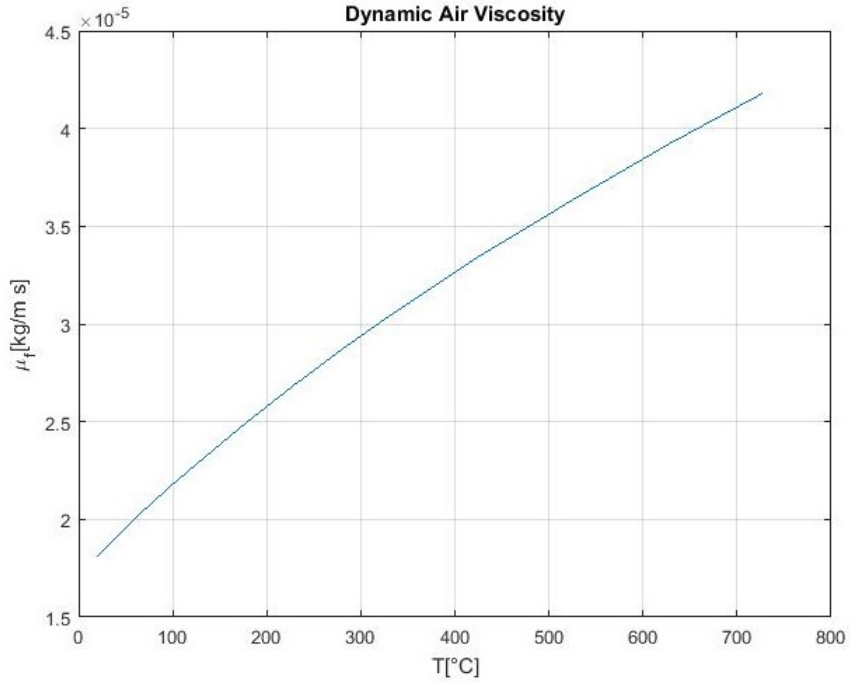

Figure 30: Representation of viscosity trend.

go beyond these temperatures because the relaxation time will be enough small

Material	Density $[kg/m^3]$	Dimension $[\mu m]$
Graphite	2,2	3,5
Boron nitride	2,1	1
Titanium oxide	4,2	0,5
Aerosil	0,05	0,012
Magnesium oxide	3,58	25
Aluminium oxide	3,95	5
Lycopodium	1,175	28
Molybdenum disulphide	5,06	1,5
Hollow glass sfere	3	10

Table 2: Particles density and dimension.

for all materials to satisfy the time scales Table 5.1. In Table 2 are shown the materials density and dimension.

Following the air dynamics velocity trend it can be deduced that also the particles time response decreasing between the bottom and the top dead center. Four time scales have been calculated in order to evaluate the seeding quality in three different crank angle degree (CAD) or rather bottom dead centre (BDC) 180°, maximum piston linear velocity 270° and top dead center (TDC) 360°, Table 5.1 [8].

- Engine time scale: It has been evaluated the flow variation rate imposed by the time varying boundary conditions. The engine time scale τ_e is calculated from the number of revolutions per minute $\tau_e = S/V_p$ where S is the piston stroke ($210mm$) and V_p is the average piston speed (for $600rpm$ is $4,2m/s$).

- Mean swirl turn-over time scale: the mean swirl turn-over time scale τ_s is calculated with the formula $\tau_s = 1/\omega_s$, where ω_s is the angular velocity of the swirling flow in the cylinder. $\omega_s = SN\omega$, where SN is the swirl number and ω is the rotation rate of the engine $\omega = 2\pi n$ where n in the speed engine. In Figure 89 are shown the SN trend for the three different mass flow rate. For each CAD analyzed (180°, 270° and 360°) the higher SN has been chosen in order to using the worst possible condition. Thus for 180° $SN = 2,37$, for 270° $SN = 3,28$ and for 360° $SN = 2,45$.

- Turbulent turn-over time scale: In this case is evaluated the time scale due to the global properties of the turbulent flow in the combustion chamber. The turbulent time scale τ_t is obtained from $\tau_t = L/u$ where L is the size of the energy containing eddies and u is the rms magnitude velocity associated to these eddies. These parameters are estimates for each CAD or rather for 180° $L = b/6$ and $u = V_p$, for 270° $L = b/6$ and $u = V_p/2$ finally for 360° $L = p/6$ and $u = V_p/2$ where b is the cylinder bore ($170mm$), p is the depth of the bowl ($16,6mm$) and V_p is the average piston speed. The results are indicate in the table. Also in this case $\tau_t >> \tau_p$.

- Turn-over time scale of small eddies. For PIV, the smallest turbulent scale that can be detected is around $\Delta = 2,5mm$ [8]. The time scale of small

eddies τ_Δ is obtained from $\tau_\Delta = \tau_t(\Delta/L)^{2/3}$. The results are indicate in the table3.

Time scale results are shown in Table 3. it is possible to see in figure 31 that for

Time scale	180°	270°	360°
τ_e $[s]$	$5 * 10^{-2}$	$5 * 10^{-2}$	$5 * 10^{-2}$
τ_s $[s]$	$6,7 * 10^{-3}$	$4,85 * 10^{-3}$	$6,49 * 10^{-3}$
τ_t $[s]$	$6,73 * 10^{-3}$	$1,34 * 10^{-2}$	$1,31 * 10^{-3}$
τ_Δ $[s]$	$1,33 * 10^{-3}$	$2,65 * 10^{-3}$	$1,23 * 10^{-3}$

Table 3: Relaxation time limits.

180° when the flow temperature is around 40°C, Molybdenum disulphide and Hollow glass sphere have τ_p closed by τ_s and thus it is advisable don't use them because could involve a response delay in the velocity variation. Furthermore, observing the lycopodium trend it is possible to see that its τ_p is always over the limit of the turbulent turn-over time scale. For this reason the lycopodium has to be excluded from the materials list. For what concern the others materials it is noted that they have always an order of magnitude smaller that the smallest time scale and thus they don't present any problem delay.

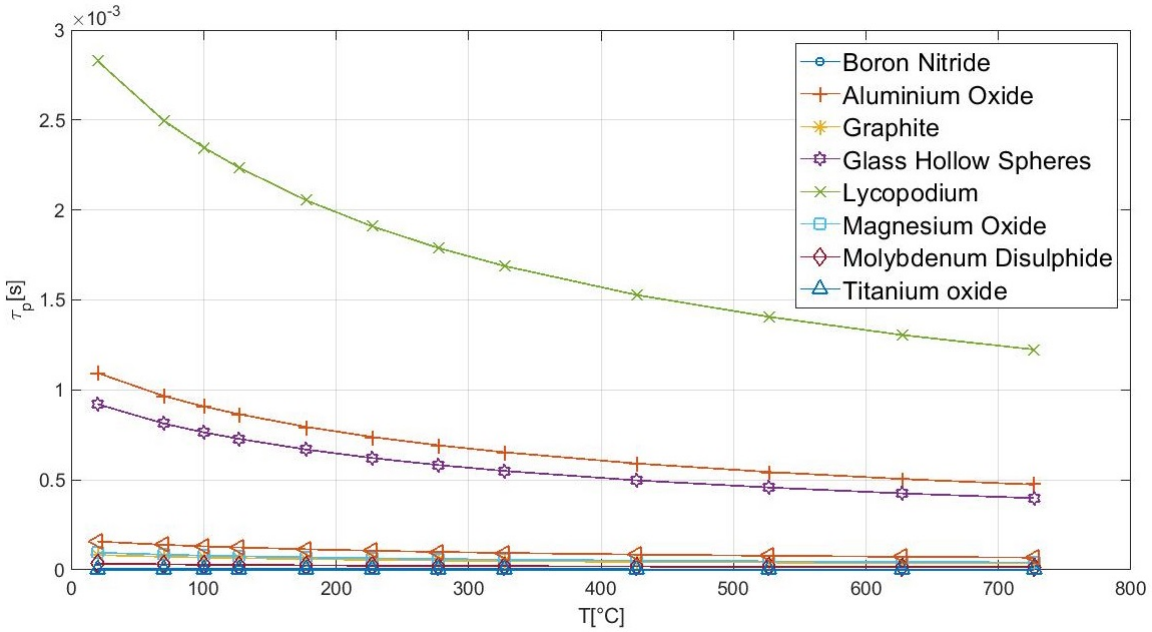

Figure 31: Relaxation Time τ_p for different materials.

5.2 Hardness

Working with solid particles may cause scratch in the experimental apparatus where the flow runs in particular the glass parts. This involves that materials with lower hardness should be given preference. In the literature it is not easy to find the hardness of material dust. However some materials can be considered

Material	Mohs hardness
Graphite	lubricating capacity
Boron nitride	lubricating capacity
Titanium oxide	6
Aerosil	7
Magnesium oxide	5,8
Aluminium oxide	9
Lycopodium	/
Molybdenum disulphide	lubricating capacity
Hollow glass sfere	6

Table 4: Materials hardness.

lubricant and thus their hardness can be not considered. In Table 4 are shown the Mohs hardness with which it is deduced that Aluminium oxide has the hardness value too high for which it is excluded from the material list. Finally, Aerosil is excluded for its high hardness value and for its particle diameter too small to be detect from the background.

5.3 Deposition

An important aspect to keep in mind during a PIV measurement is the level of particles deposition on the optical access. Indeed, when the engine works and the seeding material is supplied, there is the possibility that seeding material particles and other residue can occlude the optical passes. This involves a pictures noise increment and consequently poor results. In order to understand the different materials behaviour it has been projected a test bank that simulated engine condition. The test bank has been designed using the same cylinder head and intake system mounted in the engine. To simulate the combustion chamber a commercial Plexiglas pipe with approximately equal cylinder diameter is chosen. The representation of the test bank is shown in Figure 32. In

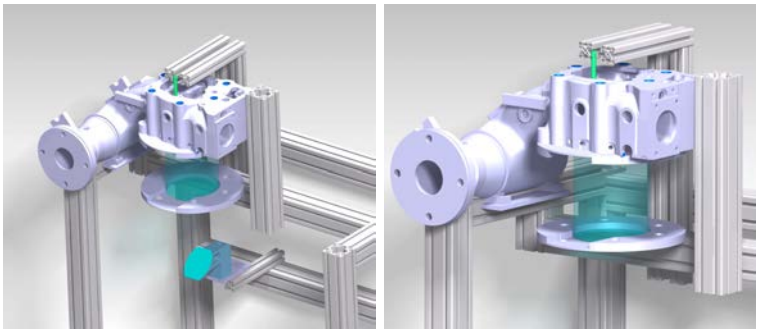

Figure 32: Test bank representation.

order to simulate the piston position, the bottom plate can sliding into the Plexiglas pipe. A blower is connected by a plastic pipe to the intake system. All the lengths have been taken considering the real engine dimension to evaluate the state of the cohesion between the particles during the trip into the engine. Indeed, adjusting the blower pressure it can be reproduced different

mass flow rate values and therefore obtaining an optimal value of particles generator pressure and laser power. For time reason, it was not possible to build it in order to test materials behavior and set the testing parameters to use in the real experiment.
In the literature it has been found similar experiments that simulate the seeding behaviour. In the V.M. Neubert work [58], many experiments are played with graphite, Molybdenum disulphide and Boron nitride. It has been established that these materials present a good solution in order to use them in the engine. More it has been evaluated the particles deposition during the run. In Figure33 are shown the deposition for each materials.

Figure 33: Material deposition [58]: Molybdenum disulphide (On the left), Boron nitride (In the center), Graphite (On the right).

The Molybdenum disulphide and the Boron nitride form a particles layer in the pipe border that impede the laser light to illuminate the particles and even at the camera of capture the light scattering. This means that it would be necessary to stop the engine frequently to clear the optic parts. On the contrary, the graphite presents a good feeling with the Plexiglas pipe and only little particles are attached to the wall.

5.4 Material choice

Taking into account all the considerations done before, there is not an optimal material to use for all the temperature range. It depends mainly from the conditions in which the measurement happens. Thus, it is possible divide the cycle in four parts, Table 5. Graphite and Boron nitride are the first choice

Best Material	Temperature range °C
Graphite	< 450 [58]
Boron nitride	$450 < x < 900$ [58]
Titanium oxide	$900 < x < 1800$ [32]
Magnesium oxide	> 1800 [19]

Table 5: Materials range.

until their temperature limit, indeed, they have the best compromise between light scattering, deposition, particle dimension and lubrication. When fired test has to been done, it is necessary switch to material with high temperature resistance. Titanium dioxide and magnesium oxide are the best choice for temperatures warmer than 900°C.

6 Equipment and Instrumentation

The Chair of Internal Combustion Engines at Technical University of Munich is currently studying engines and mechanisms in order to identify and apply new systems. For what concern the engine optical test, they are practiced in a single-cylinder experimental engine that could works in motored and in fired operation. The engine is mounted in a test bench in a dedicated room in which are supplied structural components and others systems that allow to run the engine. The engine is equipped with an optically accessible bowl piston with external diameter of $168.8mm$ and internal optical diameter of $105mm$. In the piston basement has been created the mirror seat. The mirror allows to place the camera perpendicularly to the piston axis. Finally an optical access has been created on the cylinder in order to allow the combustion chamber illumination by a laser beam. In this way the horizontal plane is studied. It is also possible to switch camera and laser and thus studying the vertical plane. In Figure34 an engine section is shown highlighting to the optical accesses.

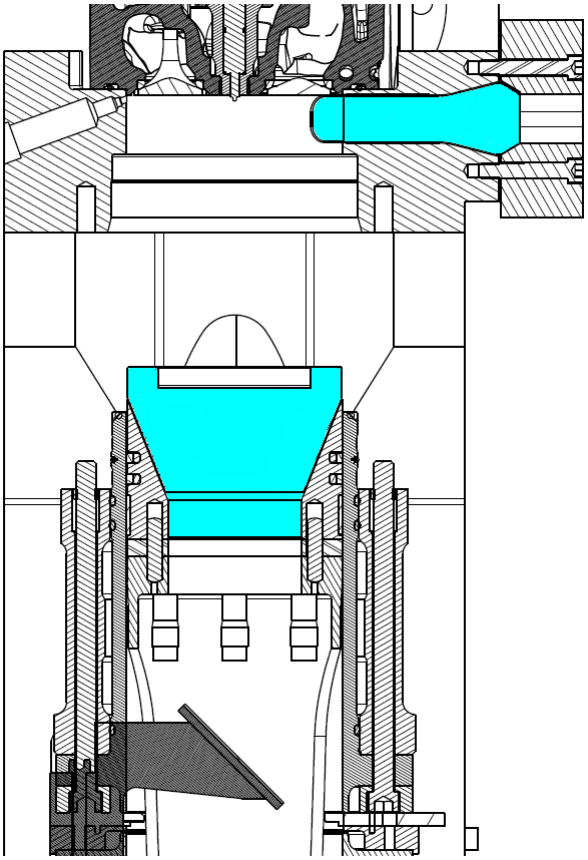

Figure 34: Large bore dual fuel engine: cylinder cross-section.

The measurement and control technology are implemented with a modular system based on a PXI from National Instruments. PXI automates the data acquisition and control tasks. PXI is controlled by two programms in LabView. In order to control in real time the gas injection and ignition timing, it has been installed a CompactRIO module from National Instruments [45]. In the motored operations, the engine is put in rotation by an electric motor fixed

in the engine crankshaft. In the fired operations, the engine is braked by the eddy current brake. The SPARC controller, using a software developed in house, controlled the fired and motored operations and it allows to maintain a constant engine speed even during the transition from fired to motored. The motor is conditioned and supplied by the periphery. The periphery can be divided into four supply lines which allow the engine to work. A peripherals description is given in the following points [45]:

- The air line: it provides the engine with fresh air and disposed of the exhaust gases. It is possible to control independently the air pressure, temperature, mass flow and exhaust back-pressure. The air pressure is generated by a screw compressor.

- The gas line: the engine on the test bench can use gas as fuel during the fired operations. The gas line supplies the fuel gas with which the engine is fired. It is possible to use either natural gas or natural gas mixed with another type of fuel. The natural gas is heated by the gas heater and immediately thereafter the natural gas mass flow is measured by a Coriolis mass flow meter. The pressure of the natural gas line is regulated by a pressure reducer. In the admixed gas line, the mass flow is also measured by a Coriolis mass flow meter and the pressure is set via a pressure reducer. The gas line injects the gas in the air line. The module that allows the gas injection consists of 12 gas valves controlled separately in three groups by the cRIO. In this way is possible to regulate the gas mass flow injection.

- Coolant system: in the test bank water mixed with frost and rust protection (glycol) are used as coolant. The coolant is pumped by a water pump through a closed circuit. On the route are mounted a heating element and a heat exchanger. The cooling water flow through the heat exchanger is adjusted by a proportional valve. The heating element and the proportional valve of the heat exchanger are controlled by the test bench automation. As a result, the coolant temperature is regulated in the circuit.

- Oil circuit: the lubricating oil for the engine is heated in the oil sump by three immersion heaters. The oil is then pumped by a pump and cooled by a heat exchanger until a define temperature. The oil line is divided into three pressure levels strands. One strand supplies the oil spray nozzles in the gearbox, in the cylinder head and in the mass balance bearings. Another strand supplies the engine camshaft and crankshaft bearings. The third strand supplies the oil spray nozzle in the piston.

6.1 Explosion protection measures

During engine operation, an important aspect to evaluate is the explosions possibility. Indeed the engine is used to investigate thermodynamic processes and combustion development. This means that several parameters in the engine can be changed such as periphery conditions, camshafts timing, injection timing, intake pressure, oil pressure and many others. This could lead to the

risk that components and operations do not work in the right way. The uncontrolled or unwanted fuel ignition poses the greatest risk during the test. The charge area is the most dangerous zone because it could happen a backfire or an explosion. There are some explosion protection measures that have to be take into consideration in order to reduce the explosion risk [45]:

- Measures which prevent or restrict the formation of hazardous explosive atmospheres (avoid explosive atmospheres).
- Measures to prevent the ignition of hazardous explosive atmospheres (avoiding effective ignition sources).
- Constructive measures that limit the effect of an explosion to an acceptable level (constructive explosion protection) for example pressure release plates in the intake and exhaust system.
- Application of process control technology in the context of explosion protection measures.
- Protective measures during repair work.
- Explosion protection document.
- Organizational measures.

6.2 Laser

The laser used in the experiments is a $nanoPIV$ made from $LitronLaser$ [34]. The serie of the laser is $NanoL\ PIVPulsed\ Nd:YAGLasers$ that offers repetition rates to $100Hz$ and energies to $200mJ$ at $532nm$. The PIV head is formed by an aluminium plate onto which two standard Nano series heads are mounted. The output beams are combined by dielectric polarisers and then frequency doubled. The specifications are shown in the table 6. An overview

Model	$NanoL200-15PIV$
Repetition Rate per laser head (hz)	$0-15$
Output Energy at 532nm per Laser Head (mJ)	200
Pulse - Pulse Stability ($\pm\%$)	2
Beam Diameter (mm)	$6,5$
Beam Divergence ($mrad$)	-3
Pulse Length at 1064nm (ns)	$6-9$
Lamp Life (pulses)	$> 5 * 10^7$
Voltage (VAC)	$110-250$
Frequency (Hz)	$47-63$
Cooling	Air
Power Supply	LPU550

Table 6: Laser specification.

of the Laser system is shown In Figure 35

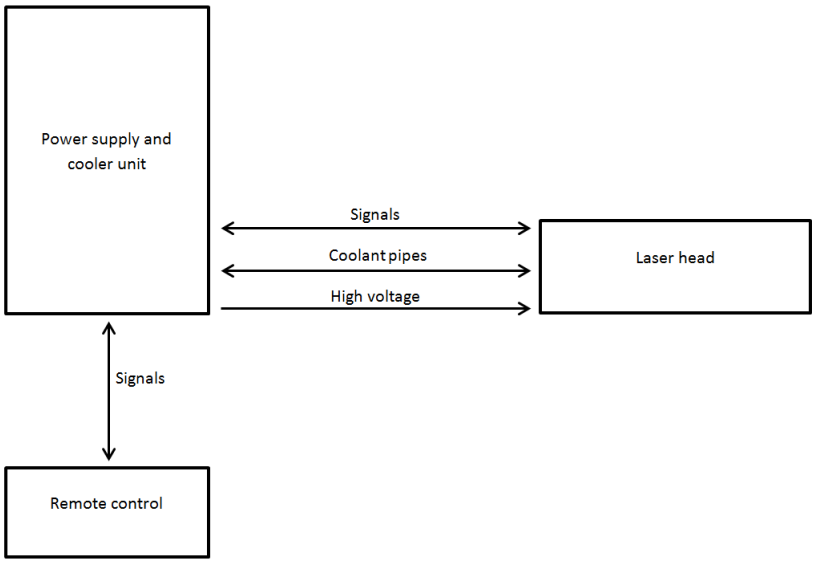

Figure 35: Laser system.

6.3 Camera

The cameras used in the experiment is the $ImagerproX2M$ and $sCMOS$ both made from LaVision [28]. This cameras have a digital image output, a separate camera control unit and different image sensor that allow to get different spatial resolution and exposure time as mentioned before. The cameras have an interline transfer chip that allows to readout and up to 1 GB memory in the camera head to store the images and than transfer the data to the computer [28]. General system specification are shown in Table 7.

Model	$ImagerproX2M$	$sCMOS$
Interframing time (ns)	110	120
Cooling system	Peltier	Peltier
Lens mount	F-mount, C-mount	F-mount, C-mount
Number of pixels	$1600x1200pixels$	$2560x2160pixels$
Pixel size (μm^2)	$7.4 * 7.4$	$6.5 * 6.5$
Spectral range (nm)	$290 - 1100$	$370 - 1100$
Frame rate $(frame/s)$	29	50
Peak quantum efficiency at $532nm$	55%	55%
Exposure time	$550ns - 1000s$	$15\mu s - 100ms$
Memory	$1GB$	/

Table 7: Camera specification.

An overview of the Camera system is shown in Figure 36

6.4 Seeding generator

The Seeding generator used in the experiment is the $PB200$ made from LaVision [29]. The seeding generator is made up of many components: high pressure

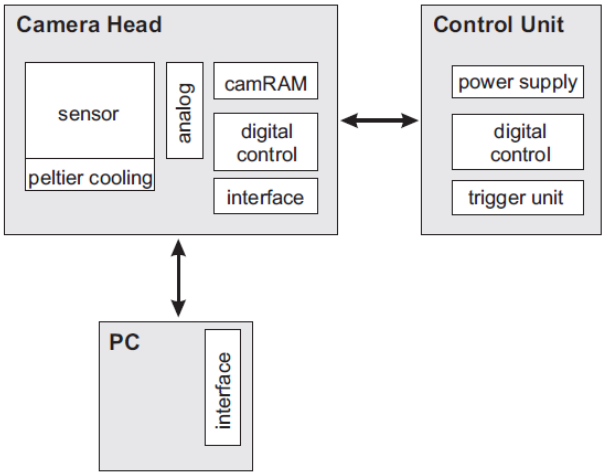

Figure 36: Camera system [28].

vessel, inlet and outlet pipe, dispersion plate, safety valve and pressure regulator (Figure 37). The $PB200$ can be used only with solid particles. To fill the

Figure 37: Seeding generator $PB200$. On the right: Top view; on the left: Dispersion plate [29].

$PB200$ with seeding material, the air supply has to be stopped and particles poured into the cylinder. After the refilling, it is necessary check the correct position of the O-ring furthermore the O-ring groove has to be cleaned before to re-assembly the top plate in order to avoid leakages. The maximum filling level is $25cm$ above the dispersion plate (volume of $8000cm3$). General system specification are shown in Table 8. The by-pass line Figure38 is an important feature because it allows to regulate the air flow in the seeding generator. When the seeding generator works, the air flow measured in the intake system drops because part of the flow is diverted in the seeder. Because of the sustainable pressure from the tools connected in the air system, the maximal pressure achievable is $7bar$ that allows to reach around $6bar$ in the seeding generator. Despite the low pressure reachable compared to the maximal pressure supportable, the particles amount that have been got is resulted enough in the

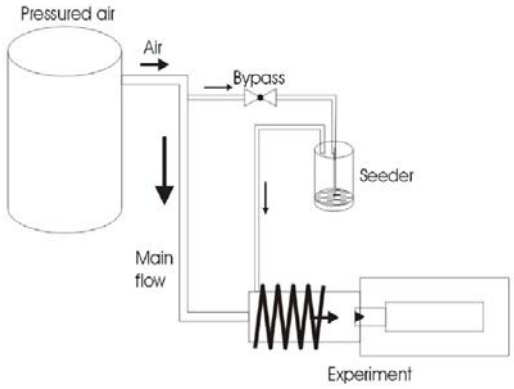

Figure 38: By-pass system [29].

Model	$PB200$
Maximum pressure	$20bar$
Safety valve	$22bar$
Minimum flow rate	$1l/s$
Size	$370mm * 750mm$
Particles	Aerosil, Titanium oxide, glass hollow spheres

Table 8: Particle generator specification.

bigger part of the engine cycle. The main problem originated from the seeding generator remain the flow channels creation in the powder vessel that reduces the particles density over time.

6.5 LaVision software

The software used during the experiment is $DaVis8.4.0$ [26]. The company LaVision has developed this software that allows to elaborate directly the pictures taken by the camera in order to get the flow analysis. Indeed, $DaVis8$ allows to apply a large and detailed number of filters for mitigate unwanted visual effects and for enhancing the particles in the image. Thanks to a complicated and consolidated algorithm, the pictures are analyzed and shown in a dedicate window in which is possible to adjust the results through the post-processing and finally export them in many different extensions. DaVis main menu is shown in Figure39. The first step is to select the pictures set to ana-

Figure 39: Davis initial menu [26].

lyze. Loading the images in the software is possible to set the scaling and the calibration of the pictures. DaVis allows to calibrate the captured images in order to have the transformation from *pixel* to mm and getting thus results in m/s. It is now possible to elaborate the images by the *processing* button. In

the processing dialog can be use up to nine different functions. The program works sequentially from the first to the last function (The result of the last function is used as input for the next operation). In Figure 40 is shown an example of operation list.

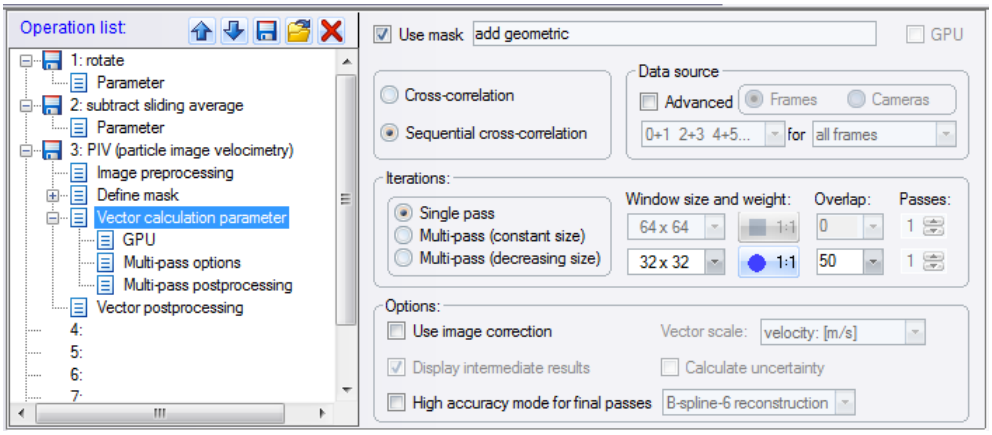

Figure 40: Davis operation list [26].

In the operation list it is possible to decide between many different type of operations. A quick explanation is provided below:

- Basic Arithmetic: the basic arithmetic allows to apply simple mathematical operations as constant values or to apply masks and to change buffer dimension.
- Image properties: it allows to do Data Type Conversion, Re-size, Extract Volume, Scalar Components and Convert image to vector.
- Image mapping: it allows to do Geometric Transformations, Image Correction and Distortion, Image Reconstruction, Image Stitching and more.
- Scales: it allows to do Set Scales, Transfer Scales and Convert Intensity Scale.
- Attributes: it allows to do Basic Attributes, Add Overlay, Add Default Attributes, Add Camera Attributes.
- Statistics: Sum, Average, Standard Deviation, Min, Max, Probability Density Function, Histogram.
- Masking Functions: it is often necessary adding a mask in the pictures in order to exclude some areas that are not useful in the process and that could make the process slower. It is possible to add a geometric or a algorithmic mask.
- Time Series: it allows to do Difference to First Image, Normalization to First Image, Shift and Rotation Correction, Time Filter (very helpful in order to delete the background), Bright-Field Correction.
- Linear Filter and Non-Linear Filter.

- Copy and Reorganize Frames.
- Profiles and Time Plots.
- Intensity Correction as Energy Correction.
- Self-Calibration.
- Convert Image to RGB.

LaVision provides a detailed manual where are explained all the software operations and some practical examples with a video guide. After applying operation the program are ready to process the data and to provide the results. The results are available in the left tree. With the results is possible to evaluate many aspects of the flow as vector length, velocity component x-y or vorticity.

Finally Davis can export the results in different formats as movie (AVI), simple bitmap (BMP), ASCII text (TXT), LaVision set (vc7) and more but DaVis does not save directly the result in matrix format. LaVision provides a MATLAB function to read DaVis results and to transform a picture in DaVis format (.im7) in order to import in DaVis pictures from an other acquisition system. In Figure41 is reported the DaVis result window.

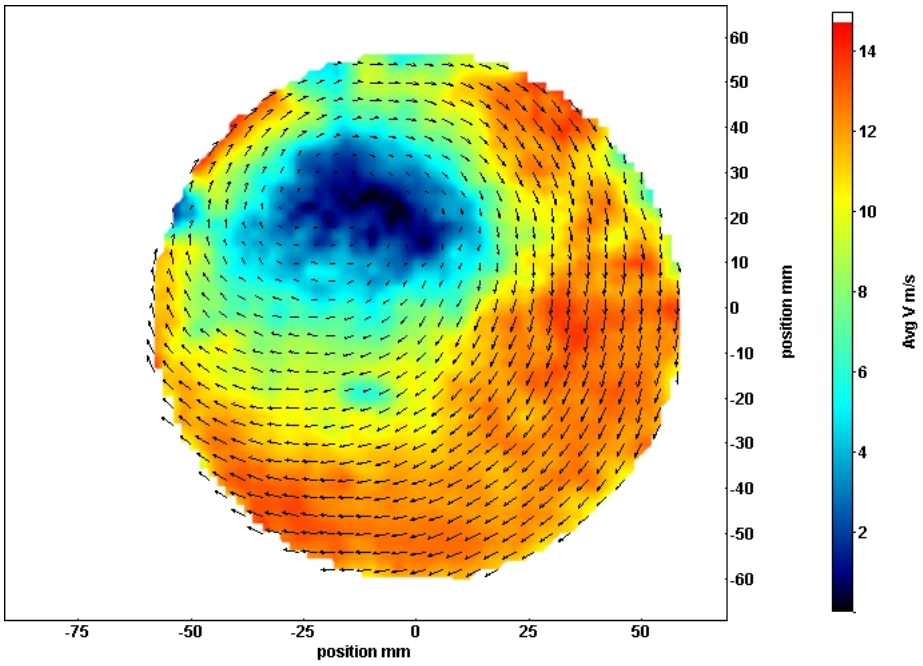

Figure 41: Davis result window: engine test with Titanium oxide as tracer at $CAD = -100°$ [26].

6.6 MATLAB toolbox

During the first data processing, Davis showed long work time and a poor possibility of results manipulation, moreover there was not a test against to evaluate the results goodness. For these reason, it has been decided to improve a MATLAB toolbox and match the results from these two programs. On the

web there are many MATLAB toolboxes for PIV, the three main toolboxes are described:

- PIVlab: it is a complete toolbox that allows to elaborate frames from pre-processing to post-processing [15, 52, 53, 54].
- openPIV: it is very simple to use, but it does not have some important functions for processing control [51].
- PIVmat: it is only a functions package for MATLAB for elaborating and displaying results already processed with another software (it supports DaVis results) [13].

The most similar program to Davis is PIVlab. It has a user-friendly software configuration that allows to understand and evaluate quickly the results and to adopt the best process configuration. More, PIVlab allows to save the setting parameters and recall them when it is necessary. The PIVlab welcome page is shown in Figure 42.

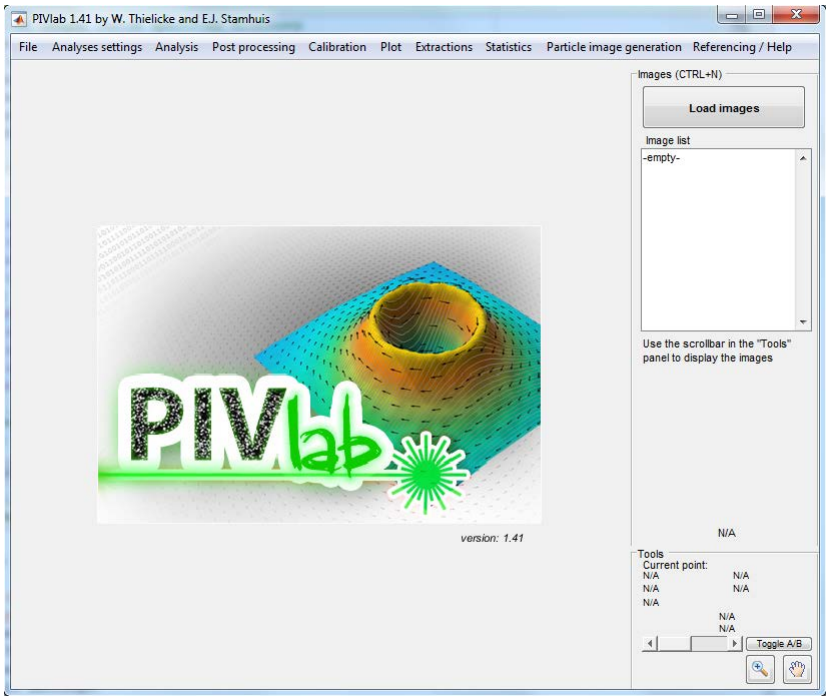

Figure 42: PIVlab main menu [52].

PIVlab works only with pictures couple imported in sequential mode in such a way that the first picture is the frame $1A$ and the second picture the frame $1B$, then the third picture is the frame $2A$, the fourth $2B$ and so on. After the pictures loading, is possible to apply filters, mask and decided the interrogation windows with respective overlap. After the processing PIVlab allows to apply post processing filters and export the results in images formats, matrix format or in PIVlab format (that can be re-loaded). For using PIVlab it is necessary to have frames in pictures format. As mentioned before, the camera output is in DaVis format ($.im7$) and consequently it is not possible to use PIVlab directly with this format. The solution is to use the LaVision package in order to read

the frame by MATLAB and then transform it in picture. The procedure to obtain images in the correct format is described below and in the Figure43:

1. Getting the image in *.im7* format by the camera.
2. Utilizing the GUI script to import all the frames in MATLAB and save them in a matrices cluster.
3. Utilizing another script to transform the matrices cluster in pictures in format decided by the user. (The script saves the picture in a selected folder renamed the pictures with data test and number).
4. Importing the pictures cluster in PIVlab.

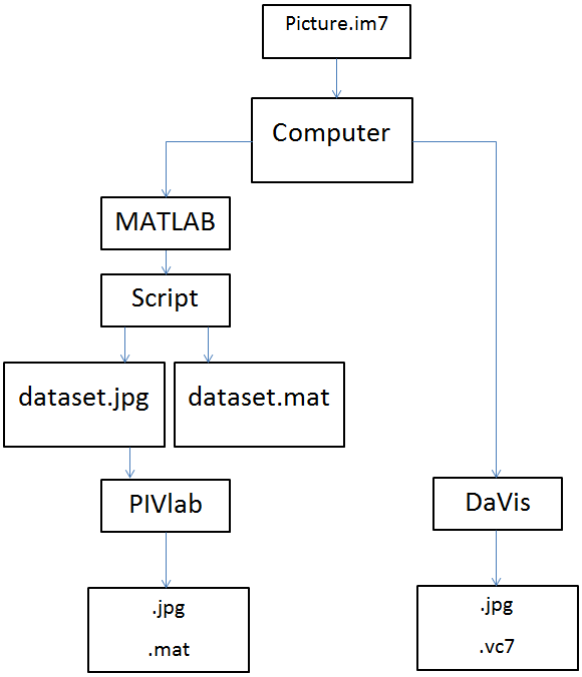

Figure 43: Sequence to transform the pictures in order to use them in PIVlab.

The whole procedure required a lot of time, mainly due to the time necessary to transform the LaVision format in matrix format. Since, it has be implemented a script derived from PIVlab that allows to use the toolbox without GUI but directly with the command prompt. This method allows to reduce the time for the processing particularly when the processing parameters are always the same. The script shows the results by pictures. It has been implemented the possibility to save the results in picture format or/and in matrix format. Finally, it has been created a script to group all the scripts and having a complete image processing automation (in order to run the script is necessary selecting the pictures folder from the camera and selecting a new folder where the user wants to save the transformed pictures and the results).

6.7 LaVision and PIVlab way of working

The main purpose to use two different programs is that to compare the results. Compare the results means studying differences as vorticity, velocity and swirl motion in the same frame by the two programs. The evaluation could be done by mathematical comparison with the result matrices. But first it is necessary to understand how the programs solve the elaboration. The vectors number is defined by the window size. It is necessary to understand how the programs work:

- DaVis: In Davis it is possible to set the window size (it only allows to select a default number of sizes), the type of interaction (single-pass or multy-pass), the window shape, the overlap between two interrogation windows and the passes number. The figure 44 allows to see how the overlap works. The interrogation window size and the window overlap

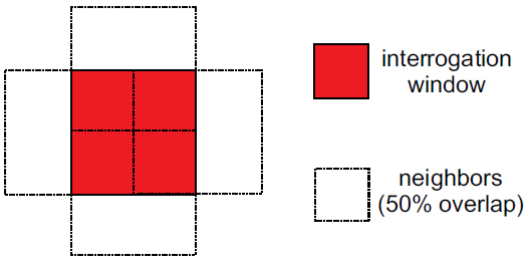

Figure 44: Overlap: first interrogation window (red) and the following interrogation window with 50% of overlap [27].

determine the vector field grid size. In DaVis, an image of $320x320$ pixels and a window size of $32x32$ pixels with 0% of overlap, it provides a matrix $10x10$ with 100 vectors. With the same image size and the same windows size but with 50% of overlap it provides a matrix $20x20$ with 400 vectors. An important feature to consider is the position of first interrogation window in the picture top left corner. Indeed, as will be possible to see later, the position of the first interrogation window influences the vectors number. In DaVis the grid size is defined as the distance between the centers of two consecutive interrogation windows. Thus, the top left window is positioned at half of the grid size, for example if the grid size is 32 pixels, the top left window center will be located at the position $(16, 16)$ and if the grid size is 16 pixels the vector will be located at the position $(8, 8)$. This convention allows an arithmetic vectors calculation:

$$nv_x = np_x/gs \qquad nv_y = np_y/gs \tag{8}$$

In which np_x and np_x are the picture pixels number respectively in x and y, nv_x and nv_x are the result vectors number in x and y and gs is the grid size value. In Figure45 are shown some examples of interrogation window position for different parameters.

- PIVlab: The PIVlab algorithm works in a different way respect Davis's algorithm. In PIVlab there is not the Overlap option, but it is necessary

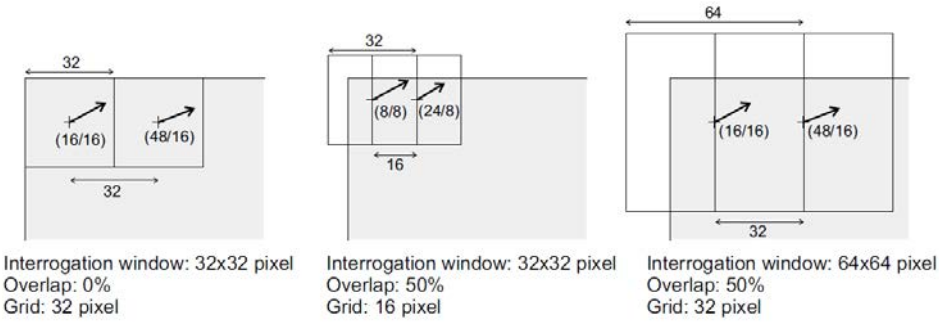

Figure 45: Vector position [27].

to define the step in pixels between two interrogation windows. For example, with an interrogation window of $32x32$ pixels and setting step of 32 pixels it is like setting an overlap of 100%. Moreover, there is another fundamental difference in the first window position. Indeed PIVlab puts the first window ever in the same position independently of the window grid and it is positioned adjacent to the picture limits. This means that if the picture size is $320x320$ pixels and the interrogation window size is $32x32$ pixels with step of 32 pixels (0% overlap), it provides a matrix $10x10$ with 100 vectors as well as Davis, but with step of 16 pixels (overlap 50%), it provides a matrix $19x19$ with 361 vectors. In order to have a good results it is always necessary set an overlap and this involves a different matrix dimension between the two programs Figure 46 .

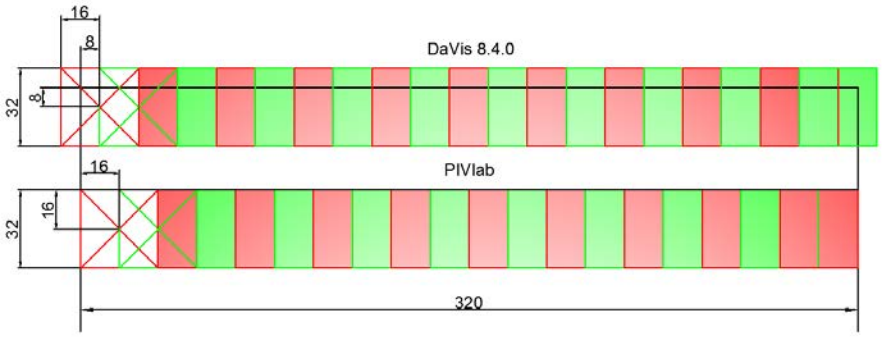

Figure 46: Interrogations windows positions in DaVis and in PIVlab for a pictur of $320x320$ pixels and interrogation window of 32 pixels with 50% of overlap.

In order to verify the effects of the different windows positions, some reference pictures has been created. The reference pictures have defined dimension of $320x320 pixels$ and the some particles are printed. In Figure 47 is shown an example of reference picture.
The pictures are processed with window size of $64x64 pixels$ and 75% of overlap in both programs. With this setup, PIVlab provides $17x17$ vectors while DaVis provides $20x20$ vectors. The imposed particles displacement is $12 pixel$ only in the horizontal plane. In Appendix A are shown the results matrix for the velocity v_x (Figure 90).

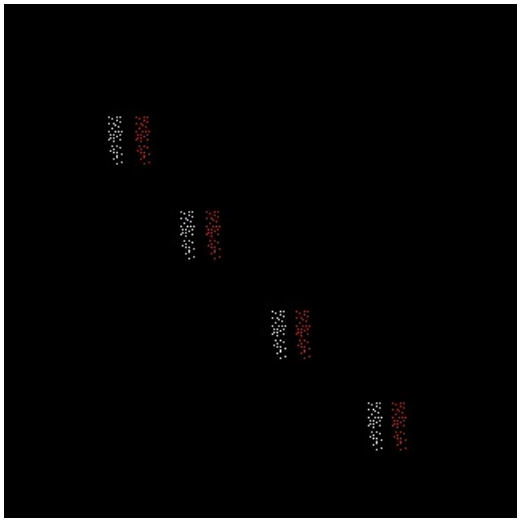

(a) Reference picture

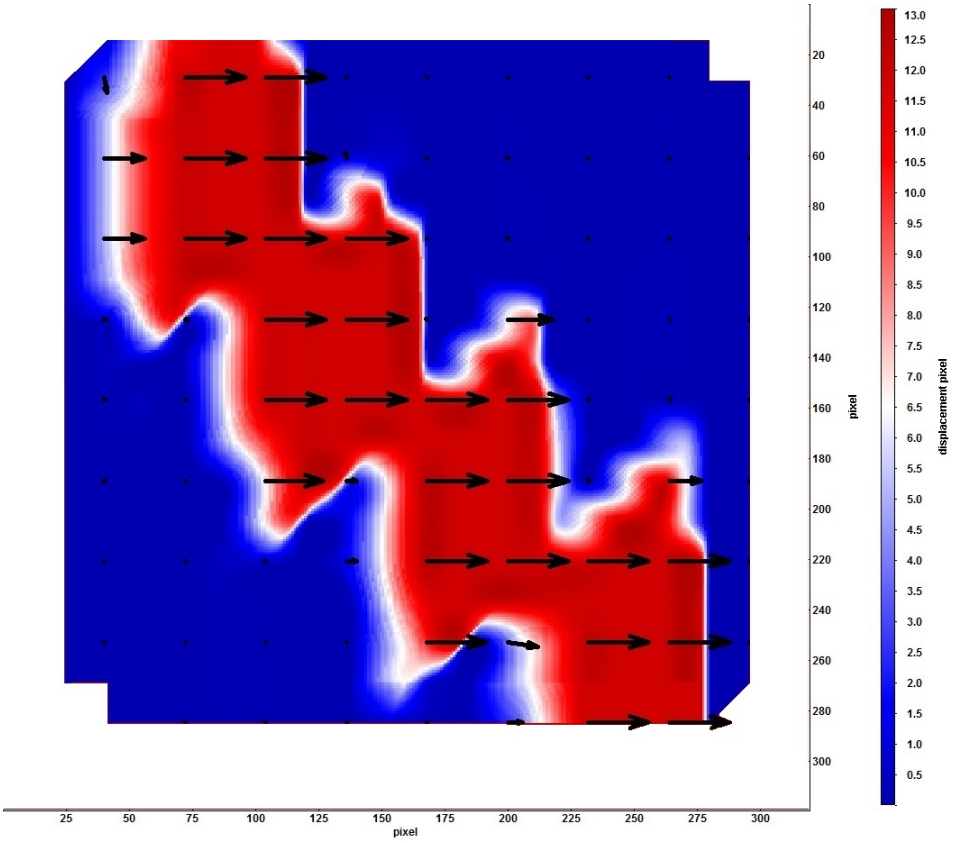

(b) Flow field Result

Figure 47: White particles are from the first frame while red particles are frome the second frame. It has been imposed a particles shift of 12 pixels.

7 Results comparison between PIVlab and DaVis

In order to verify the results goodness, it is necessary to compare the same flow field in both programs. About this, will be used some pictures taken in different contexts to have the possibility to evaluate completely the software behavior. For the comparison it has been decided to use the result average of the whole pictures set. In this way are neglected local errors.

7.1 Simple flow field

For the first evaluation are analyzed example pictures from the LaVision tutorial. The images refer to a simple fluid flow with particles addition. These pictures allows to test the principal PIV functions and to understand the programs features. The flow type is shown in Figures 48: This example has 10

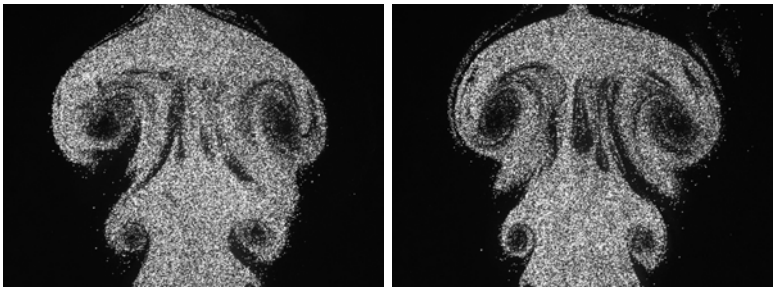

Figure 48: Test images: two different frames of a sequence.

different pictures in which there are 2 frames for each situation. In order to have the same unit of measure in both programs, it is necessary to set the same image scale and frame timing ($200\mu s$). Before to launch the processing, it is a good rule to impose a mask to avoid non-influential areas contribution that could involve results distortion and extra processing time. It has been decided to use a window size of $64x64pixels$. In the follow pictures are shown the programs results imposing the same scale range and the same vector appearance. In the left side are shown the result from PIVlab while in the right side are show the result from DaVis. As first analysis, it has been taken into account the flow velocity. Pictures 49 shown the velocity trend applying a color scale from $0m/s$(blue) to $3,6m/s$(red). The velocity is a combination between x-component and y-component, called $VectorLength$ in DaVis and $VelocityMagnitude$ in PIVlab. Visually, the velocity field perfectly fits. The velocity progress is the same and the maximum velocity is around about $3,5m/s$. In order to get a mathematical comparison, the velocity has been evaluated along a line between the two superior vortexes. The result is shown in Figures 50. With these graphics, obtained directly from the programs, it is clear that the velocity trend is the same. To complete the analysis, in Figure 51 are shown the vorticity results.

It is possible to identify the presence of four vortexes. The vorticity results fit perfectly for both programs, but with opposite sign.

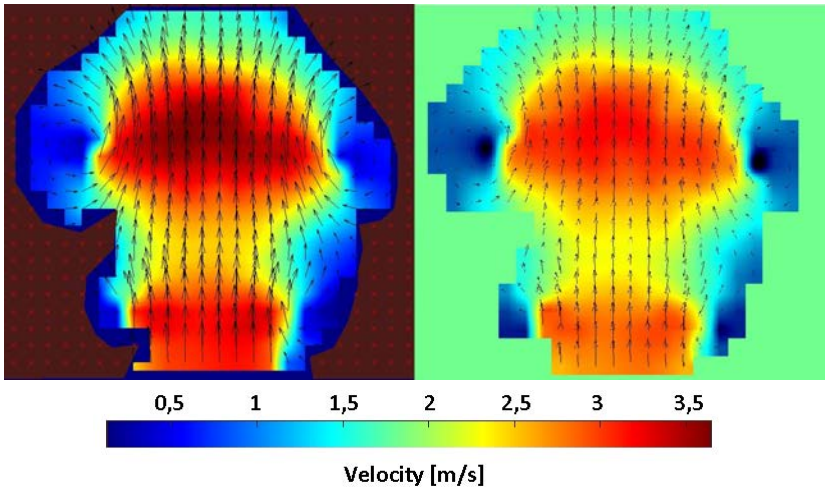

Figure 49: PIV test pictures. Average result PIVlab (left) and DaVis (right): Velocity.

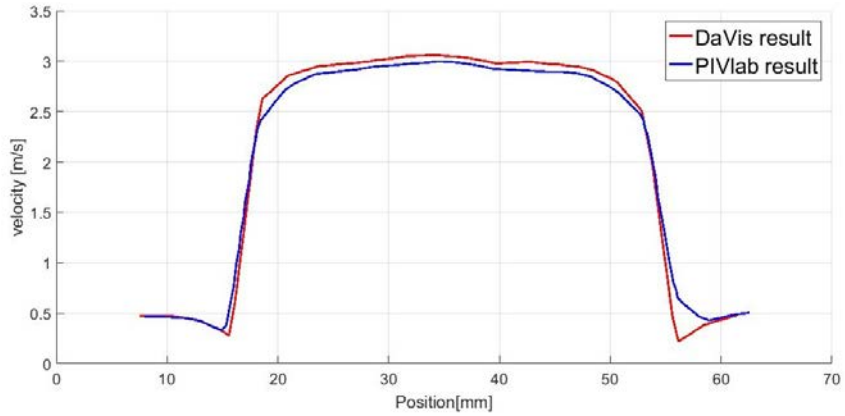

Figure 50: Velocity values along a line in PIVlab and DaVis.

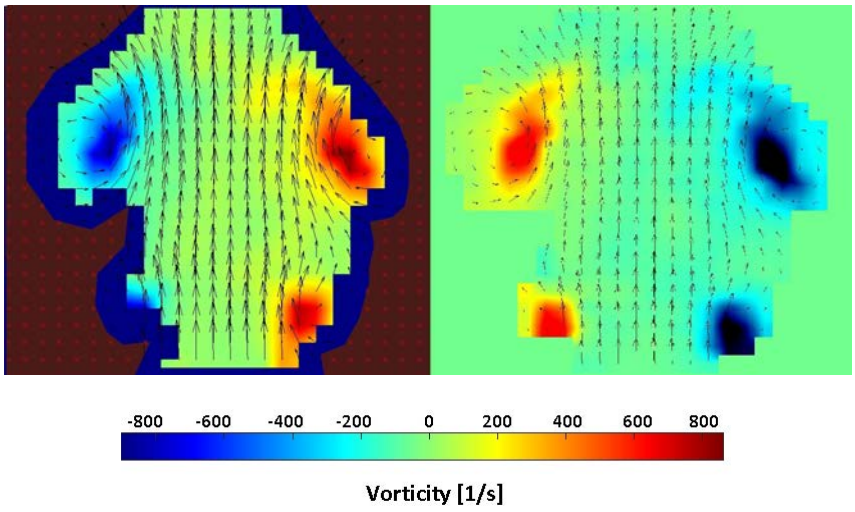

Figure 51: PIV test pictures. Average result PIVlab (left) and DaVis (right): Vorticity.

7.2 Engine flow field

For the second test it has been taken into consideration pictures from the engine. In this case the pictures are 50. In Figure 52 it is represented a picture captured from the camera after the pre-processing (background subtraction). Compared to the previous ideal case, it is clear that applying the PIV in the engine it is a challenge: non-uniform particles density, light peak, particles dimension and background effects are problems likely to be encountered in this pictures.

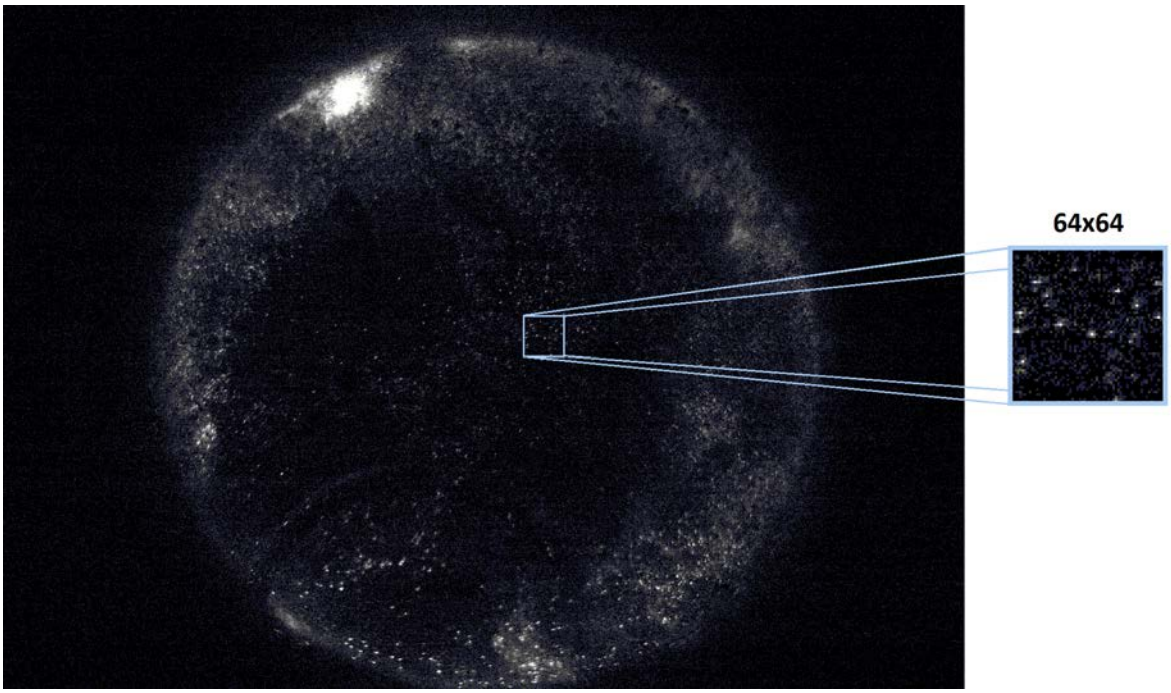

Figure 52: Engine flow picture: Window magnification of $64 * 64 pixels$.

The analysis is done by a $64 * 64 pixels$ window size with 75% of overlap. Even in this case the flow velocities (Figure 54) have the same course but there are little differences in their value. It could be attributed at the different mask size and position. In both cases it is recognizable a swirl centre. By a vertical line passing through the swirl center, the velocities are analyzed and the results are shown in Figure 53. It is possible to identify the same trend (the first three vectors in DaVis are due to the different mask position). An important aspect is that PIVlab does not allow to set the axis position differently from DaVis. This involves a different axis position.

7.3 Engine flow analyzed with lycopodium particles

During the first PIV setup test, pictures have been taken in some situations during the crankshaft rotation. These pictures have been helped to define the best camera timing and to adjust the particles density. Lycopodium has been chosen because it is a natural material (Lycopodium clavatum spores) in such a way as to be able to manipulate it without restrictions. More, in this phase, it is not necessary to analyze the entire engine cycle, thus the lycopodium

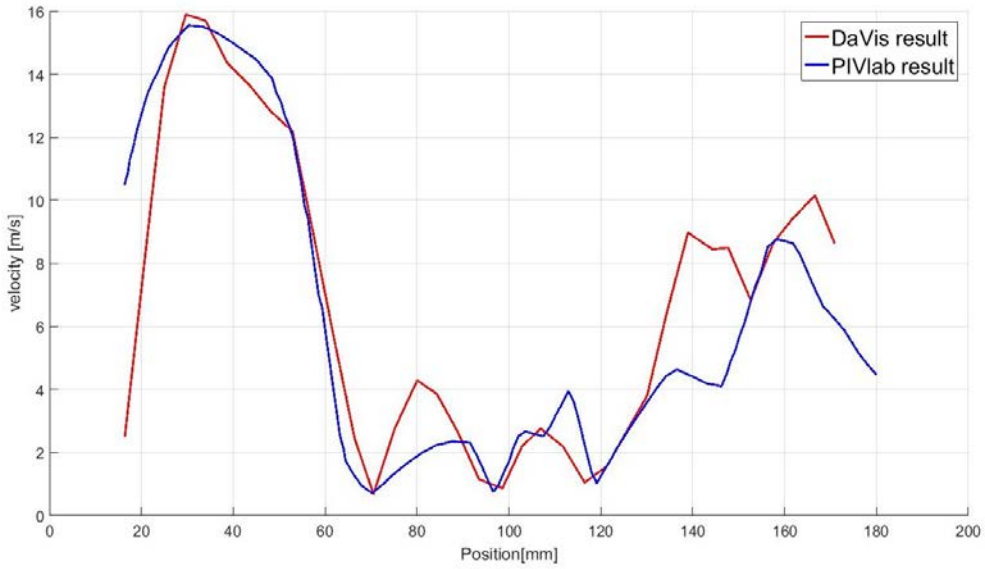

(a) PIVlab

Figure 53: Velocity comparison between PIVlab and DaVis along the red line displayed in Figure 54.

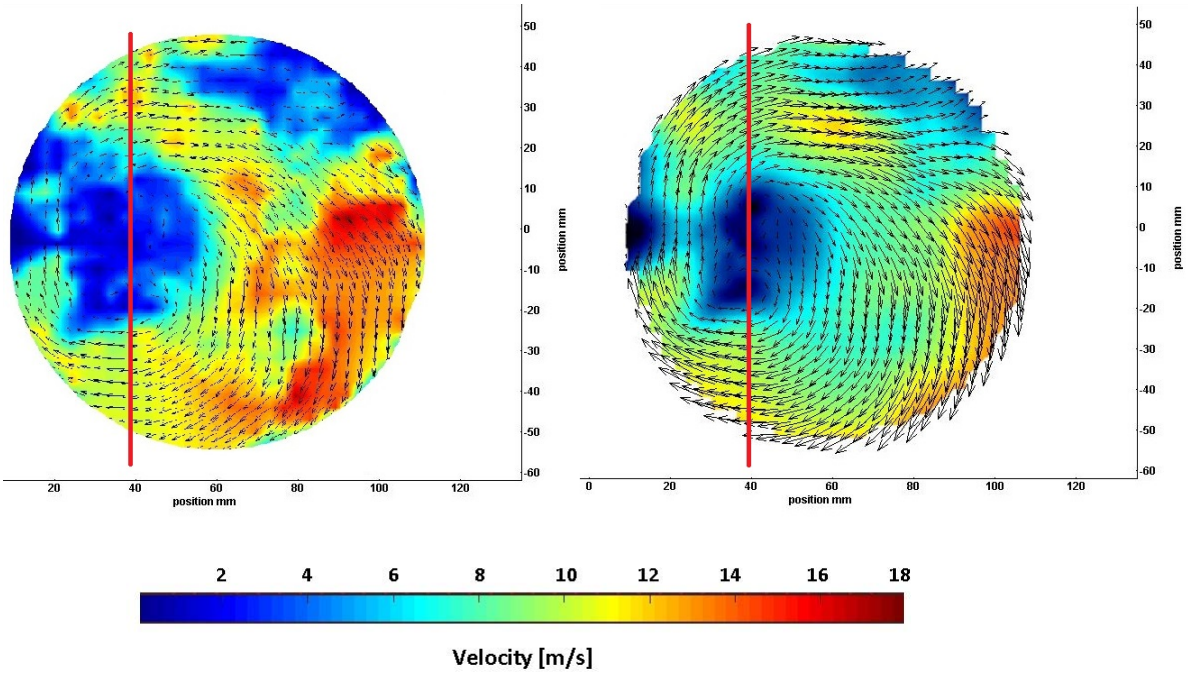

Figure 54: PIV result engine at TDC: average Velocity PIVlab(on the left), DaVis(on the right).

thermal capacity meets the requirements. The tests have been done without diesel injection. For the comparison it has been decided to study the flow during the exhaust stroke when the exhaust valves are open and the intake valves are still closed. The CAD is $-420°$ from TDC as it is possible to see in Figure61. In Figure 55 are shown the programs results with same velocity scale. At $CAD = -420°$, the flow presents poor quantity of particles. This condition

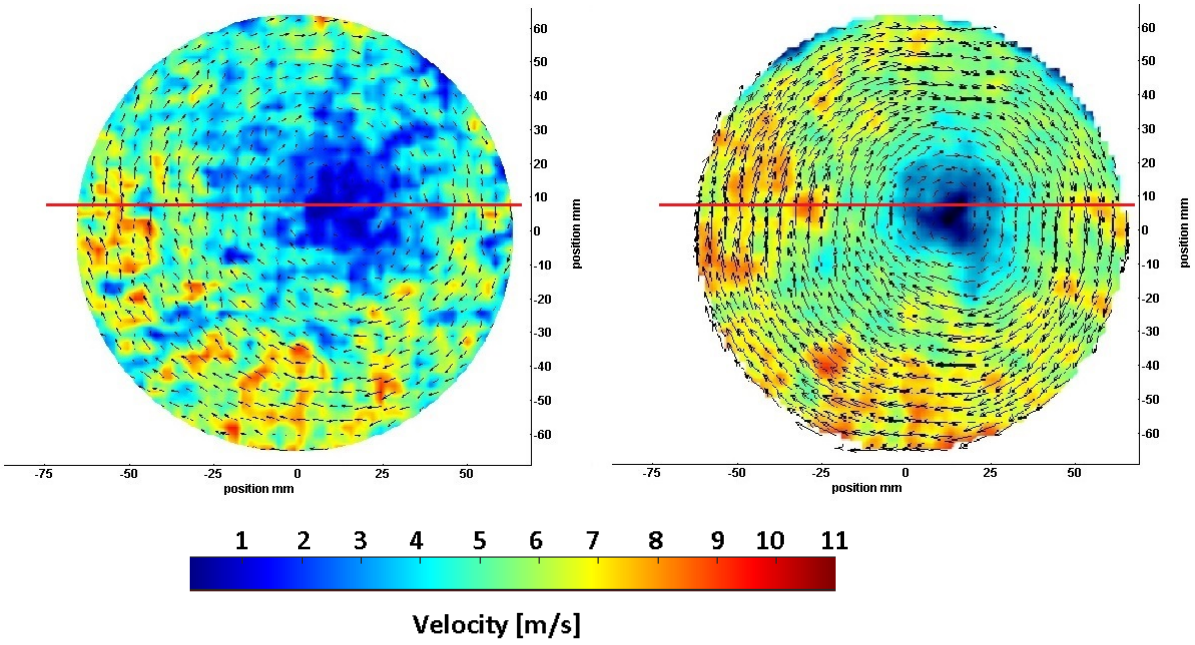

Figure 55: PIV results, Lycopodium, Vector field in the plane $z = 20mm$ at $CAD = -420°$ and $n = 600min - 1$, $\dot{m} = 210kg/h$.

is more burdening for PIVlab that shown non-uniform results, instead DaVis grants good results. The problem is evident plotting the velocity value (Figure 56). The velocity trend is the same for both programs but in the PIVlab case there are a lot of peaks which means that some interrogation windows don't have enough particles.

7.4 Engine flow analyzed with titanium dioxide particles

As last comparison, it has been studied the flow in the bottom dead center, with titanium dioxide as tracer. This condition is particular critical because the chamber volume reaches its maximum value and the pictures have relevant density gradients. This involves, combined with the small dimensions of the particles, to have areas with no results, Figure 57. As it is possible to see in figure 58, with this flow condition, PIVlab does not allow to get good flow information.

The Figure58 does not allow to have the whole flow field comparison. As seen previously, Figure 46, the different position of the interrogation windows in the programs, does not permit to compare directly the results. It has been studied a method to get around this problem. Adding a pixels frame (a quarter of the interrogation window) around the pictures to elaborate in PIVlab,

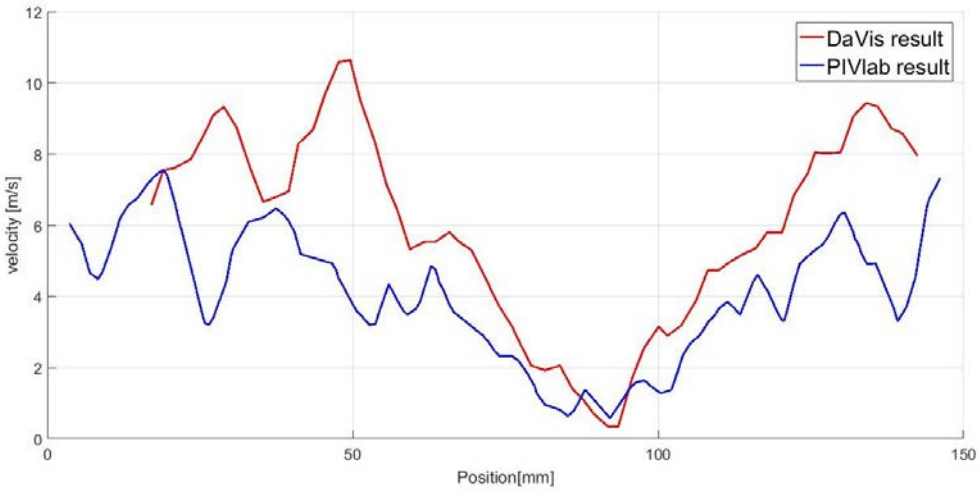

Figure 56: Velocity values along the red line displayed in Figure 55, Lycopodium, Vector field in the plane $z = 20mm$ at $-420°$ and $n = 600min - 1$, $\dot{m} = 210kg/h$ in PIVlab (on the left) and Davis (on the right).

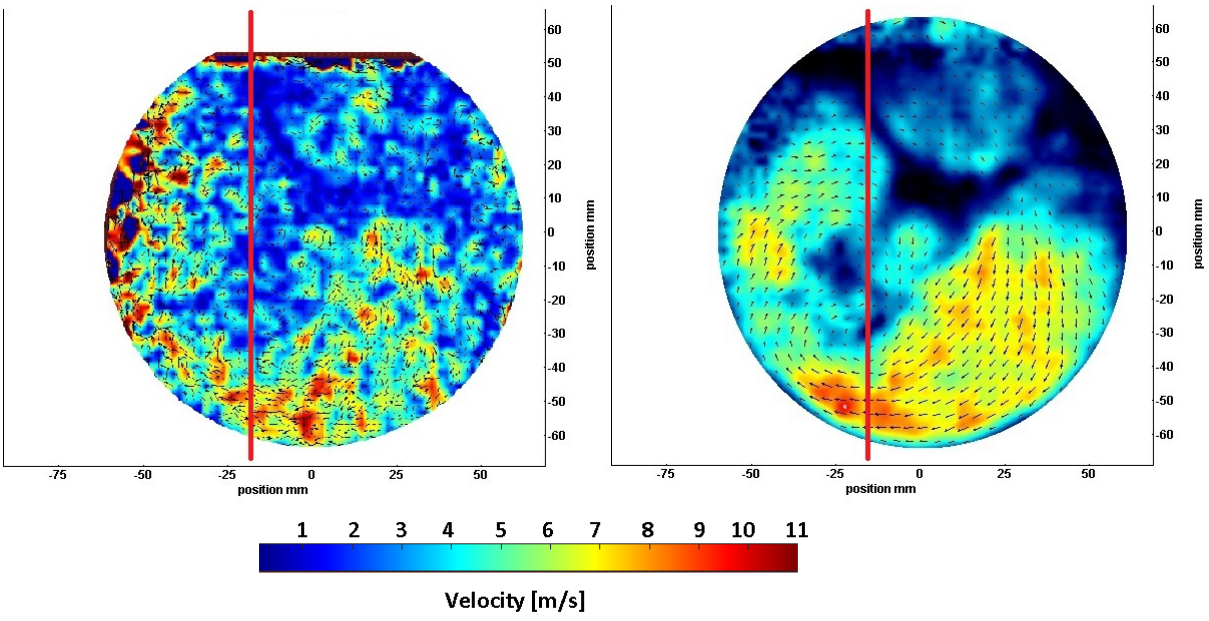

Figure 57: PIV results, Titanium dioxide, Vector field in the plane $z = 20mm$ at $CAD = -180°$ and $n = 600min - 1$, $\dot{m} = 210kg/h$. PIVlab (on the left) and Davis (on the right).

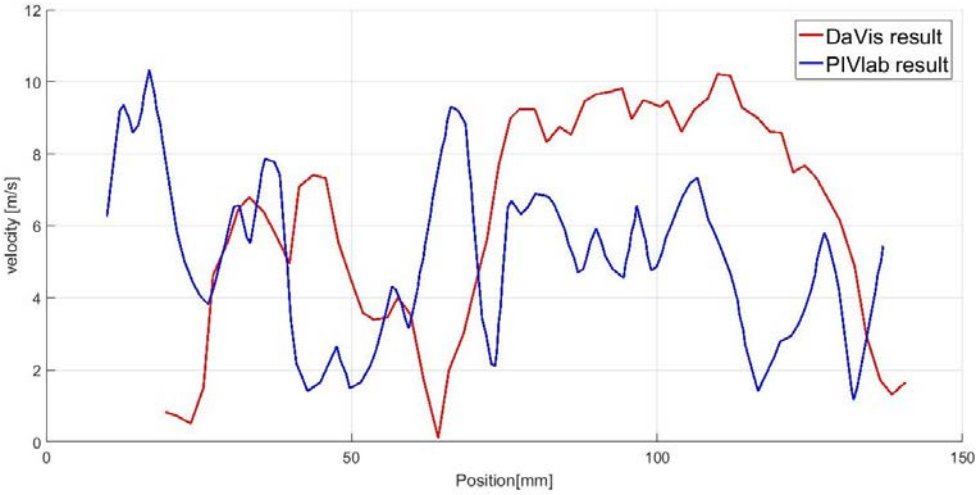

Figure 58: Velocity values along the red line displayed in Figure 57, Titanium dioxide, Vector field in the plane $z = 20mm$ at $CAD = -180°$ and $n = 600min - 1$, $\dot{m} = 210kg/h$.

it has been obtained the same overlap between the interrogation windows in the programs. This means that the vectors are in the same position, and then, the results can be mathematically compared. The velocity results have been imported as matrices in MATLAB. Having a picture dimension of $2560x2160$ pixels for DaVis and of $2592x2192$ pixels for PIVlab (due to the pixels frame), the matrices results have $68x80$ vectors. It has been decided to apply two types of comparison: Percentage difference and Absolute difference. The pictures 59

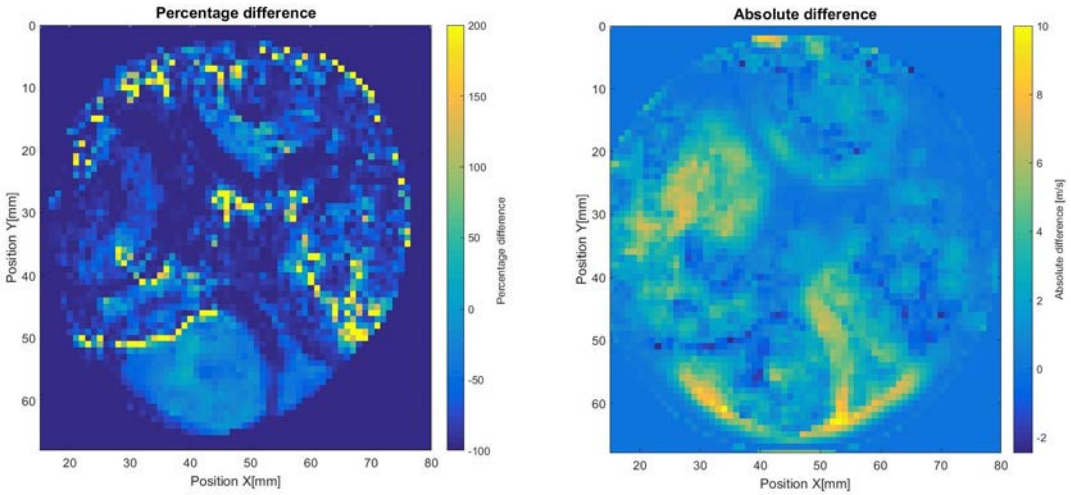

Figure 59: PIV results, Titanium dioxide, Vector field in the plane $z = 20mm$ at $CAD = -180°$ and $n = 600min - 1$, $\dot{m} = 210kg/h$: Percentage difference and Absolute difference.

shown the comparison. The Absolute difference has been obtained subtracting from DaVis result the PIVlab result. This means that, when the difference is greater than zero, the velocity in DaVis is higher than PIVlab, while when it

is less than zero, the velocity in PIVlab is higher than DaVis. It is possible to see that around the valves seat and in cylinder contour, where there are high background effects, DaVis has the velocity trend higher than PIVlab. This could be imputed at the fact that, as expected, PIVlab can not obtain good result where the particles are hard to see stating that, also in this case, the results are highly influenced by the background. In the Percentage difference, if the percentage is greater than zero, means that the PIVlab vector value is higher that DaVis vector value and vice versa. Also in this case it is possible to draw the same conclusions as in the previous case.
The cases at $CAD = -180°$ is extremely difficult to analyze because it has the most critical situation, due to the poor particles quantity. Studying another CAD it is possible to achieve more information about PIVlab behaviour. Thus, it is now studied $CAD = -90°$. In Figure60(a) is shown the flow field result coming from Davis. Instead, in Figure60(b) is shown the flow field result coming from PIVlab. It is clear as, the different pre-processing in the programs, involves different results. In Figure60(c) is shown the absolute difference in the programs results. Also in this case, it is easy to deduct that the main problems are around the valves seat.
In order to understand if it is only a problem of pre-processing or if the problem in PIVlab is in the calculation algorithm also, it has been used the pictures already pre-processed by DaVis and import them in PIVlab. The flow field result is shown in Figure60(d). Whit this new evaluation it is clear that, in order to obtain the same result, it is necessary to improve the pre-processing function of PIVlab. Finally, it has been compared, by absolute difference, PIVlab result 60(d) with DaVis result 60(a), obtaining Figure60(e). Again, this picture confirm a good PIVlab behaviour with pictures pre-processed with the "subtract time filter".

The comparison highlighted PIVlab difficulties to analyze the pictures when the flow condition become severe, or rather, when the particles dimension make difficult to recognize them from the background. Instead, DaVis allows to have good results for its elevated filters quantity and the possibility to adjust the pictures before the processing. To use PIVlab automation will be necessary,in a future work, to improve the pre-processing done with the script and adding a "subtract time filter" that remove the background objects present in the all set of pictures.
In this work, DaVis has been chosen to evaluate the engine experiments done with titanium dioxide.

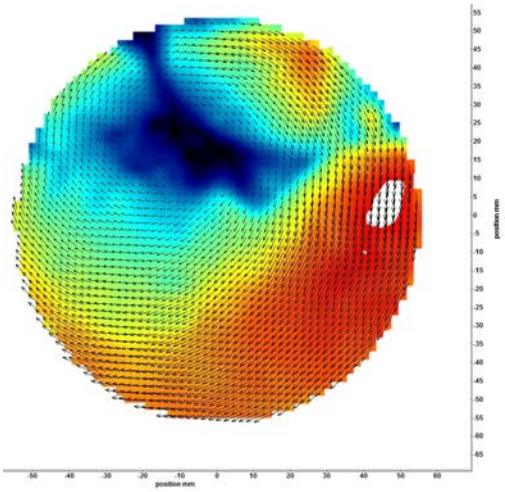

(a) DaVis

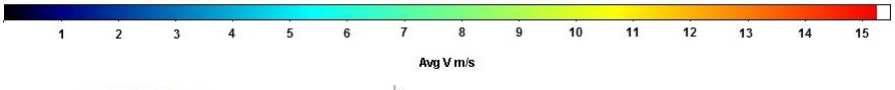

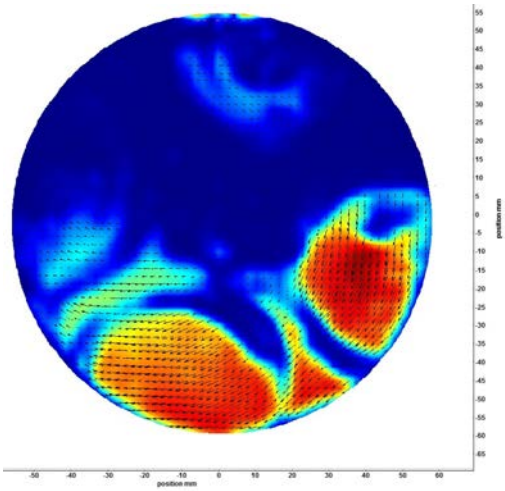

(b) PIVlab

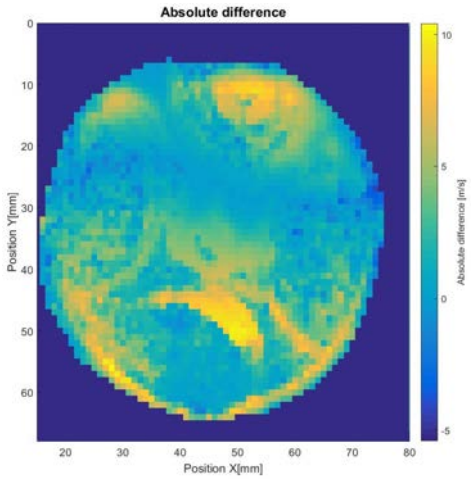

(c) Absolute difference

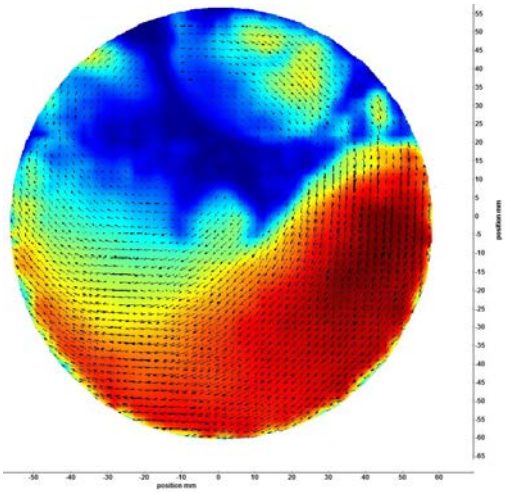

(d) PIVlab with time filter

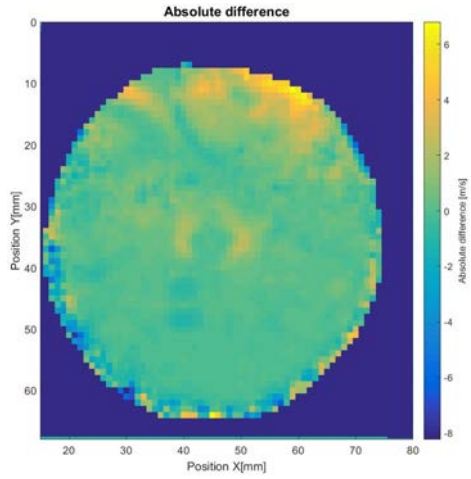

(e) Absolute difference with time filter

Figure 60: PIV results, Titanium dioxide, Vector field in the plane $z = 20mm$ at $CAD = -90°$ and $n = 600min - 1$, $\dot{m} = 210kg/h$.

8 Data processing

Material	**CAD[°]**				
	Air mass flow [kg/h]			**plane [mm]**	
	160	**210**	**260**	**10**	**20**
Lycopodium	/	Sweep [−410°/0°]	/	/	210
Titanium Dioxide	Detailed, even 5° [−410°/+26°]	Detailed, even 2° [−410°/+26°]	Sweep [−410°/0°]	210	All

Table 9: Schematic illustration points measured.

The first set of experiments has been done with lycopodium. The lycopodium has the advantage to have large diameter that makes it easily recognisable in the pictures. Pictures cluster have been captured in different crankshaft angle. Unfortunately, after some cycles, the particles started to burn, thus compromising the engine and the optical system and forcing to stop the experiment. The pictures made with lycopodium are too little and they do not cover the whole engine cycle. The reason why the lycopodium ignited it is not clear, but it is probably due to the progressive accumulation of particles in the intake system. The low ignition point of the lycopodium does not allow to use it for this test. The other available materials in the department during the test were titanium dioxide, graphite and aerosil. Since the graphite ignition temperature is about the same of the lycopodium and the experience in past experiments, it was decided to avoid to use the graphite. The aerosil was avoided too because its particle diameter is around $12nm$ and it involves difficult during the processing. Therefore, the only material available was the titanium dioxide. Titanium dioxide allows to reach around 1800°C and its particle diameter is around $0,5\mu m$.
It has been decided to analyze the flow in different engine work points 9. The mass flow rate is changed in three values: $160kg/h$, $210kg/h$ and $260kg/h$. Furthermore, it has been taken different points in the engine stroke, in particular, they have been taken with step by 2 crank angle degrees in the points of major interest as valve lifts and top dead centre and with step by 5 degrees during the compression stroke. Finally, it has been evaluated the flow in two different planes, at $20mm$ and at $10mm$ from the cylinder head. In this way, it is possible to evaluate the flow field in different operation points and assessed the particles trend. As it will be possible to see in the following chapters, the particles number and distribution, change continuously during the piston stroke. Furthermore, in the pictures, there is a blurred zone where it is difficult to distinguish the particles from the background. This effect was not debilitating with lycopodium particles because their dimension were big enough to be always discernable, but for particles with smaller diameter like titanium oxide, the problem becomes more evident. These characteristics involve difficulties in the evaluation and oblige to use an accurate pre-processing.
The piston stroke, together with the valves lift, imply a continuous variation

of particles density and velocity in the studied plane. In order to have always a good parameters setting it is necessary to change the pressure in the particle generator, the laser energy and the Δt between the frames. Another tied problem, due to the small particles diameter, is an easier formation of flow channels in the particle generator. Indeed, it has been ascertained that the number of particles added to the air flow in the case of lycopodium was almost constant. On the other hand with the titanium dioxide, the number of particles supplied to the air flow has a peak in the successive instants (after the valve opening in the particle generator) and then it decrease dramatically. This involve a non-sufficient number of particles in the combustion chamber. In order to solve this problem it has been added a system which allows to set the time and the frequency of the generator valve opening. In this way, it has been possible to solve partially the particles density problem. Indeed, the particles density, remains not constants and the pictures have a trend with large concentrations followed by a small concentrations, with the same opening and closing frequency of the generator valve. For this reason, it has been necessary to increase the pictures number for each crank angle in such a way to increase the number of pictures with good particles concentration.

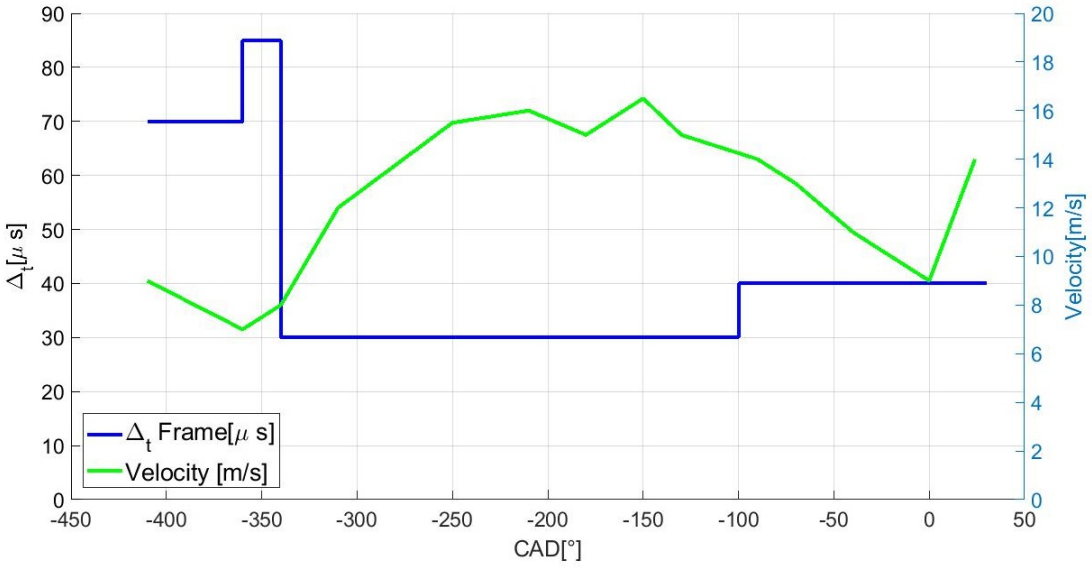

Figure 61: Δ_t variation during the cycle.

The frames timing has been chosen based on the maximum particles velocity, trying to get a maximal particle displacement of a quarter of the interrogation window size ($64x64pixels$). This means having a maximum displacement of $16pixels$. This serves to avoid to lose the slower particles contribution. Apparently, the particles velocity change is based on the piston position. Therefore, in the beginning, measurements have been done in order to understand the velocity in whole engine range. Finally, four different δt have been chosen:

- $\Delta t = 70\mu s$ in the range from $-410°$ to $-360°$.

- $\Delta t = 85\mu s$ in the range from $-360°$ to $-340°$.
- $\Delta t = 30\mu s$ in the range from $-340°$ to $-100°$.
- $\Delta t = 40\mu s$ in the range from $-100°$ to $26°$.

The timing optimization should be done for smaller crank angle range, but for practicality, it is divide only in four steps.

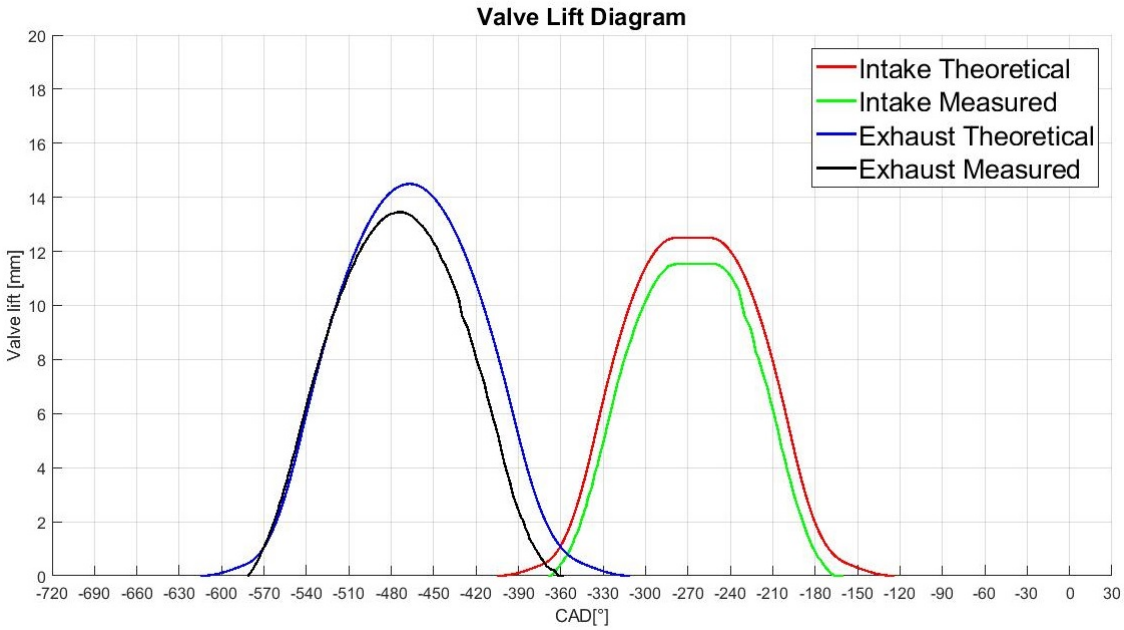

Figure 62: Valve Lift Diagram [Measured by S. Eicheldinger, S. Gleis].

It has been noted that from $CAD = -26°$ to $CAD = 26°$, or rather around the top dead centre, the pictures presents an elevate noise. It can be attributed to the fact that the piston overlaps the cylinder glass window. Indeed, this could involve reflexes due to the presence of residues between the glass and piston, and the possibility that the laser lights some particles filed in the top of the piston. Thus, the pictures in this zone are difficult to process because the particles are masked from the residues.
Background pictures have been taken for each crank angle position. In this way it is possible to subtract the background from the pictures during the pre-processing in order to reduce the environment effects. Unfortunately, it has been seen that this approach has not the expected aftermath, or rather there is not an effective results improvement. Instead, a good result improvement comes from using the DaVis filter "subtract time filter". With this tool it is possible to choose three different type of subtraction: minimum average, normal average and Gaussian average. It is recommended to use the normal average because it leads to good results.
During the entire testing time, the pictures have been analyzed in real time by DaVis in order to adjust the record setting.
The particularity of the background (the cylinder head) leads to problems during the processing indeed, valves seats, shadows, injector and construction details, make that the particles are not uniformly visible. To work around this

problem, background pictures have been taken for each CAD in order to subtract the background from the flow pictures. The necessity to take the background for each CAD drifts from the fact that the dimension of the analyzed window is dependent directly from the piston position. Indeed, the optical

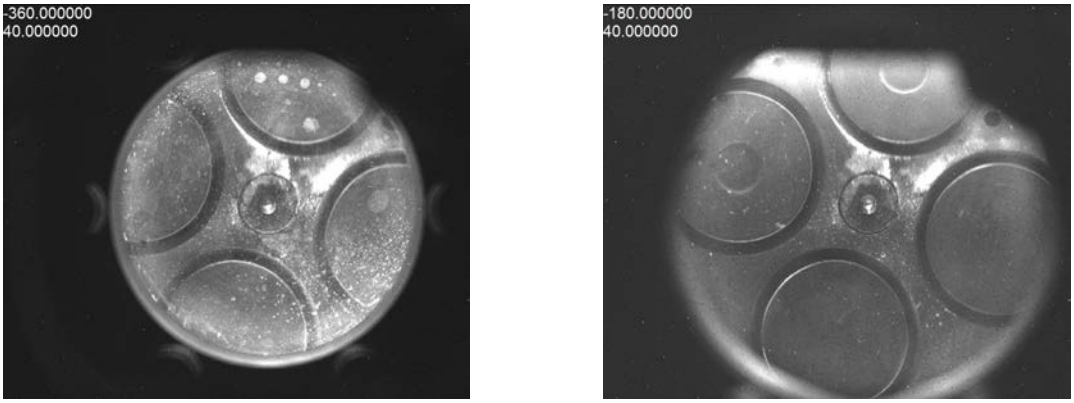

Figure 63: Different background dimension. On the right TDC; On the left BDC.

access in the piston is defined and constant while its position is based on the crank angle. Thus, when the piston is on the bottom dead centre (therefore the piston is near the mirror), the optical cone allows to see a large part of the cylinder head. Instead, in the case when the piston is on the top dead centre, the optical cone will be reduced at the limit that it is possible to see only the surface equal to the dimension of the optical access in the piston. This involves a continuous variation of the background dimension.
The smaller is the particle dimension, the more is difficult to detect it. Unfortunately, in the case of titanium dioxide, the background subtraction from the pictures hasn't improved the results neither in DaVis nor in PIVlab. To solve partially this problem it is useful to use the DaVis function "subtract time filter" that allows to remove the constant pictures parts in the whole dataset.

8.1 Flow evolution in the compression stroke

In this section it has been analyzed the whole compression cycle with titanium dioxide as tracer, with mass flow rate of $210kg/h$ and at $20mm$ from the cylinder head. With this flow condition, the pressure in the seeding generator has been leaved constant at $5bar$ because the particles density was satisfying for all the measurements.
The referent points have been taken with step of $2°$, from $-410°$ to $26°$. With reference at Figure 61, the data have been analyzed. Starting from $-410°$, the most interesting points are shown.
At $-410°$ Figure64(a) the exhaust valves are closing while the intake valves are still closed. In this position, the cycle is in the exhaust stroke then the piston is moving upward. In this cycle part, the flow preserves a swirl motion coming from the compression stroke. The maximal velocity is around $10m/s$ and it is possible to observe a residual swirl motion with center under the exhaust valves zone. The velocity field is decentralized and divided in two parts, once at high velocity while the other one at low velocity, that suggests the presence of a tumble motion. This movement is appreciable until $-388°$ when almost

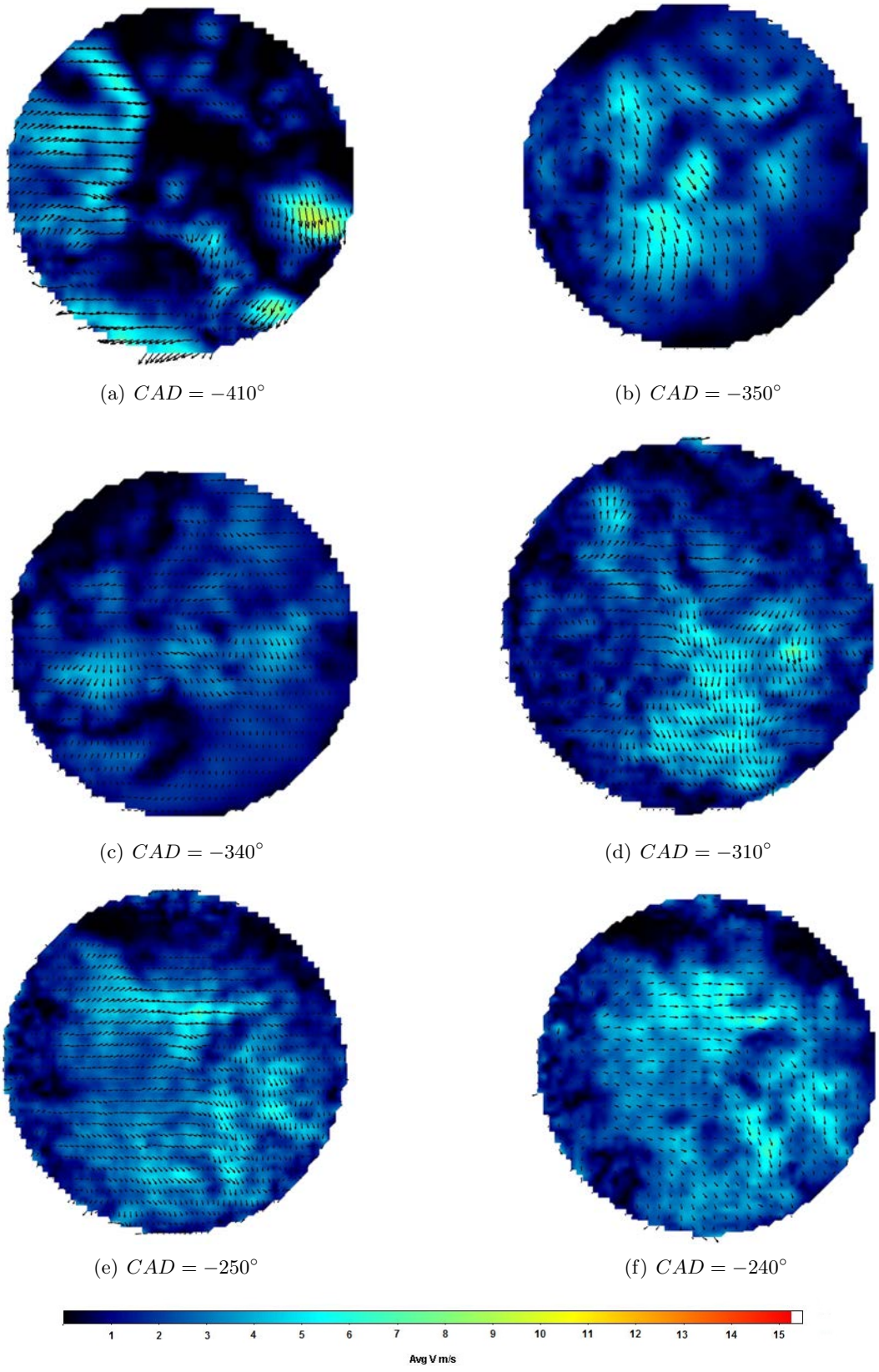

(a) $CAD = -410°$

(b) $CAD = -350°$

(c) $CAD = -340°$

(d) $CAD = -310°$

(e) $CAD = -250°$

(f) $CAD = -240°$

Figure 64: Instantaneous Velocity, Titanium dioxide, plane $z = 20mm$ at $n = 600min - 1$, $\dot{m} = 210kg/h$ from $CAD = -410°$ to $CAD = -240°$.

all flow is going out. In fact, in this phase, there are only few particles inside the chamber and they are gradually decreasing until when the intake valves are sufficiently open to bring new charge. The poorest flow is around $-350°$ Figure64(b), or just after the top dead centre, and the flow velocity reaches $6m/s$. In this phase, all the valves should be still opened in such a way that the gas inertia pushes the flow to exit. When the piston starts to go down again, the flow changes progressively its direction and new charge comes from intake valves. The flow has a disordered phase in which the motion does not have a principal direction. Around $-340°$ Figure64(c), the flow coming from the intake valves is direct towards the exhaust valves. This trend, initially confused, becomes ordered around $-310°$ Figure64(d) when the exhaust valves are definitively closed and it is possible to observe a velocity increments until $7m/s$. The flow maintains this trend until about $-296°$ when swirl motion starts to form in clockwise. The fresh charge keeps entering and the swirl motion is always more defined. At around $-240°$ Figure64(f), the zero velocity centre starts to form and it is positioned near the cylinder side, in the bottom left. At $-210°$, the swirl is completely formed and the velocity poses a large increments with a peak around $16m/s$ (maximal velocity measured in whole cycle). From $-210°$ Figure65(a) to $-130°$ Figure65(d), or rather when the intake valves are closing, it is possible to observe the swirl centre moves upwards and the velocity is holding steady around $13m/s$. At $-180°$ Figure65(b) the piston reaches the bottom dead centre (BDC) and the combustion chamber volume reaches its maximum value. In this crank angle, the particle density, in the flow, reaches the lowest value. Indeed, it is possible to see that there is a big area with no results in Figure Figure65(b). This means that, it was necessary to increase the seeding generator pressure to evaluate the bottom dead center and and nearby points, this problem will be studied later. At $-90°$, Figure66(a), the piston reaches its maximum linear velocity, but the flow velocity is lower in relation to the earlier stages ($12m/s$). At around $-70°$ Figure66(b), the centre motion starts to decrease again as well as the velocity. At $-40°$ Figure66(c), the center swirl motion heads to the cylinder center and it is possible to observe a perfect swirl motion with a symmetrical trend and with mean value around $11m/s$. At $-20°$ Figure66(d) until $24°$ Figure66(f)the velocity continues to fall until $7m/s$.

The results in Figure64, 65, 66 are an average of 50 pictures for each crank angle. It is possible to see that in some cases as Figure64(a), 65(b), 65(c), 65(d) there is the background influence. Regarding Figure64(a), the background effect can be accounted for the decrease of particles numbers, due to the fact that the combustion chamber is almost empty. For cases as Figure65(b), 65(c), 65(d), the low results quality can be imputed at the chamber volume that it is at its maximum value and this involve a low particles density in the air bulk. The background effect is always positioned under an intake valve zone. Analyzing the pictures it is possible to understand the problem Figure67.

As it is possible to see, there is a blurred area in all the pictures. This effect has affected the whole results because it does not allow to identify some particles. In order to solve this problem, the mirror has been changed and the camera filters have been cleared but there's been no improvement. As it is possible to see in the Figure69, 70, 71, this problems become more relevant for

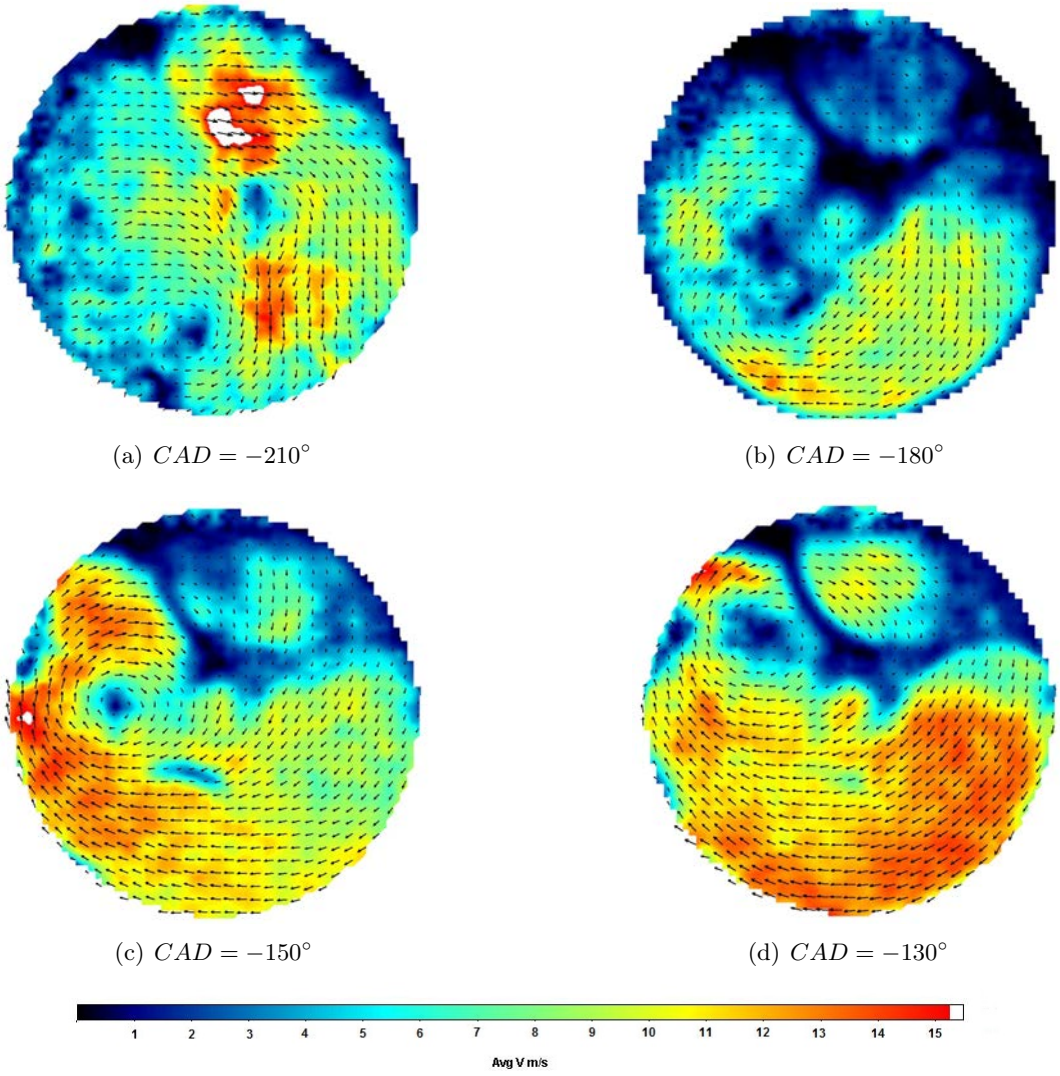

(a) $CAD = -210°$

(b) $CAD = -180°$

(c) $CAD = -150°$

(d) $CAD = -130°$

Figure 65: Instantaneous Velocity, Titanium dioxide, plane $z = 20mm$ at $n = 600min - 1$, $\dot{m} = 210kg/h$ from $CAD = -210°$ to $CAD = -130°$.

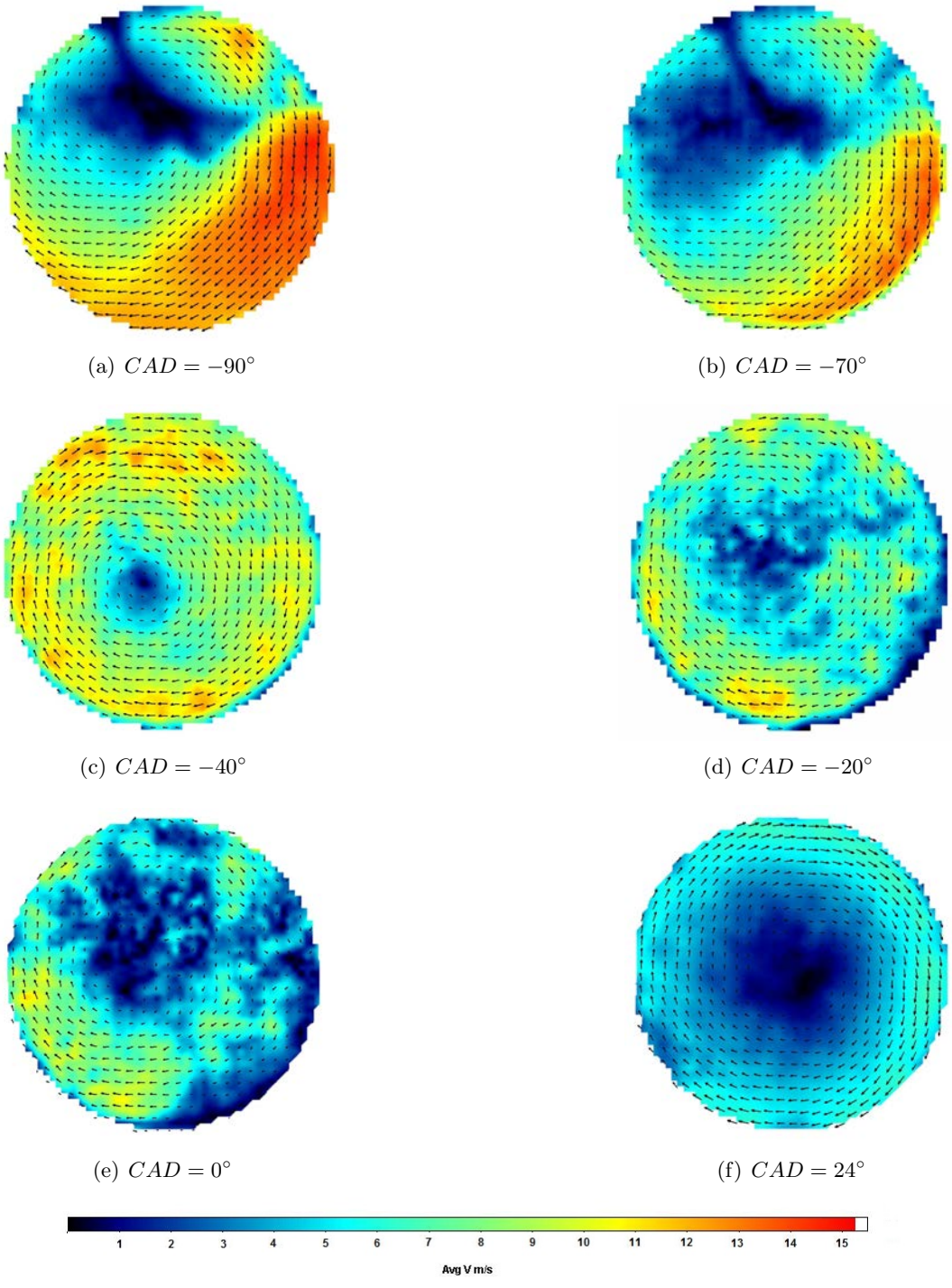

(a) $CAD = -90°$

(b) $CAD = -70°$

(c) $CAD = -40°$

(d) $CAD = -20°$

(e) $CAD = 0°$

(f) $CAD = 24°$

Figure 66: Instantaneous Velocity, Titanium dioxide, plane $z = 20mm$ at $n = 600min - 1$, $\dot{m} = 210kg/h$ from $CAD = -90°$ to $CAD = 24°$.

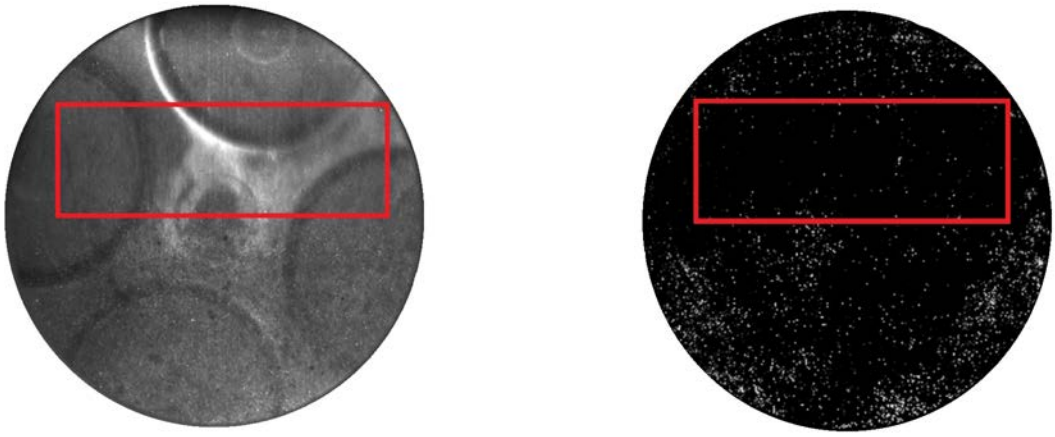

(a) Without time subtraction

(b) With time subtraction

Figure 67: Shadow: Titanium dioxide, plane $z = 20mm$ at $n = 600min - 1$, $\dot{m} = 210kg/h$ $CAD = -30°$.

the others two mass flow rate values. On the other hand, to solve the problem at $CAD = -180°$, it is necessary to increase the particles density adjusting the seeding generator pressure.
It is now analyzed the mean velocity during the compression stroke. This parameter is calculated taking into consideration the result average (whole circle) for different CAD. The evaluation is focused in the range from $-210°$ to $0°$, Figure68. With reference at Figure62, the mean velocity trend is analyzed. The mean velocity, during the cycle, reaches its lowest value at $-180°$ of $5m/s$ concomitantly with intake valve closing. After this point the velocity increases and at $-100°$, it reaches the maximum value of $9,2m/s$. From $-100°$ to $-60°$ it is possible to see a gradual decrease due to the swirl motion development. Thereafter, it returns to grow until $-40°$ in which it is possible to see a perfect swirl motion Figure66(c). Finally, it decreased definitely to the top dead center. Since background effect, mentioned in the Figure67, could affect the mean velocity value, due to the fact that big areas are useless. It has been decided to try to calculate the mean velocity only in area where there are good results. Despite this expedient, the result trend does not change underpinning the fact that the trend shown in Figure68 can be accepted as valid.

8.2 Flow behavior for different intake pressure

In order to analyze the effects of different parameters, which could affect the combustion chamber flow, three different mass flow rate have been analyzed ($160kg/h$, $210kg/h$ and $260kg/h$). In the engine it is possible to change the supply pressure, simulating the turbocharger effects and, in so doing, the mass flow rate is varied. Moving away from the initial value of $\dot{m} = 210kg/h$, the particles density problem has become more evident, indeed, it has been noted a big density fluctuation between the first picture, just after seeding generator aperture, and the pictures obtained after some cycles after opening thereof. In order to solve this problem, a clocked function has been added to the generator valve controller. This function allows to set the valve aperture frequency and its

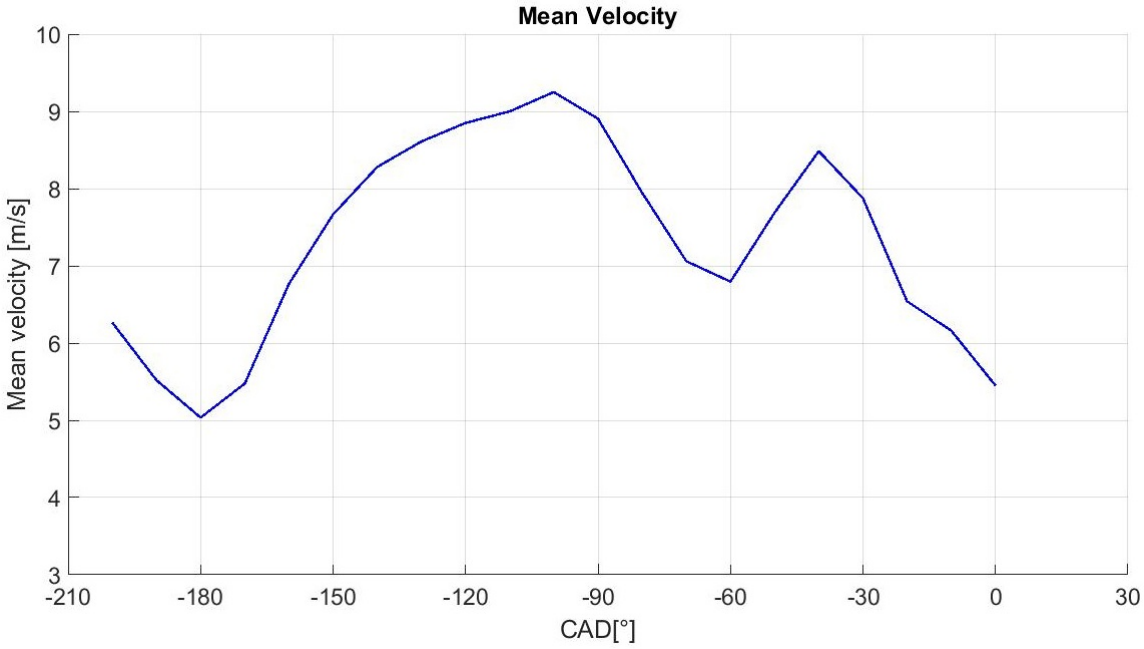

Figure 68: Mean Velocity: Titanium dioxide, plane $z = 20mm$ at $n = 600min - 1$, $\dot{m} = 210kg/h$.

work time. Properly applied, the clocked function allows to get better pictures because, opening and closing the generator, the created channels (in the tracer container) closing, thus enabling to achieve good mixture and homogeneity of incorporation between air and particles. Furthermore, a bigger pictures number have been taken to have a large number of significant pictures. These precautions have increase the results quality, but not enough to be compared with the cases with $\dot{m} = 210kg/h$. Trying to increase the particles generator pressure, it has been got opposite effect, indeed, initially there is an excessive growth in particles density and then a decrease sharply, reaching insufficient values.
The Figure69, 70, 71, 72, display the different velocity development for each mass flow rate. At $CAD = -410°$ it is possible to observe that during the exhaust stroke for Figure69(a) the velocity is fastest ($13m/s$) than Figure69(b), 69(c) (10m/s), probably due to the bigger air bulk remained in the chamber. In this phase, the background influence largely all cases in particular for $\dot{m} = 210kg/h$ in which it is not possible to understand the real flow motion. For $CAD = -350°$ and $CAD = -340°$, the flow behavior is the same for all the cases. At $CAD = -310°$, it is possible to observe that the result for Figure69(j) is entirely without meaning. This is caused by an insufficient number of pictures taken for this point. This problem remains until $CAD = -210°$ Figure70(g) while, for the others two cases, there is not background effect Figure69(k), 69(l). From $CAD = -310°$ to $CAD = -240°$, the flow with $\dot{m} = 210kg/h$ Figure70(k), 70(b), 70(e) and $\dot{m} = 160kg/h$ Figure69(l), 70(c), 70(f) has the same behaviors and for $\dot{m} = 160kg/h$ cases, it continues to maintain a velocity greater than $\dot{m} = 210kg/h$ of around $2m/s$. At $CAD = -210°$, the $\dot{m} = 210kg/h$ (Figure70(h)) condition, presents a sharp velocity increase ($16m/s$),

but this velocity increase there is not in the others two cases Figure70(g), 70(i). This suggests that the results with $\dot{m} = 160kg/h$ and $\dot{m} = 260kg/h$ are not reliable and more experiments are necessaries in order to get more pictures. The velocity trend for the subsequent points confirms the precedent theory, in fact from $CAD = -180°$ to $CAD = 0°$, all the tests have the same behaviour both for velocity intensity and for flow trend. At $CAD = -180°$, the background effect is always present for all the cases Figure70(j), 70(k), 70(l) and it remains constants until $CAD = -130°$ Figure71(d), 71(e), 71(f). This confirms the necessity to adjust the particles density when the chamber volume reaches its maximum value.

The initial analysis suggests that the flow behavior remains constant regardless the mass flow rate. To check it, it has been studied the different mean velocities for the three mass flow rate values. In Figure73 are shown the results.

The three mean velocities follow the same description given previously for the Figure68. It is possible to see that the mean velocity with $\dot{m} = 210kg/h$ remains the highest until $-60°$ while the velocity trend with $\dot{m} = 260kg/h$ and $\dot{m} = 160kg/h$ have a similar trend. This effects may be attribute at the different results quality between the tests as a matter of fact that the mean velocity is calculated for the whole result picture, also covering the black areas where there are not results (due to the background and at the effects mentioned in Figure67). Hence, poor results quality lead to a mean velocity reduction. Like it did before, it has been applied a window in the lower picture part where the result quality is better. With this new check Figure74, it is evident that result quality is responsible of the difference mean velocity value between different $\dot{m}$ values. It can be concluded that the mass flow rate (and therefore the boost pressure) has no influence on the structure and on the average velocity of the in-cylinder flow.

8.3 Flow behavior for different cylinder heights

To evaluate the flow behavior for different heights, two sections have been analyzed. Changing the laser height, in the cylinder, it is possible to evaluate different section thereof. Indeed, the laser beam position determines the analysis section. The setting operations to change the laser beam height are easy since, it is sufficient to change the height of the divergent (chapter 4.2.2), collimator optics (chapter 4.2.2) and the last mirror. To measure the effective laser position in the cylinder, a calibrated tool, provide with a magnet, is attached in the cylinder head. Two different plane have been evaluated: at $20mm$ and at $10mm$ from the cylinder head 75. For a complete cylinder overview should be necessary to evaluate the flow in a greater number of planes, along the entire cylinder, in such a way as to understand completely the flow trend. The figure Figure77,78,79,80,81 display the flow trend in the two different planes. Starting from $CAD = -410°$, it is possible to see some differences in the velocity behaviour between the two planes. From $CAD = -410°$ to $CAD = -310°$, the pictures are always better for the plane at $10mm$ Figure77(a) than the other plane Figure77(b), probably due to the increased presence of particles that are going outside during the exhaust stroke and enter during the intake stroke, in the plane nearest the valves. Still for this reason, the velocity in the plane at

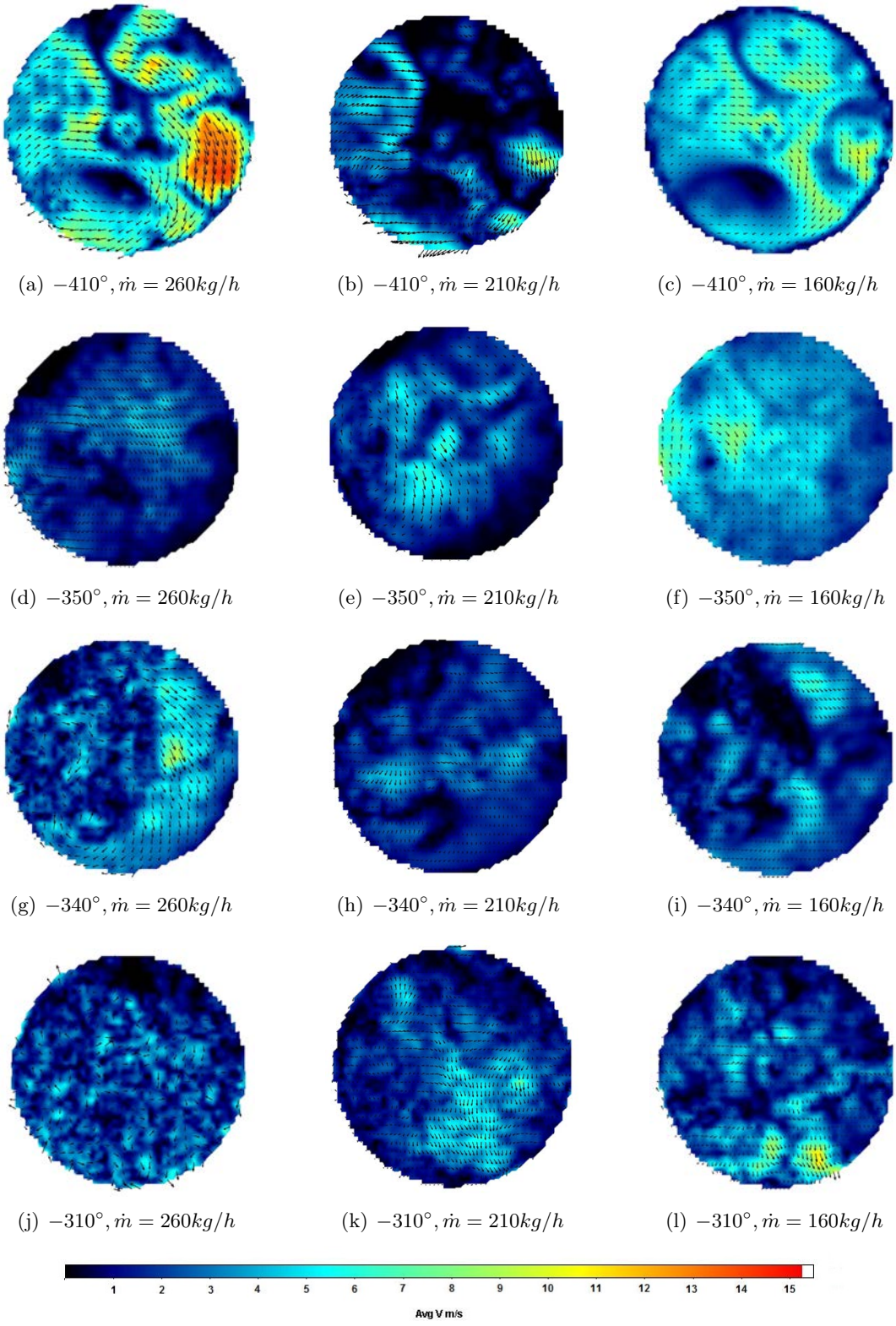

(a) $-410°, \dot{m} = 260kg/h$ (b) $-410°, \dot{m} = 210kg/h$ (c) $-410°, \dot{m} = 160kg/h$

(d) $-350°, \dot{m} = 260kg/h$ (e) $-350°, \dot{m} = 210kg/h$ (f) $-350°, \dot{m} = 160kg/h$

(g) $-340°, \dot{m} = 260kg/h$ (h) $-340°, \dot{m} = 210kg/h$ (i) $-340°, \dot{m} = 160kg/h$

(j) $-310°, \dot{m} = 260kg/h$ (k) $-310°, \dot{m} = 210kg/h$ (l) $-310°, \dot{m} = 160kg/h$

Figure 69: Instantaneous Velocity comparison, Titanium dioxide, plane $z = 20mm$ at $n = 600min - 1$, from to $CAD = -410°$ to $CAD = -310°$.

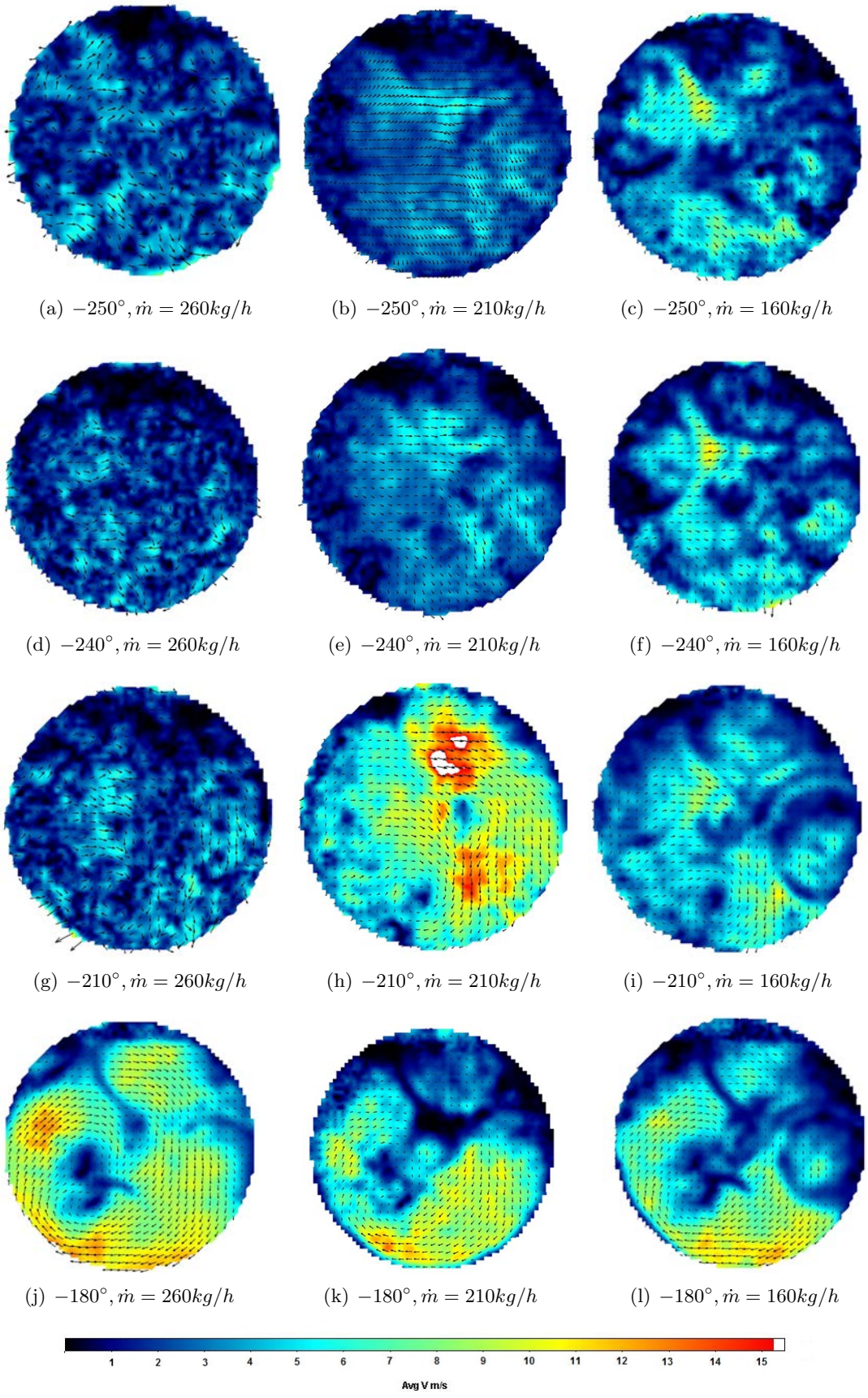

(a) $-250°, \dot{m} = 260kg/h$ (b) $-250°, \dot{m} = 210kg/h$ (c) $-250°, \dot{m} = 160kg/h$

(d) $-240°, \dot{m} = 260kg/h$ (e) $-240°, \dot{m} = 210kg/h$ (f) $-240°, \dot{m} = 160kg/h$

(g) $-210°, \dot{m} = 260kg/h$ (h) $-210°, \dot{m} = 210kg/h$ (i) $-210°, \dot{m} = 160kg/h$

(j) $-180°, \dot{m} = 260kg/h$ (k) $-180°, \dot{m} = 210kg/h$ (l) $-180°, \dot{m} = 160kg/h$

Figure 70: Instantaneous Velocity comparison, Titanium dioxide, plane $z = 20mm$ at $n = 600min - 1$, from to $CAD = -250°$ to $CAD = -180°$.

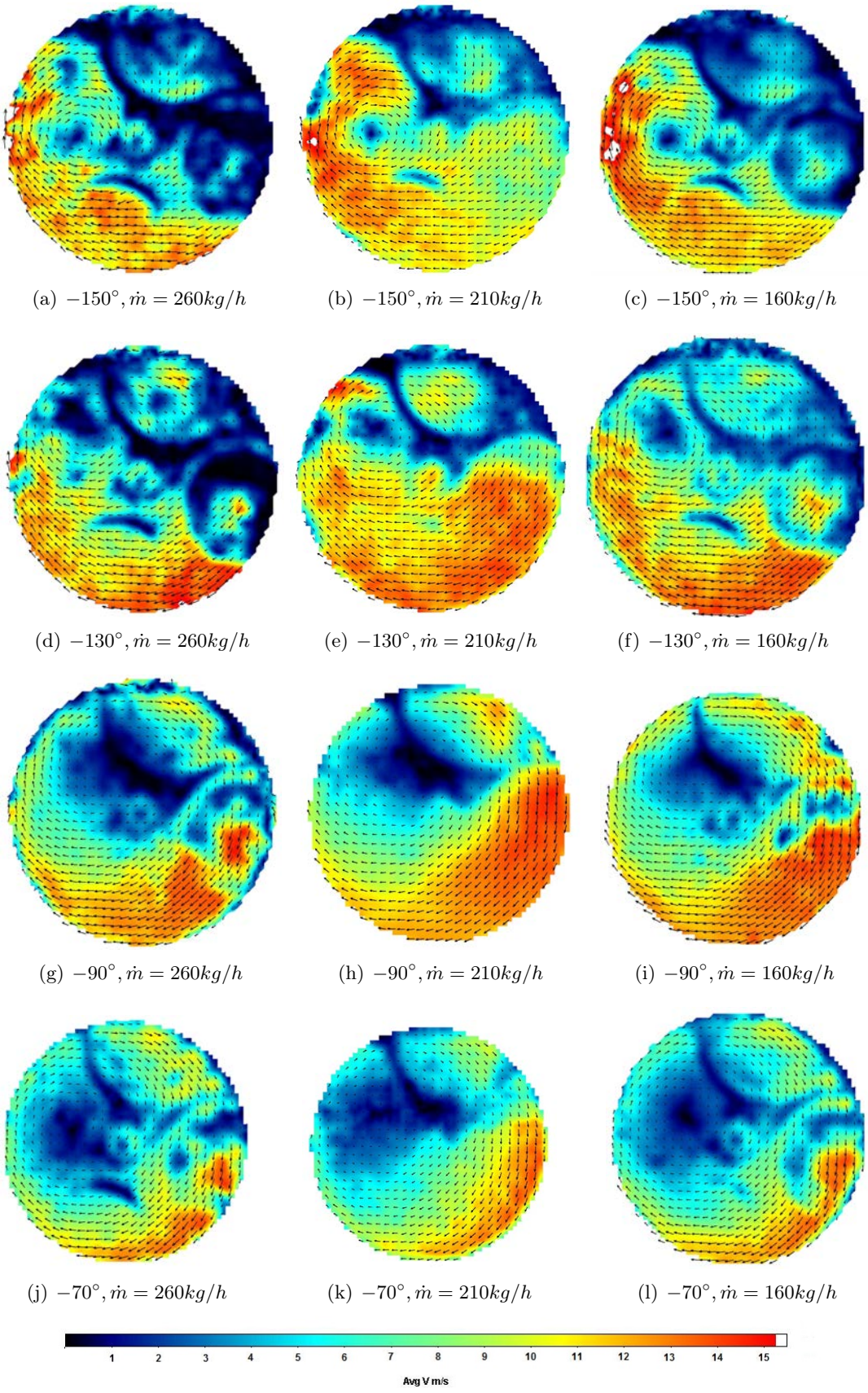

(a) $-150°, \dot{m} = 260kg/h$ (b) $-150°, \dot{m} = 210kg/h$ (c) $-150°, \dot{m} = 160kg/h$

(d) $-130°, \dot{m} = 260kg/h$ (e) $-130°, \dot{m} = 210kg/h$ (f) $-130°, \dot{m} = 160kg/h$

(g) $-90°, \dot{m} = 260kg/h$ (h) $-90°, \dot{m} = 210kg/h$ (i) $-90°, \dot{m} = 160kg/h$

(j) $-70°, \dot{m} = 260kg/h$ (k) $-70°, \dot{m} = 210kg/h$ (l) $-70°, \dot{m} = 160kg/h$

Figure 71: Instantaneous Velocity comparison, Titanium dioxide, plane $z = 20mm$ at $n = 600min - 1$, from to $CAD = -150°$ to $CAD = -70°$.

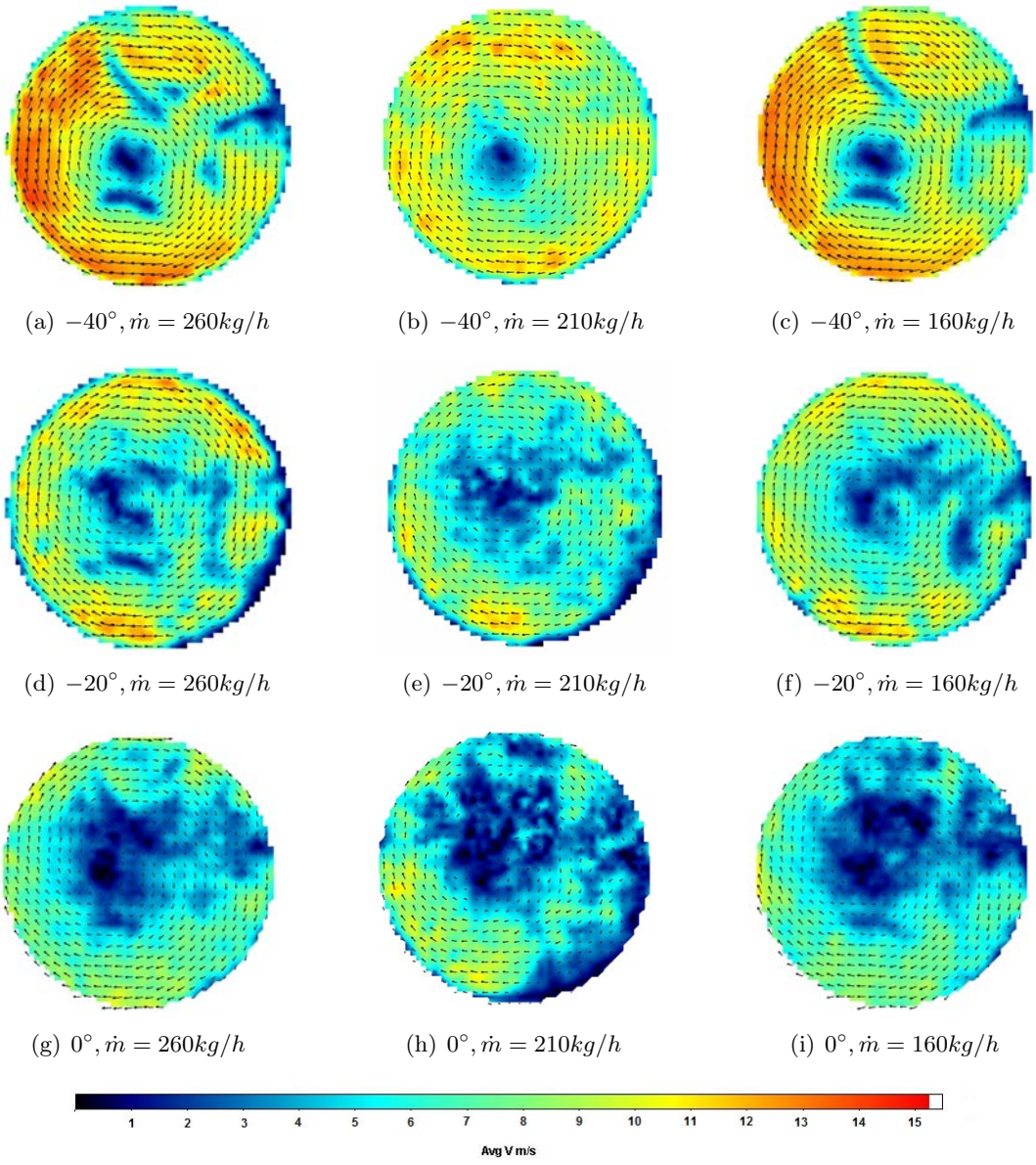

(a) $-40°, \dot{m} = 260kg/h$ (b) $-40°, \dot{m} = 210kg/h$ (c) $-40°, \dot{m} = 160kg/h$

(d) $-20°, \dot{m} = 260kg/h$ (e) $-20°, \dot{m} = 210kg/h$ (f) $-20°, \dot{m} = 160kg/h$

(g) $0°, \dot{m} = 260kg/h$ (h) $0°, \dot{m} = 210kg/h$ (i) $0°, \dot{m} = 160kg/h$

Figure 72: Instantaneous Velocity comparison, Titanium dioxide, plane $z = 20mm$ at $n = 600min - 1$, from to $CAD = -40°$ to $CAD = 0°$.

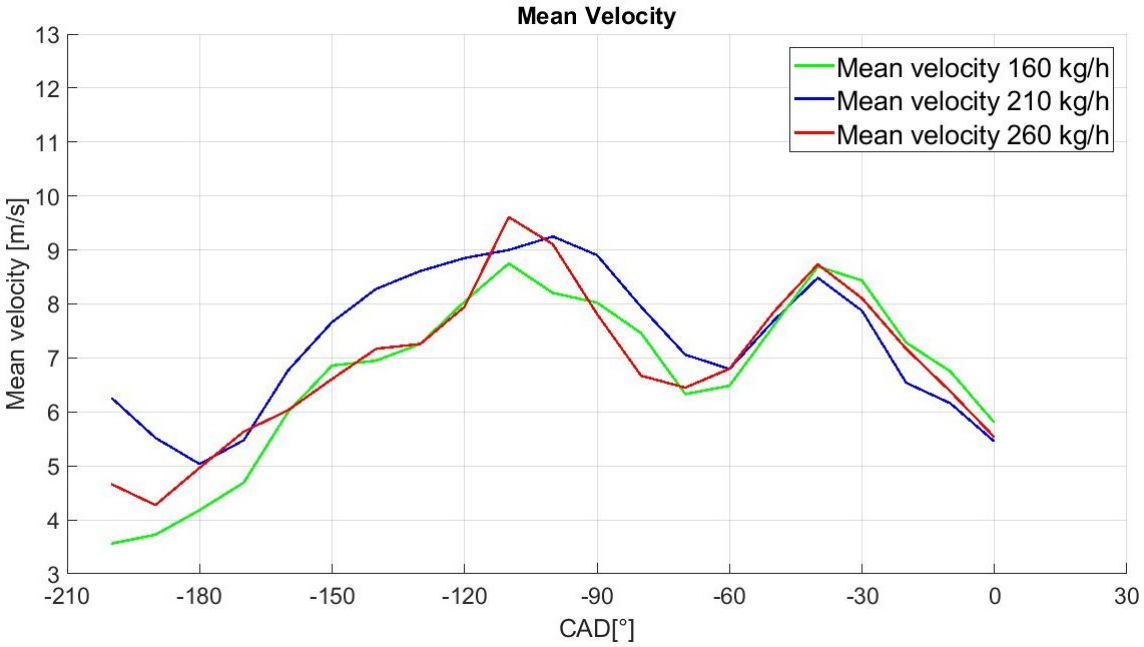

Figure 73: Mean Velocity different mass flow rate for the whole circle.

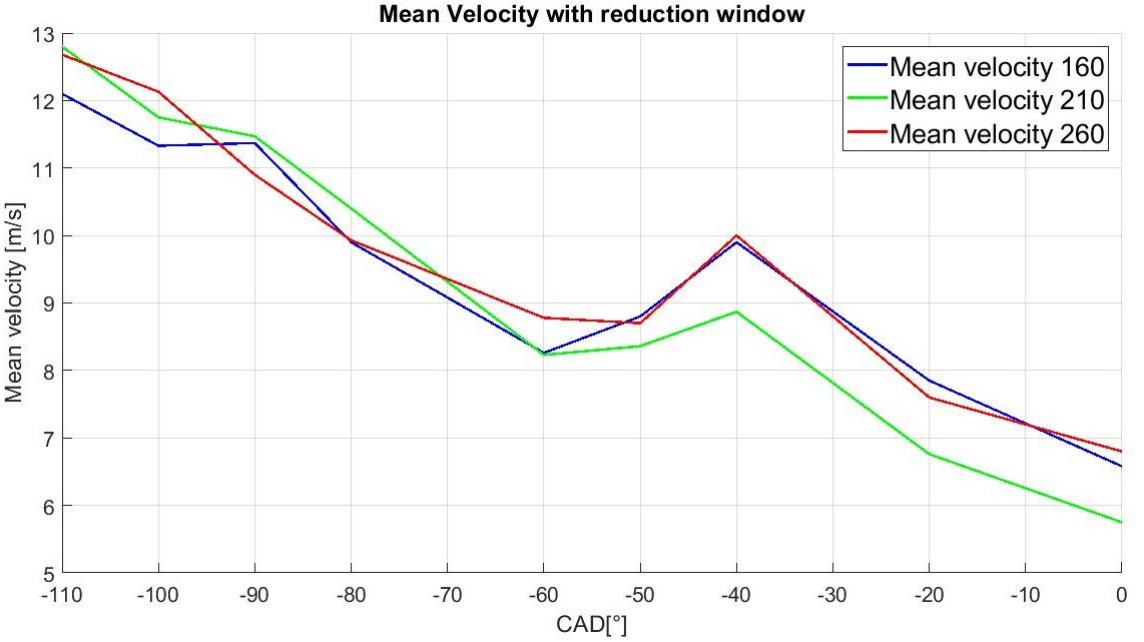

Figure 74: Mean Velocity different mass flow rate without blurred area.

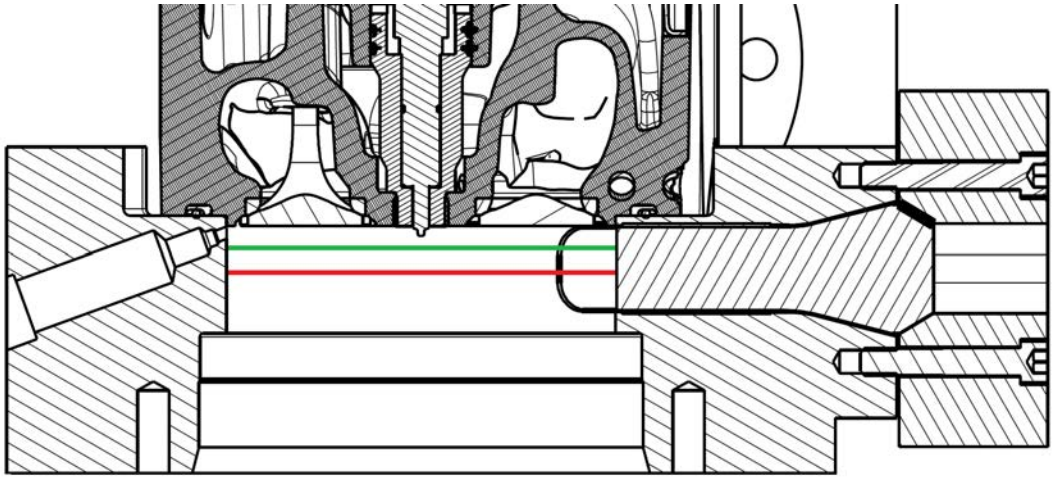

Figure 75: Plane representation: Green plane $10mm$, red plane $20mm$.

$10mm$ has a higher velocity starting from $CAD = -410°$ to $CAD = -250°$ Figure78(c),78(d). After $CAD = -250°$ the velocity in the two planes becoming the same. At $CAD = -240°$, a swirl motion starts to form in the plane at $20mm$ Figure78(f), while for the plane at $10mm$ the flow, directed to the exhaust valves, persists Figure78(e). This fact suggest that the swirl motion starts to form from the bottom up. The swirl motion, in the plane at $10mm$, starts around $CAD = -210°$ Figure79(a), but at the same moment in the plane at $20mm$, the swirl motion is already fully develop with the consequence that the velocity is growing Figure79(b). The consequence is that in this CAD, there is a big maximum velocity difference: $10,5m/s$ at $10mm$ and $16m/s$ at $20mm$. After this point, the velocity trend is starting to become similar in the two planes. Here again, it is possible to noted the background effect for the plane at $10mm$ also Figure79(c). However, the background effects is less pronounced for the plane at $10mm$, probably due to the higher density as result of a tumble motion. The velocity remains similar until $CAD = -70°$ Figure80(e), 80(f), after that, it is higher for the plane at $10mm$ (Figure81(a), 81(b)). When the piston is reaching the top dead center, it comes into contact with the laser beam and this create an optical effect. This effect starts at $CAD = -26°$ for the plane at $20mm$ while at $CAD = -22°$ for the plane at $10mm$. In Figure76 are shown two pictures before and then the piston interference.

The optical effect, comes from the piston, is worst for the pictures in the plane at $10mm$ with the consequence that the results are not good around the top dead center. The effect is visible in result Figure81(c).

In Figure82 is shown the mean velocity trend in the two planes. Until $CAD = -160°$, in the plane at $10mm$, the mean velocity remains slower that in the plane at $20mm$. As mentioned before, it is because the swirl motion starts to form from the bottom up and therefore the velocity in the highest plane reaches high values with a lag. Then from $CAD = -160°$ to $CAD = -20°$, the velocities trend remain similar to each other. After $CAD = -20°$, the optical effect, due to the piston, makes a sharp reduction in the plane at $10mm$ plane while it is milder in the plane at $20mm$. This suggest that actually the mean velocity, calculated in the plane at $10mm$, is not the real mean velocity in the

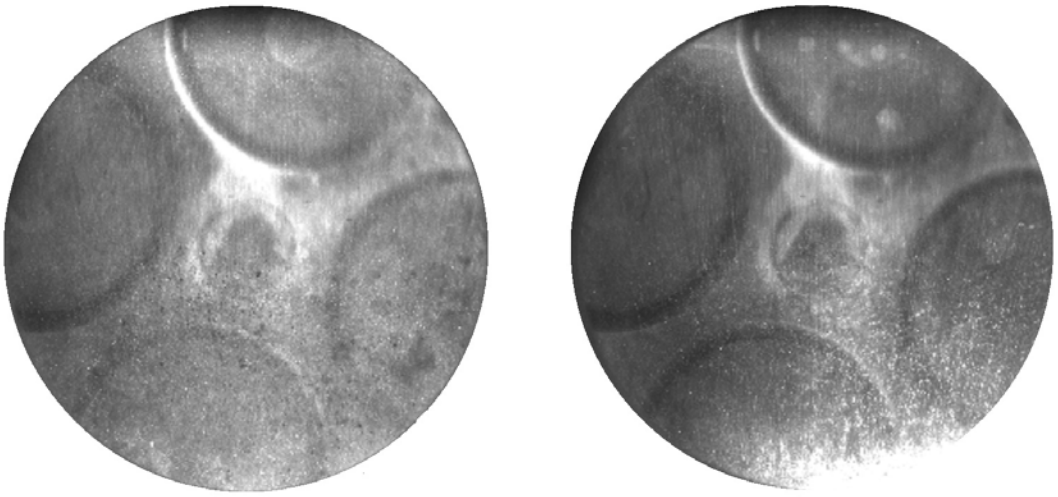

(a) $CAD = -30°$ (b) $CAD = -26°$

Figure 76: Optical interference due to the piston: Titanium dioxide, at $n = 600min-1$, $\dot{m} = 210kg/h$, plane $20mm$.

cylinder.

8.4 Materials behaviour

The lycopodium has been used two times during this work. In the first engine test was necessary stop the engine because the cylinder glass was damaged and it didn't ensure the pressure seal. During the second engine test, lycopodium was used in order to calibrate the operating parameters, in which few pictures have been taken for little CAD only. After the setup period, lycopodium became unusable due to its accumulation in the intake system that provoked a flame propagation. The ignition occurs when in the combustion chamber is reached high temperature, or rather when the piston reaches the top dead center Figure83. Unfortunately, the data got during the calibration were not enough to elaborate good results an compare them with titanium dioxide results.
Considering the pictures taken in the first part of the experiment (with lycopodium), it is possible to see the difference respects titanium oxide 84. The small particle diameter of the titanium oxide (0,2-0,5 [μm]), compared with that of the lycopodium (28 [μm]), leads problems with the light reflection and with the background. Considering its instability, lycopodium can not be used for diesel cycle because of the temperature reached.
Time problem hasn't allowed to use other materials to evaluate the dissimilarity between them.

8.5 Swirl center motion

The position of the swirl motion center is an important parameter to take into account. It can help to understand the flow field asymmetry and thus the asymmetric mixture preparation. During the compression stroke, the swirl centre changes continuously due to the intake system geometry and to the piston

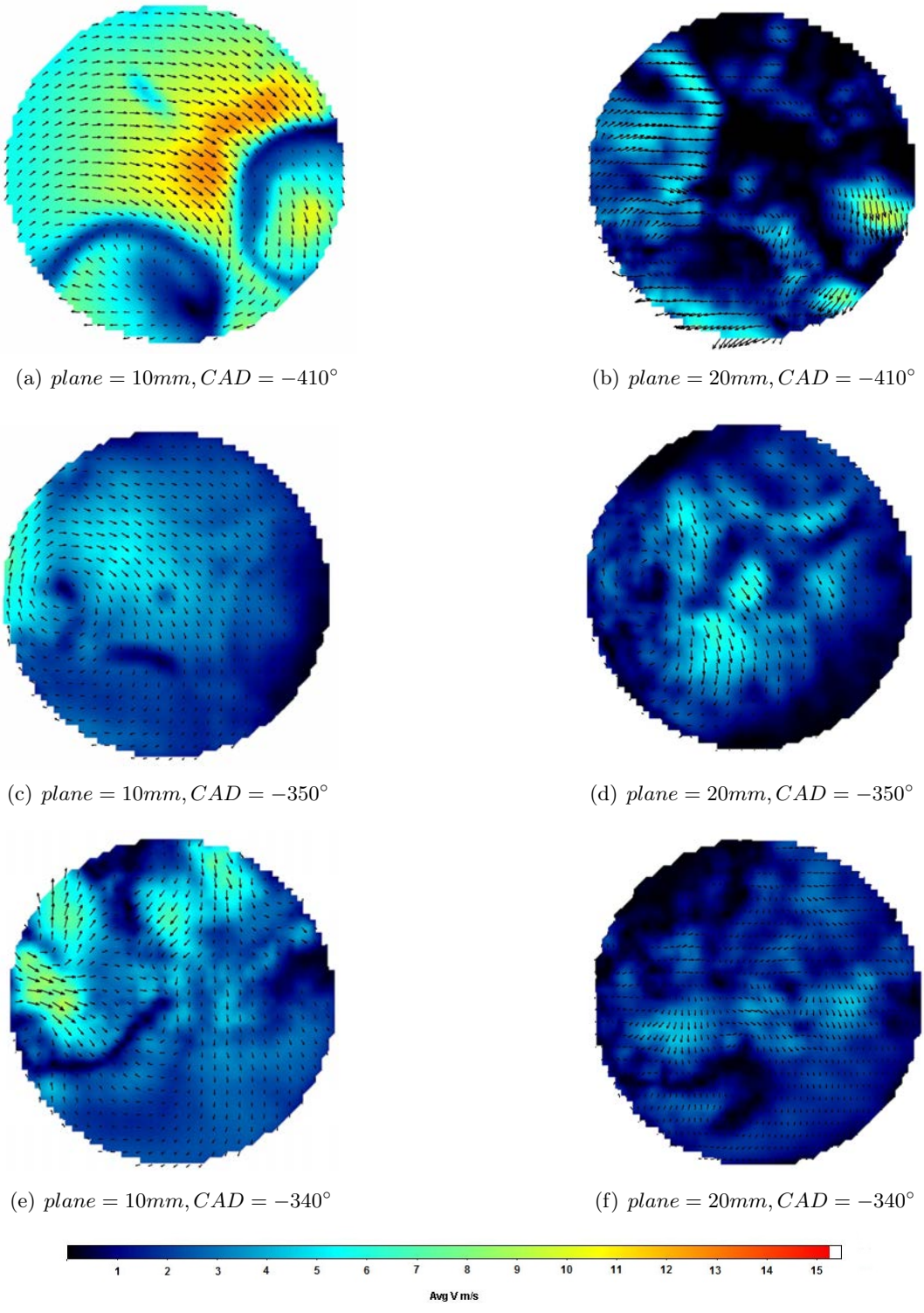

(a) $plane = 10mm, CAD = -410°$

(b) $plane = 20mm, CAD = -410°$

(c) $plane = 10mm, CAD = -350°$

(d) $plane = 20mm, CAD = -350°$

(e) $plane = 10mm, CAD = -340°$

(f) $plane = 20mm, CAD = -340°$

Figure 77: Instantaneous Velocity comparison in different planes, Titanium dioxide, at $n = 600min - 1$, $\dot{m} = 210kg/h$ from $CAD = -410°$ to $CAD = -340°$.

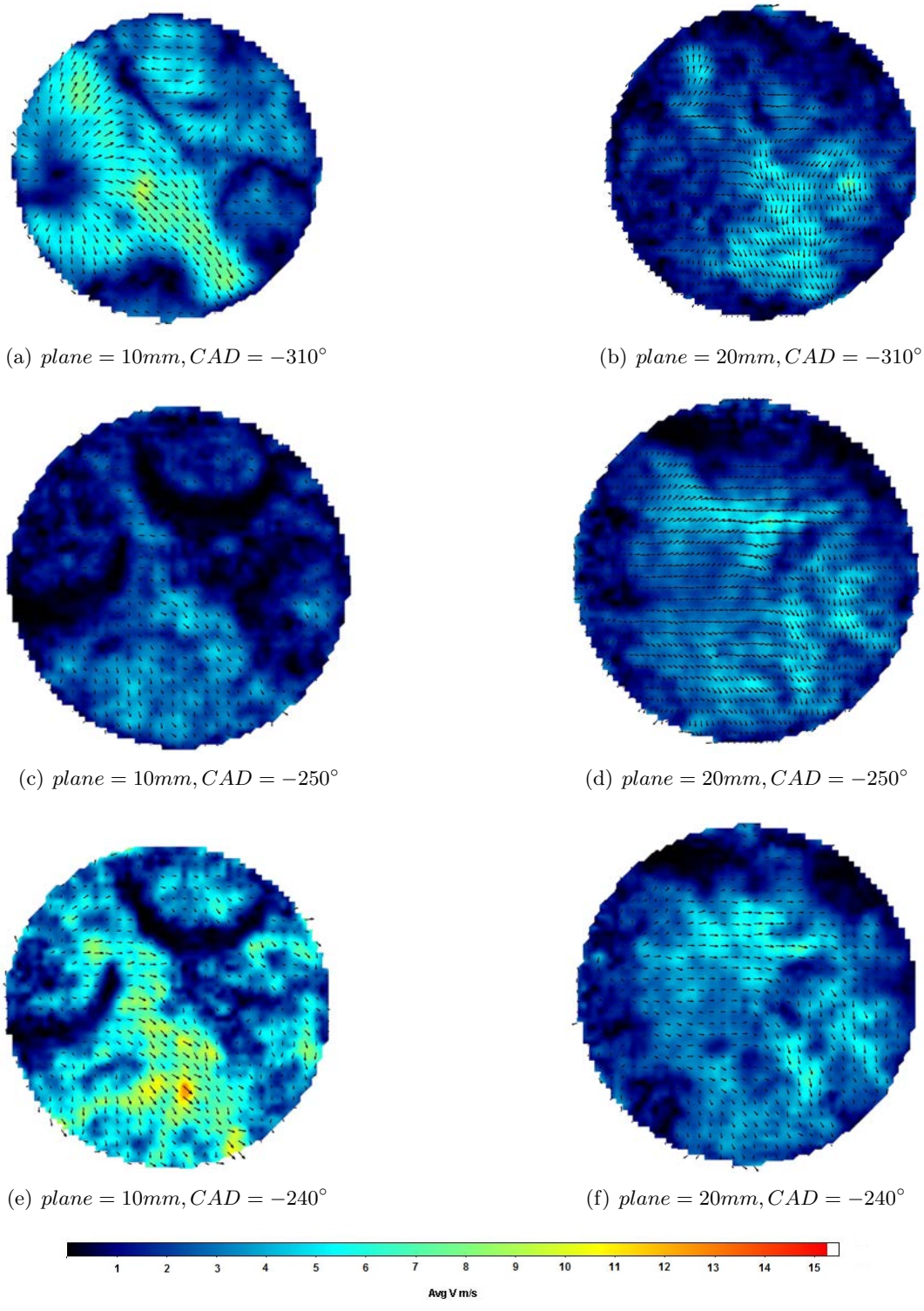

(a) $plane = 10mm, CAD = -310°$

(b) $plane = 20mm, CAD = -310°$

(c) $plane = 10mm, CAD = -250°$

(d) $plane = 20mm, CAD = -250°$

(e) $plane = 10mm, CAD = -240°$

(f) $plane = 20mm, CAD = -240°$

Figure 78: Instantaneous Velocity comparison in different planes, Titanium dioxide, at $n = 600min - 1$, $\dot{m} = 210kg/h$ from $CAD = -310°$ to $CAD = -240°$.

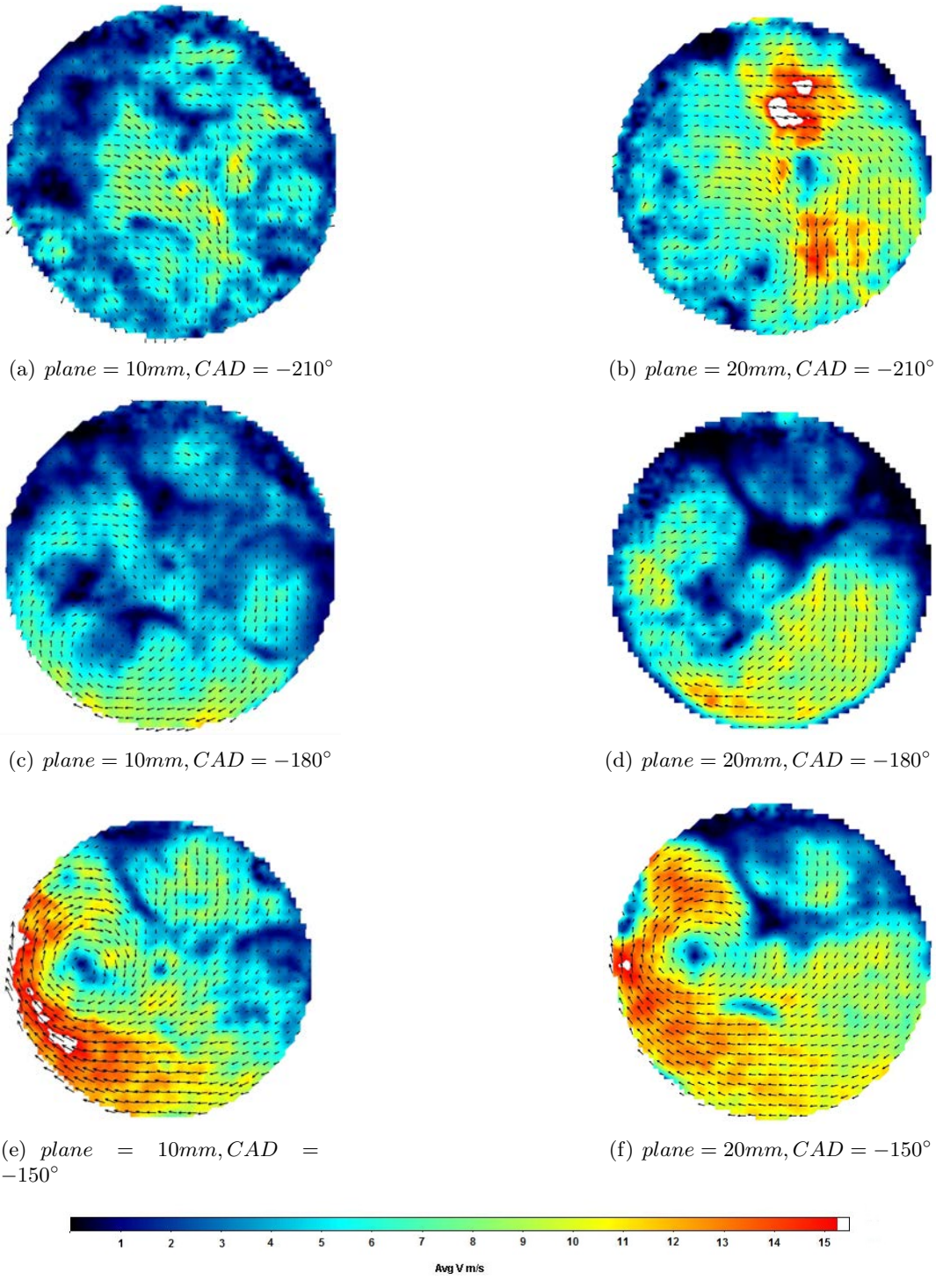

(a) $plane = 10mm, CAD = -210°$

(b) $plane = 20mm, CAD = -210°$

(c) $plane = 10mm, CAD = -180°$

(d) $plane = 20mm, CAD = -180°$

(e) $plane = 10mm, CAD = -150°$

(f) $plane = 20mm, CAD = -150°$

Figure 79: Instantaneous Velocity comparison in different planes, Titanium dioxide, at $n = 600min - 1$, $\dot{m} = 210kg/h$ from $CAD = -210°$ to $CAD = -150°$.

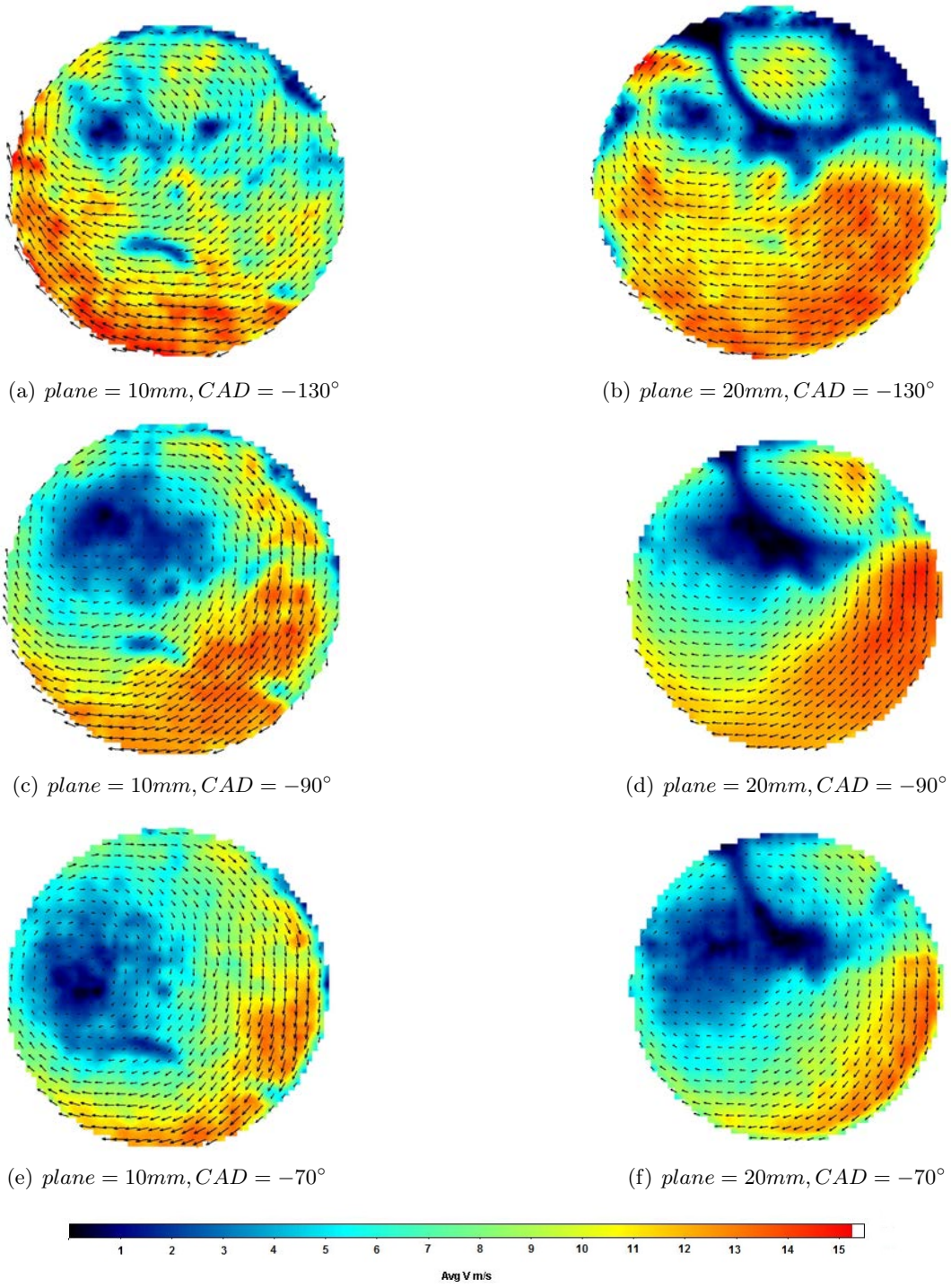

(a) $plane = 10mm, CAD = -130°$

(b) $plane = 20mm, CAD = -130°$

(c) $plane = 10mm, CAD = -90°$

(d) $plane = 20mm, CAD = -90°$

(e) $plane = 10mm, CAD = -70°$

(f) $plane = 20mm, CAD = -70°$

Figure 80: Instantaneous Velocity comparison in different planes, Titanium dioxide, at $n = 600min - 1$, $\dot{m} = 210kg/h$ from $CAD = -130°$ to $CAD = -70°$.

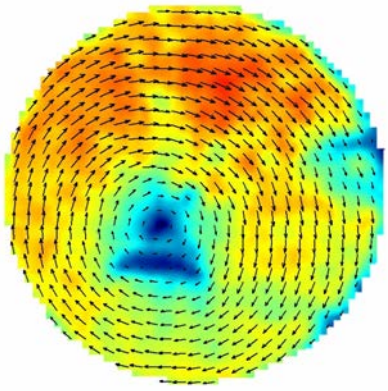

(a) $plane = 10mm, CAD = -40°$

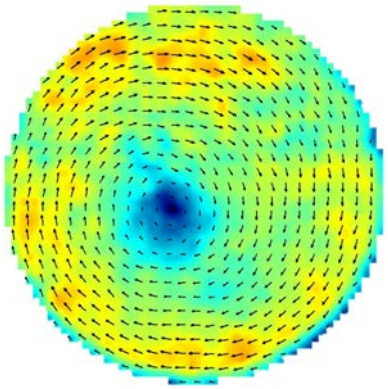

(b) $plane = 20mm, CAD = -40°$

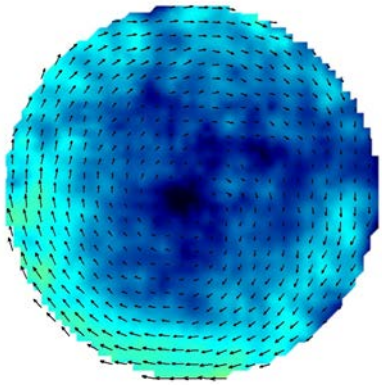

(c) $plane = 10mm, CAD = -20°$

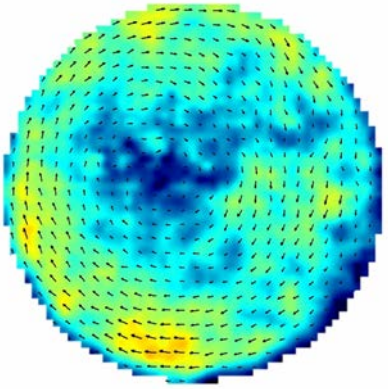

(d) $plane = 20mm, CAD = -20°$

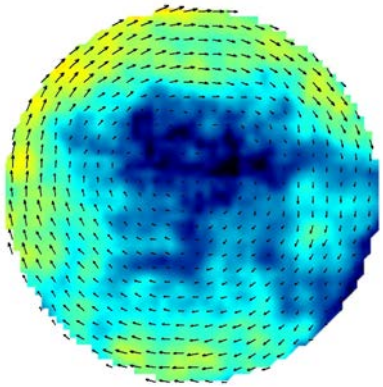

(e) $plane = 10mm, CAD = 0°$

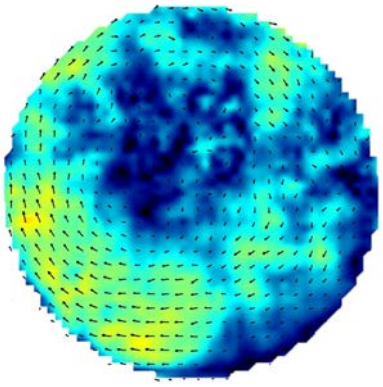

(f) $plane = 20mm, CAD = 0°$

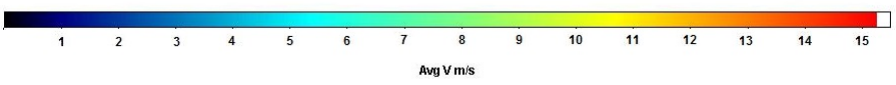

Figure 81: Instantaneous Velocity comparison in different planes, Titanium dioxide, at $n = 600min - 1$, $\dot{m} = 210kg/h$ from $CAD = -40°$ to $CAD = 0°$.

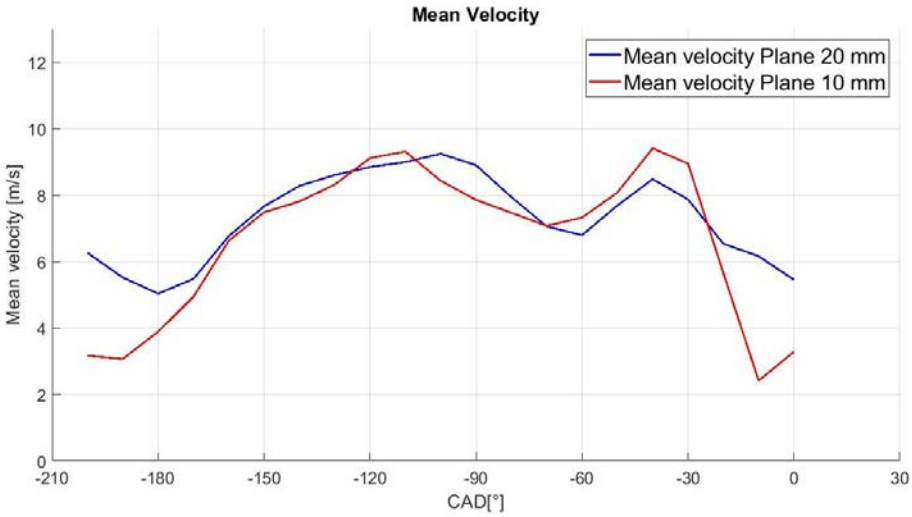

Figure 82: Mean Velocity different planes: Titanium dioxide, at $n = 600min - 1$, $\dot{m} = 210kg/h$.

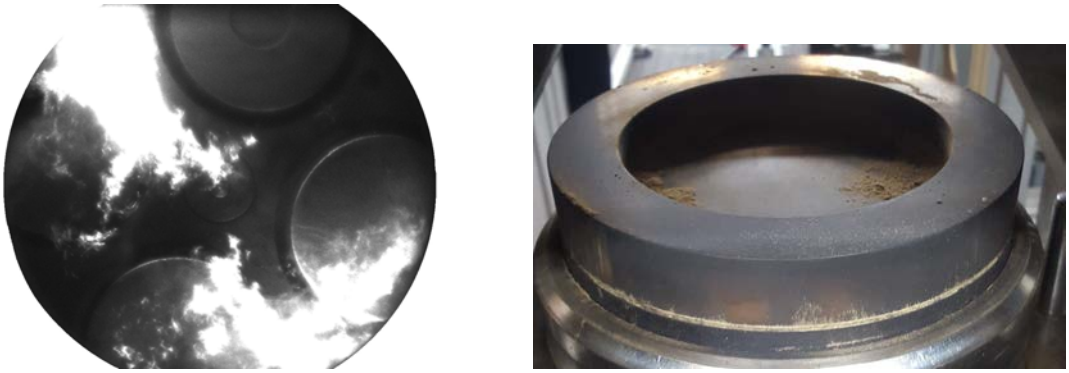

Figure 83: Lycopodium ignition and its effect in the piston.

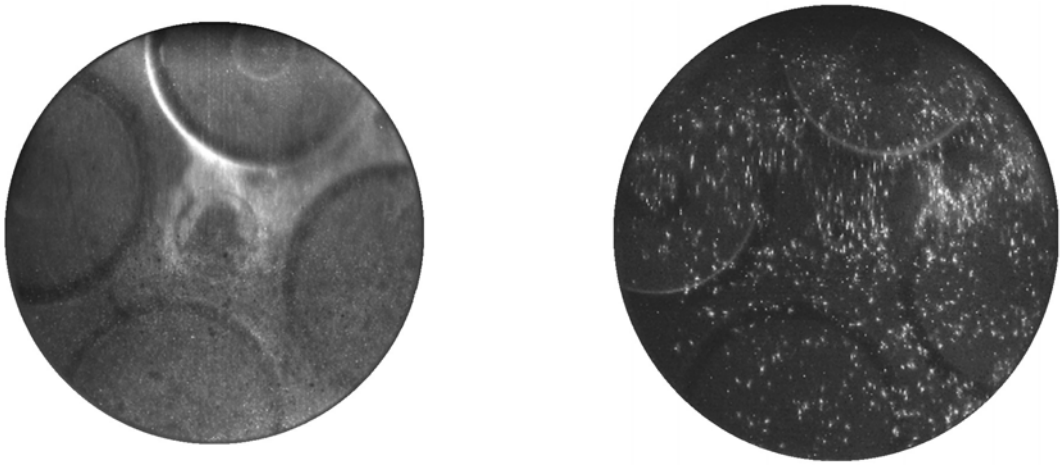

Figure 84: $CAD = -210°$, $z = 20mm$, $\dot{m} = 210kg/h$ at $n = 600min - 1$. Left: Titanium dioxide; Right: Lycopodium.

bowl. Will be considered the range from $-210°$ to $24°$ because the swirl motion starts to form during the intake stroke. The Figure85 shows the swirl centre movement in the plane $z = 20mm$ at $n = 600min - 1$ and $\dot{m} = 210kg/h$ from $-210°$ to $24°$. The swirl center locations, during the intake stroke and in the

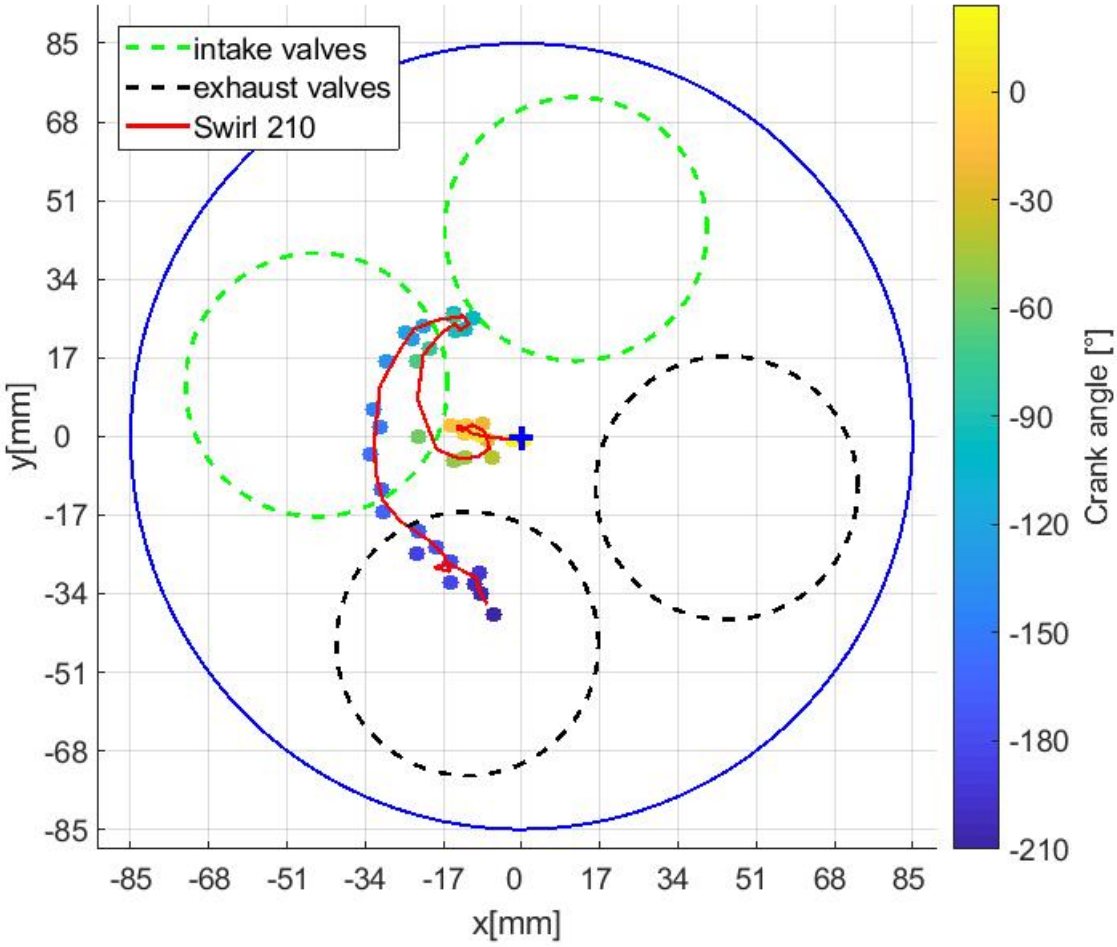

Figure 85: Centre swirl variation during the intake and compression strokes, Titanium dioxide, plane $z = 20mm$ at $n = 600min - 1$, $\dot{m} = 210kg/h$.

first compression stroke part, exhibit larger spatial variation. As can be seen in Figure85, at $-210°$, the rotation center is located under the exhaust valve. In this phase, the piston moving downwards and the rotation is clearly eccentric. The swirl center moves with the piston motion and, when the piston reaches the bottom dead center, the swirl center has moved of around $10mm$. From $-180°$ to $-90°$, the swirl center follows a clockwise semicircle trajectory with center in the cylinder center passing from exhaust valve to intake valve. This behaviour is due to the large instability of swirling flow in its initial formation stage. From $-90°$ to $-50°$, the swirl center begins to move downward, always through a semicircle trajectory, until it reaches the center height. From $-50°$ to $24°$, the movements become closer together and the swirl center approaches the cylinder center. In particular, it is possible to see that, from $-40°$ to $-10°$,

the swirl center tends to move away from the cylinder center (moving from a distance of $10mm$ to $16mm$ from the center). Thereafter, the swirl center remains in the same position until 10° where a rapid movement drives its to the center (at 24°). The position of the swirl centre, close to the cylinder centre, creates the perfect condition to inject the diesel and mix it symmetrically in the air flow in order to minimize the asymmetric mixture preparation. To analyze the mass flow rate influence in the swirl movements, in Figure86 are plotted three paths for three $\dot{m}$ values. The Figure86 shown the swirl center motion

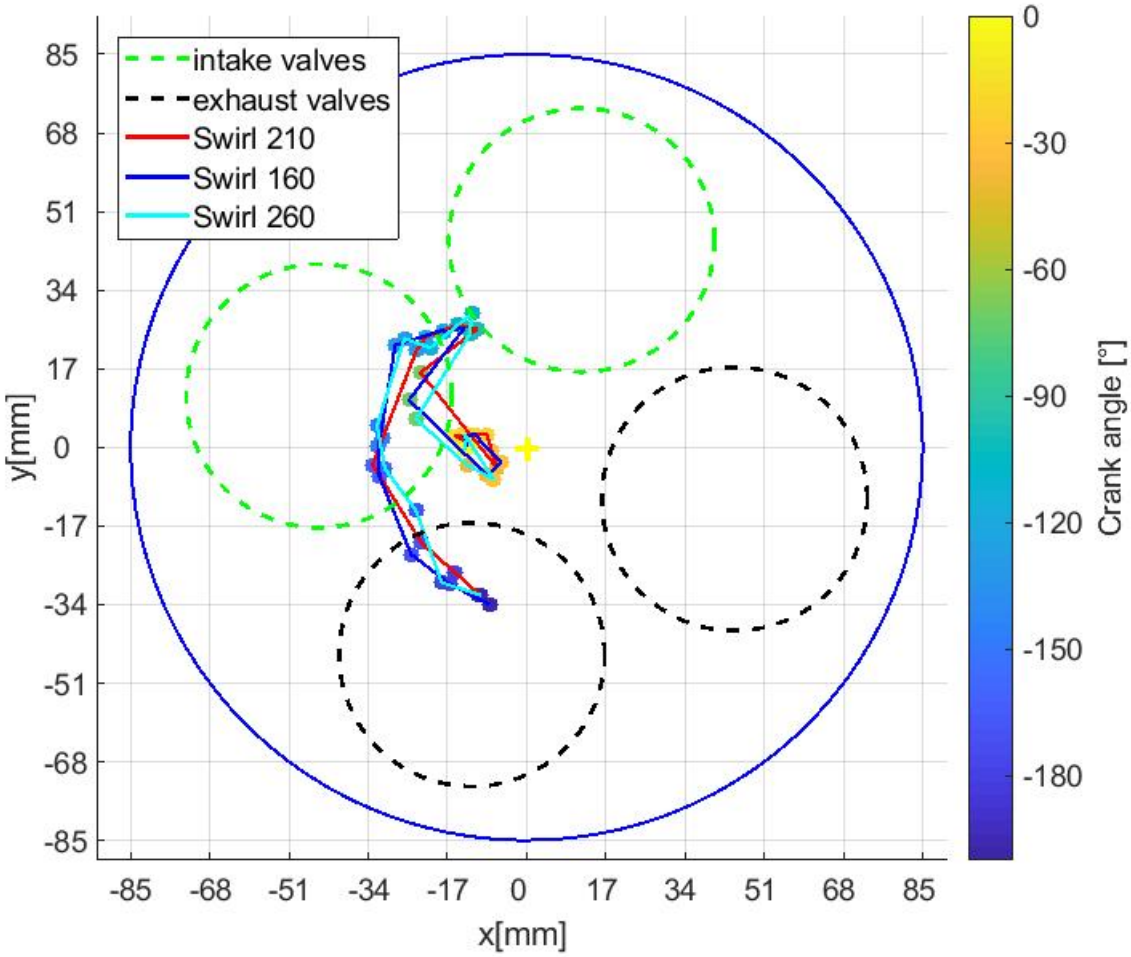

Figure 86: Centre swirl variation during the intake and compression strokes for different intake pressure, Titanium dioxide, plane $z = 20mm$ at $n = 600min - 1$.

from $-210°$ to $0°$. It is clear that all the paths follow the same trend and thus, as for the mean velocity, different mass flow rate values don't change the swirl center behaviour during the compression stroke.
The swirl center motion, for different cylinder heights, is now analyzed. In Figure87 are plotted two swirl center paths. The Figureshows that, from $CAD = -180°$ to $CAD = -90°$, the two trajectories are very similar showing that, in the first compression phase, the swirl motion develops in the same way in different cylinder heights, because the swirl motion is not completely

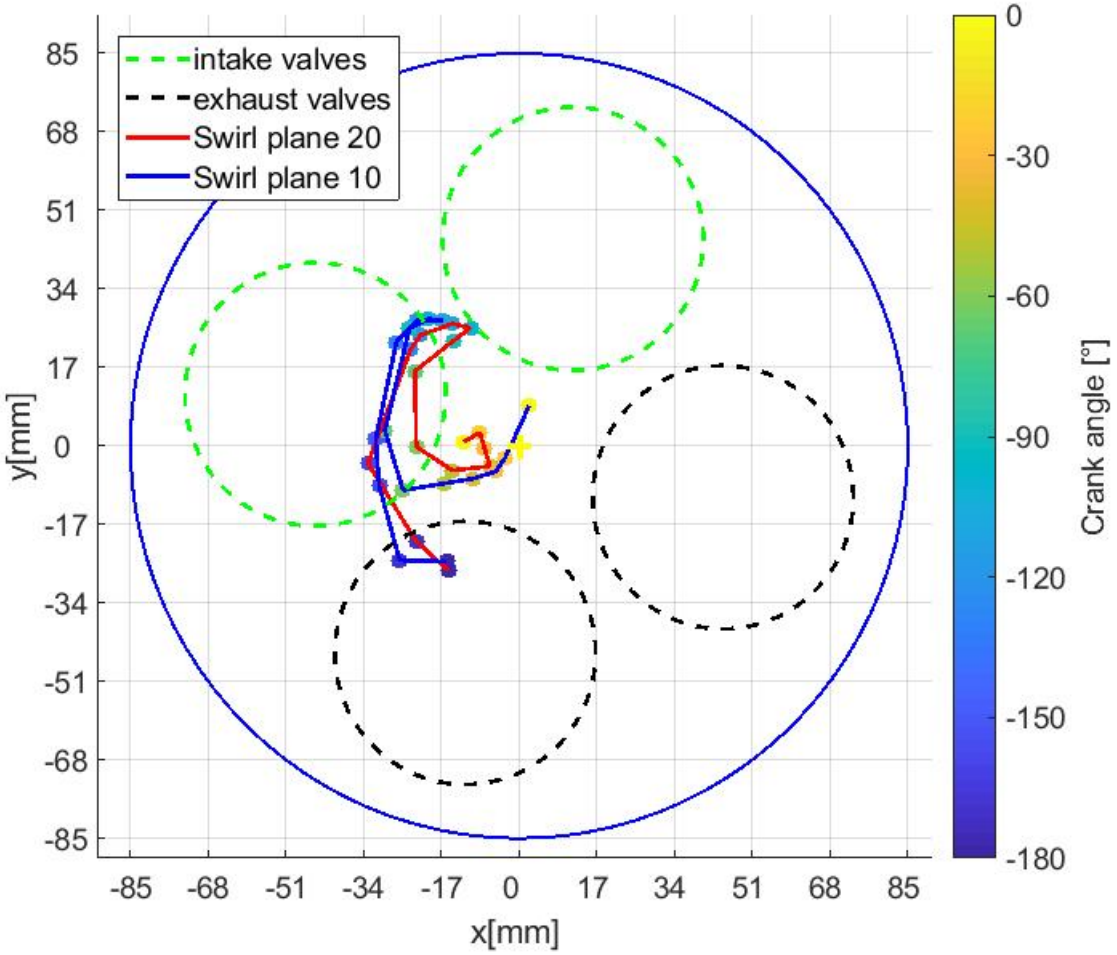

Figure 87: Centre swirl variation during the intake and compression strokes in different planes, Titanium dioxide, $n = 600min - 1$ and $\dot{m} = 210kg/h$.

formed yet. Starting from $CAD = -90°$ to $CAD = -60°$, both trajectories make a semicircle, but in the plane at $10mm$, the path radius is greater than the plane at $20mm$. After $CAD = -60°$, both trajectories head towards the cylinder center and, at $CAD = -30°$, their positions are equivalent. From $CAD = -30°$ to $CAD = 0°$, the trajectories carry out a different trend as a matter of fact that, at $20mm$, the swirl center moves to the left moving away from the cylinder center, on the other hand, at $10mm$, the swirl center moves towards the cylinder center up to exceed it.
This behavior suggests that, at the top dead center, the swirl center is located closer to the intake valves, but it changes his position based on the distance from the cylinder head.

8.6 Swirl number

Since, the angular velocity of the swirl flow in the cylinder changes in proportion to the engine speed, the swirl number represents a suitable quantity for a description of the internal engine flow. The swirl number SN thus defined as the quotient of angular velocity ω_s and the angular velocity of the crankshaft of the engine [58]:

$$SN = \omega_s/(2\pi n) \tag{9}$$

Where n describes the engine speed in revolutions per second. The swirl number, determined here, is based of vector fields measured in the engine, thus it makes a direct reference to the swirl numbers measured.
The deflection of the gas flow, emerging from the inlet valves at high speed in the piston, contributes to the formation of the swirling flow. The time-resolved measurement of the flow fields allows to observe the temporal swirl number evolution. As a result, the swirl number can be determined specifically for moments in which it has particular relevance for engine operation. For example, in the development of an engine, the intake passage geometry can be optimized with respect to a desired spin level in the desired injection time. In this work will be analyzed the main swirl number differences in different work points. In Figure88 is shown the swirl number trend for two different cylinder heights. The data range starts from $CAD = -210°$ for the plane at $20mm$ and from $CAD = -200°$ for the plane at $10mm$, or rather when it is possible to distinguish a swirl motion. The Figure88 makes it clear that, in the intake stroke and depending on the location, different flow conditions prevail. From the intake closing to $CAD = -100°$, it is possible to observe a continuous swirl number increase, for both cases, reaching a peak of $SN = 3,4$ at $CAD = -100°$ in the palne at $20mm$. After that, it drops until $CAD = -60°$ and then it returns to grow until $CAD = -40°$ for then decreased definitely. Whit reference at Figure68, it is possible to see that the swirl number following the same mean velocity trend. The two swirl number curves have the same evolution during the compression stroke, but regarding the plane at $10mm$, the swirl number always remains smaller compared to the other plane. After $CAD = -40°$, the swirl number values have the same trend for both planes. This shows that, during the first compression part, the swirl motion develops differently based on the cylinder height and then it takes a standard course, when the piston is located closer to the TDC.

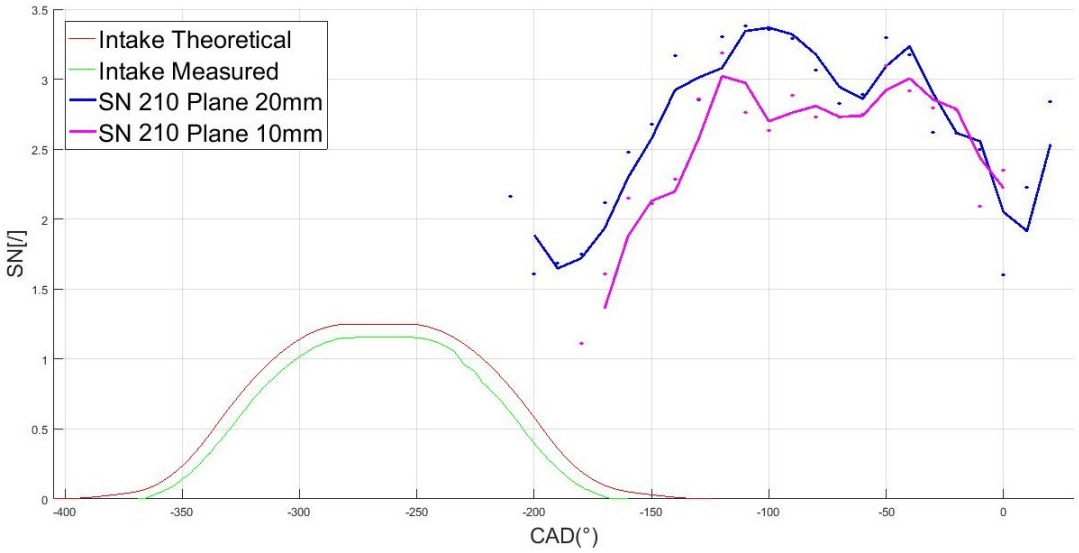

Figure 88: Swirl Number variation during the intake and compression strokes in different planes, Titanium dioxide, $n = 600min - 1$ and $\dot{m} = 210kg/h$.

Finally, the swirl number is analyzed for different mass flow rate values. In Figure89 is shown the swirl number trend for two different $\dot{m}$ values. The

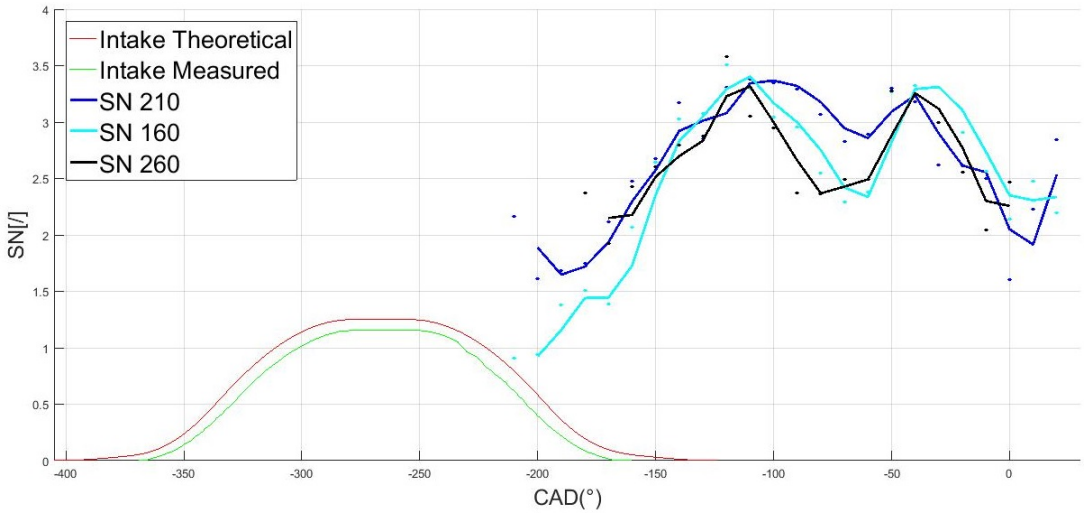

Figure 89: Swirl Number variation during the intake and compression strokes for different intake pressure, Titanium dioxide, plane $z = 20mm$ at $n = 600min - 1$.

Figure89 shows a similar trend between the swirl number values for different mass flow rate. The swirl number is affected by the results quality level, indeed, it can be deduced that, the large trend deviations, are the result of poor pictures quality. Therefore, it can be concluded that different mass flow rate values have no influence on the swirl number as for the mean velocity Figure74.

9 Conclusion and Outlook

9.1 Conclusion

In the present work Particle Image Velocimetry (PIV) problems, the instrumentation and the internal cylinder flow of a large bore dual fuel engine in non-firing conditions have been examined. Starting from the large background theory about PIV, several problems encountered in the application to a engine have been analyzed. In particular, great interest has been placed to find the ideal Δ_t between two frames. That is because, the flow direction changes in the four dimensions and thus, a wrong Δ_t choice, would cause a loss of information. Hence, reference results have been calculated for the whole intake and compression stroke to impose a maximum particle displacement, at the upper recommended limit. The imposition of the maximum particle displacement, to the higher limit, is necessary to avoid loss data in the cylinder center area, where there is low flow velocity. This is due to the presence of high velocity gradients in the combustion chamber. The volume of the combustion chamber changes during the compression stroke, involving in a different tracer density in the flow during the cycle. For this reason it has been necessary to change the seeding generator pressure in order to adjust the tracer density.The results show that, in the BDC, the particles number was not enough.
An other problem that has characterized the result is the background type. Indeed, the presence of shaded areas, caused by valves seats and not uniform color, make difficult to subtract the background from the seeding particles. Moreover, the pictures have a blurring zone that does not allow to locate the particles. These problems are more evident when small diameter particles are used, e.g. titanium dioxide. A partial solution it has been found applying a pre-processing filter.
In order to combine vector result number, displacement gradients and image shift a $64x64pixels$ interrogation window size has been chosen. An accurate alignment work has been done to focus and calibrate laser beam and camera.
Considering the cylinder thermal development and material features, a research to find different tracer solutions has been carried out. In literature, a large number of materials has been used in PIV, but the hard conditions reached in the combustion chamber cause a reduction until little available materials. Moreover, taking into account relaxation time, particle diameter, hardness and deposition a list with the best material choice for different temperature range, depending on the maximum cylinder temperature, has been provided.
To process the flow pictures, two programs have been used: DaVis and PIVlab. A scrupulous phase of study has been made to find merits and defects of each one. For what concern DaVis, it is the most used PIV program with more than 25 years of experience. However, DaVis has long dead times and there is not a test against to evaluate the goodness of the result. For this purpose, it has been decided to try using an alternative way to get results. Using a MATLAB script, internally developed and that uses the PIVlab script, it is possible to select a pictures set and, automatically, they are processed. The results are saved in MATLAB format and in *.jpg* format. However, using the automatic elaboration process, it is difficulty to get a good graphic optimization. This problem makes the automation useful only for a first result evaluation. It is

necessary to use the main program (PIVlab application) to extract particular graphic effects in such a way to compare them with DaVis results. Analysing the results get using lycopodium, it has been proved that the results match between PIVlab and DaVis. Unfortunately, the pictures made from titanium dioxide caused a difficulty for PIVlab to elaborate correctly the results, especially in areas affected from background effect. Some improvements have been got using in PIVlab the pictures pre-processed from DaVis. This means that, in order to solve PIVlab problem, is necessary highlight the particles in the pre-processing using some filters, e.g. average time filter. For this reason and for the poor rendering options available in PIVlab, it has been decided to evaluate the titanium dioxide data using DaVis only.
Three different mass flow rate values and two different cylinder heights have been analyzed, starting from the initial intake stroke phase until the compression stroke end. For what concern the flow behaviour, it has been possible to observe that, thanks to the thrust generated by the incoming flow, an initial swirl motion is generated at the end of the intake stroke (when the intake valves are still open). After valve closing, the piston ascent generates a velocity growth and the swirl motion expands throughout the cylinder. During the compression stroke, it is possible to observe a continuous movement of the swirl center until when it reaches the cylinder center. Concerning the flow velocity, it has a peak when the piston reach its maximum linear speed at $CAD = -90°$. After that, the mean velocity decrease until $CAD = -60°$, returns to grow until $CAD = -40°$ and then decreased definitely reaching the top dead center. This velocity trend has been observed for all the mass flow rate values and also for different cylinder heights, with the difference that the velocity increasing and decreasing more steeply for the plane close to the cylinder head. The center swirl has the same trend for different mass flow rate values, but not for different cylinder heights. For the plane more distant from the cylinder head, the trajectories make a strict semicircle and it stops at around $12mm$ from the cylinder center. Instead, the trajectory of the plane close to the cylinder head, makes a wide semicircle but then it starts to going towards the cylinder center up to exceed it and stopping at around $9mm$ from it. This behavior suggests that, at the top dead center, the swirl center is located closer to the intake valves but it changes his position based on the distance from the cylinder head. Finally has been made a swirl number evaluation. The swirl number follow the same trend of the mean velocity and there are not differences between different mass flow rate values. In the other hand, it is possible to highlight that, for the plane closer to the cylinder head, the swirl number is less than the plane at $20mm$ until when it reaches $CAD = -40°$, in which, the swirl number becomes similar for both planes. This shows that, during the first compression part, the swirl motion develops differently based on the cylinder height and then, when the piston is located closer to the TDC, it starts a standard course.

In conclusion, this analysis turned out that the mass flow rate value does not have any effect in the flow development both for the velocity and for swirl motion. Instead, moving along the cylinder, it is possible to observe different flow conditions.

9.2 Outlook

The experiment requires long run time to set-up the parameters in order to get the best image quality. In this phase are included tuning the laser power, seeding generator pressure, Δ_t choice, materials selection and materials deposition. All this aspects could be solved before to use the engine. In fact, building a test bench that simulates the combustion chamber condition, it is possible to be prepared in many different aspects before to run the engine and thus save the little time available to do the experiment.
During the experiment, it has been possible to observe a good behaviour for what concern the titanium dioxide and, if there hadn't been the blurred area problem, it should have been possible to get excellent results. Nevertheless, it is necessary to test others materials in order to reduce background and density problems.
One of the problems that has plagued the test is the seeding generator working. In fact, the generator geometry leads preferential sliding channels with the consequence of a tracer density reduction. A future work could be the realization of a new generator concept that allows a constant tracer supply.
In order to equalize the pre-processing tools between DaVis and PIVlab, it would be necessary to implement a time-filter in the automatic script. The time-filter should be checked the whole set of pictures to delete the constant parts found in the analysis.
Eventually, in order to have a complete engine overview, it is necessary to analyze the vertical plane and applying the same flow variation done in this experiment. Furthermore, it is still needed to study the fired condition and its consequences in the flow motion.

10 Riassunto Della Tesi

In un momento in cui la comunità europea impone sempre più severe limitazioni nelle emissioni degli autoveicoli, questa tesi si propone di approfondire un metodo di misurazione efficace per valutare lo stato della carica del cilindro dei motori a combustione interna. Con tale metodologia non solo è possibile convalidare i risultati ottenuti tramite analisi CFD, ma anche di approfondire il processo di combustione stesso ottimizzando i parametri motore e conseguentemente ridurne le emissioni.
Il metodo di misurazione studiato è il PIV o Particle Image Velocimetry. Questo metodo venne utilizzato per la prima volta da Ludwig Prandtl il quale, agli inizi del diciannovesimo secolo, studiò il moto di un flusso d'acqua in un condotto da lui realizzato. Prandtl si avvalse di particelle traccianti che, aggiunte al flusso, permettevano di visualizzare il moto tridimensionale dell'acqua. Con l'evoluzione della tecnologia, questo metodo è diventato sempre più preciso e affidabile, permettendo anche lo studio del moto di fluidi in situazioni critiche come quelle all'interno di un motore a combustione interna in cui temperatura, pressione, accessi ottici, materiali e accelerazioni portano il metodo PIV al suo estremo applicativo.
Dalla letteratura, sono state ricavate le nozioni per l'applicazione del metodo PIV: iniettando particelle traccianti nel fluido, ed illuminandole tramite un fascio laser, è possibile catturare il movimento delle particelle attraverso una sequenza di immagini scattate da una fotocamera ad alta velocità. Le immagini ottenute (chiamate frame) vengono suddivise in finestre d'interrogazione e poi elaborate tramite cross-correlazione. La strumentazione necessaria per l'esperimento si può riassumere in:

- Sistema otticamente accessibile
- Generatore di particelle
- Particelle traccianti
- Una o più fotocamere ad alta velocità
- Generatore di fascio laser
- Programma di elaborazione delle immagini

Il motore in cui è stato eseguito lo studio presenta 2 accessi ottici: uno praticato nella sezione del cilindro e l'altro nel pistone. Il motore in esame è un dual-fuel diesel monocilindrico da 4 litri con una velocità di rotazione di 600 giri al minuto in cui si raggiunge una temperatura di fine compressione di 650C. Trovare un materiale tracciante che resista ad elevata pressione, elevata temperatura, con particelle sufficientementi grandi da essere rilevato dalla fotocamera, facilmente reperibile, a basso costo e che non comprometta il funzionamento del motore stesso richiede una attenta selezione. In letteratura sono stati utilizzati molti tipi di materiali traccianti per applicare il PIV ai motori a combustione. Attraverso alcuni criteri di selezione sono stati selezionati tre materiali traccianti adatti a questa applicazione: la grafite, l'ossido di titanio e spore di Licopodio. Insieme alla selezione del materiale tracciante, altri parametri sono importanti

da ottimizzare per il corretto funzionamento del PIV come potenza del laser, tempo fra 2 frame, dimensione delle finestre di interrogazione, overlap tra due diverse finestre di interrogazione, pressione del generatore di particelle e programma di elaborazione delle immagini. Proprio su quest'ultimo è stata fatta un'approfondita analisi comparando due diverse tipologie di programma. Il programma più utilizzato dai ricercatori è DaVis, un software fornito dall'azienda LaVision che fornisce anche il generatore di particelle, materiali traccianti, fotocamere e filtri. Per verificare i risultati ottenuti con DaVis si è invece utilizzato un toolbox di MATLAB che permette di elaborare le immagini ricavate dalla fotocamera con un più alto livello di automazione di analisi e consentendo quindi una riduzione del tempo di calcolo.
Durante la fase di test si è cercato di analizzare diversi punti motore variando parametri come pressione in ingresso (simulando l'effetto del turbo), altezza del piano di analisi rispetto alla testa del cilindro e materiali traccianti. In questo modo si è potuto tracciare delle linee guida per futuri esperimenti riuscendo ad analizzare il moto in diversi angoli di manovella.
Dai risultati ottenuti si è potuto valutare lo stato del fluido durante la fase di aspirazione e compressione. Più in dettaglio, si è potuto vedere come già alla fine della fase di aspirazione si crei un moto di swirl generato dalla conformazione del condotto di aspirazione. Durante la fase di compressione, il moto di swirl diventa più marcato e la velocità del fluido aumenta con l'avanzare del pistone verso il punto morto superiore. All'incirca a 90 dell'angolo di manovella, coincidentemente alla massima velocità lineare del pistone, la velocità del moto di swirl raggiunge il suo valore massimo. Superati i 90 la velocità assoluta del fluido si abbassa conseguentemente all'effetto della compressione dello stesso. Un andamento simile lo si ha per l'evoluzione del numero di swirl durante il ciclo: esso raggiunge il valore massimo di 3.5 (a 90 dell'angolo di manovella).
E' stato analizzato il comportamento del flusso al variare della pressione di ingresso, simulando così la presenza di un turbocompressore. I risultati ottenuti hanno dimostrato che la pressione in ingresso non altera il campo delle velocità e nemmeno l'andamento del numero di swirl.
Analizzando altezze diverse rispetto alla testa del cilindro, si è evidenziato come il moto del fluido vari in base al piano di analisi: lo sviluppo del moto della carica cambia nei due piani cosi come il numero di swirl e l'andamento delle velocità assolute.
L'analisi è stata effettuata utilizzando particelle di ossido di titanio. Sono state anche utilizzare spore di licopodio per valutarne pregi, come le elevate proprietà riflessive, e difetti, come il ritardo nella risposta all'accelerazione del moto. A causa di un accumulo di particelle nel condotto di aspirazione però, le spore si sono incendiate compromettendo le rilevazioni e l'impianto.
In conclusione, l'analisi del metodo e la risoluzione dei problemi legati all'uso del PIV è servito ad ottenere una maggiore conoscenza del metodo e una migliore configurazione dei parametri per la lettura effettiva del moto della carica. I risultati ottenuti saranno da linea guida per le successive ricerche nel laboratorio di motori a combustione interna del politecnico di Monaco Di Baviera.

A Matrix result comparison

In Figure 90 are shown the result vector matrices resulting from the elaboration of the same reference picture 47 for DaVis and for PIVlab.

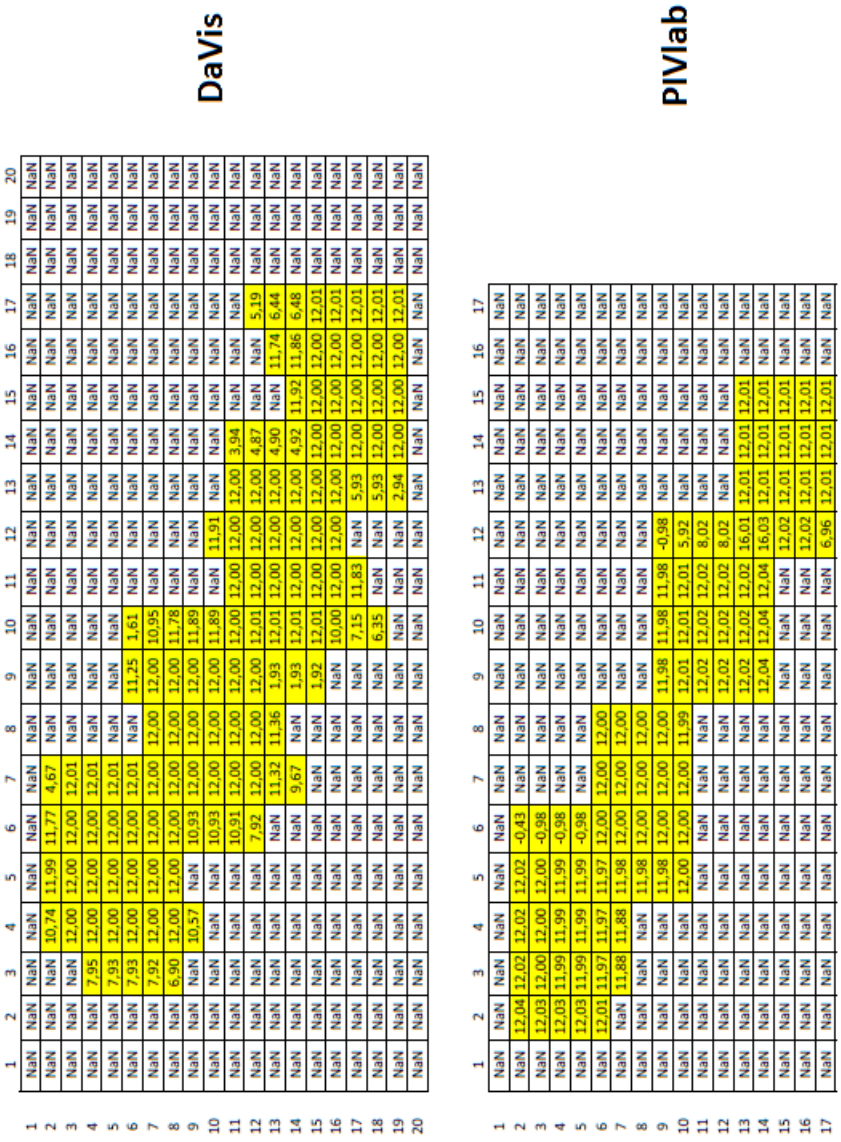

Figure 90: Result matrices.

B Flow field results with cylinder head scale

Some flow field results, with cylinder head scale, are given in the followed pictures 91, 92. The pictures allow to understand the results size changes, during the compression stroke, due to the optical cone between camera and piston.

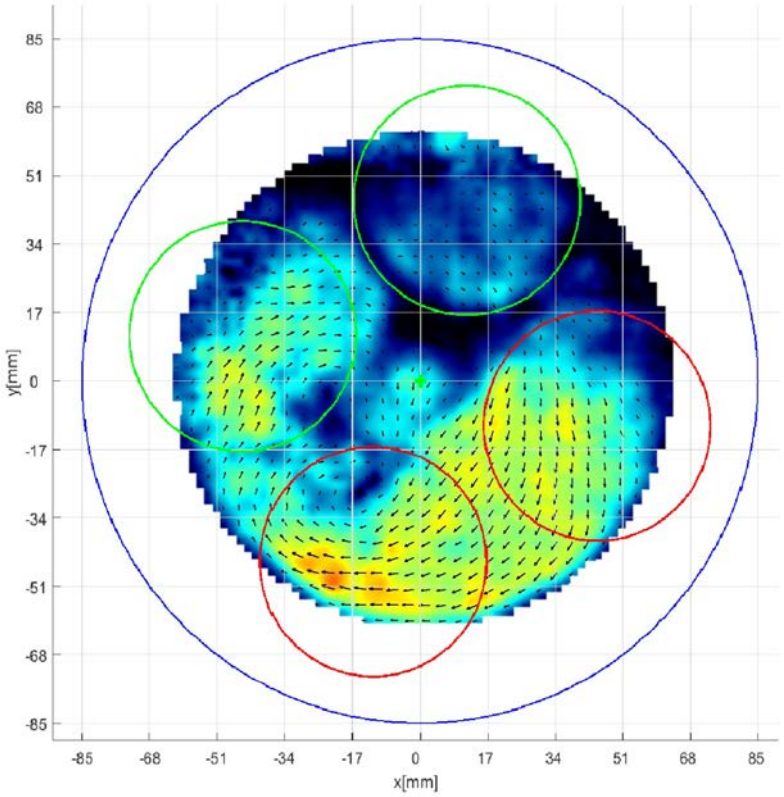

(a) $CAD = -180°$

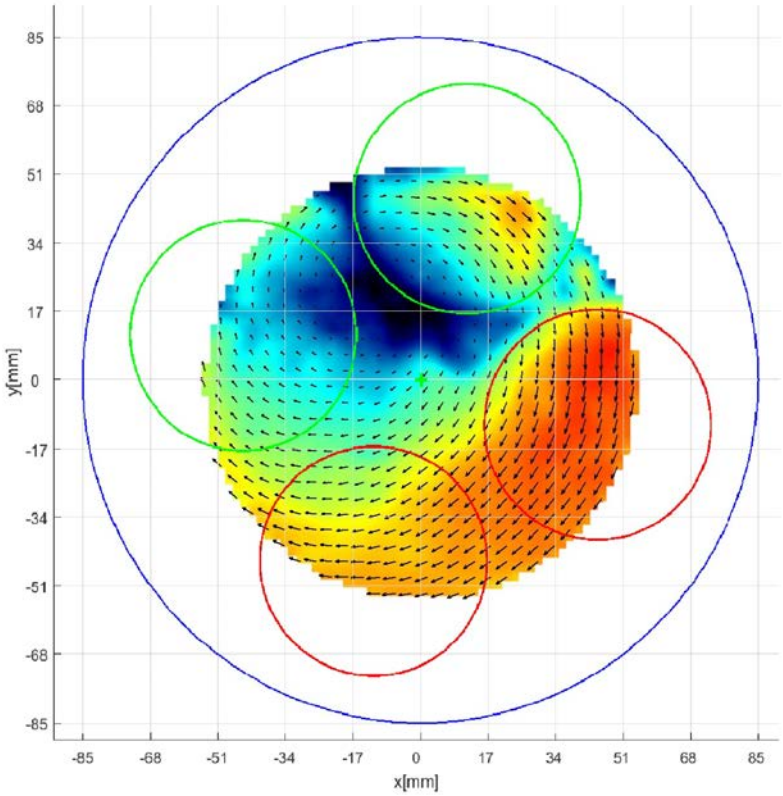

(b) $CAD = -90°$

Figure 91: Results scale, Titanium dioxide, plane $z = 20mm$ at $n = 600min - 1$, $\dot{m} = 210kg/h$ for different CAD.

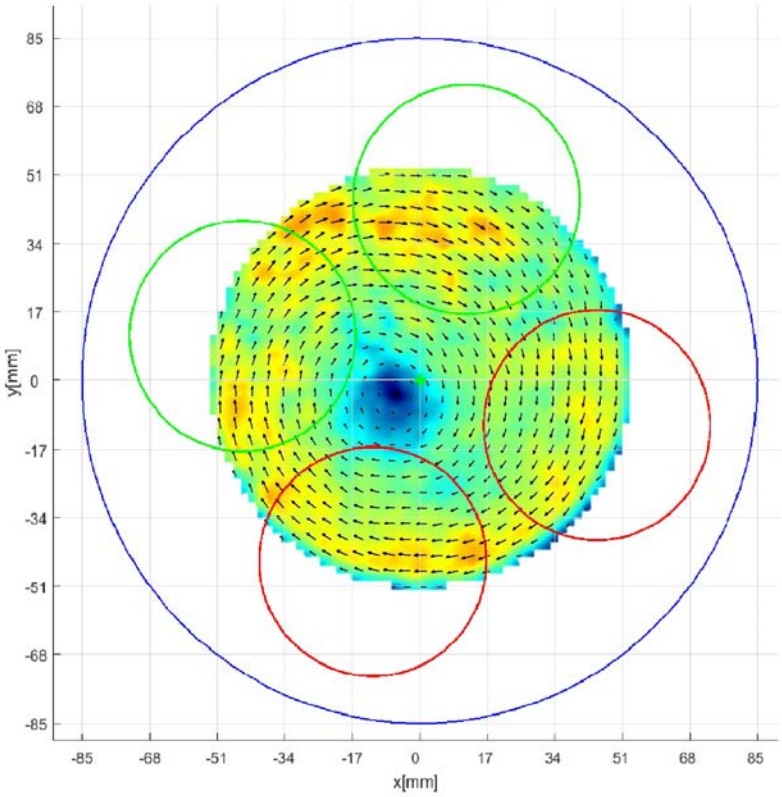

(a) $CAD = -40°$

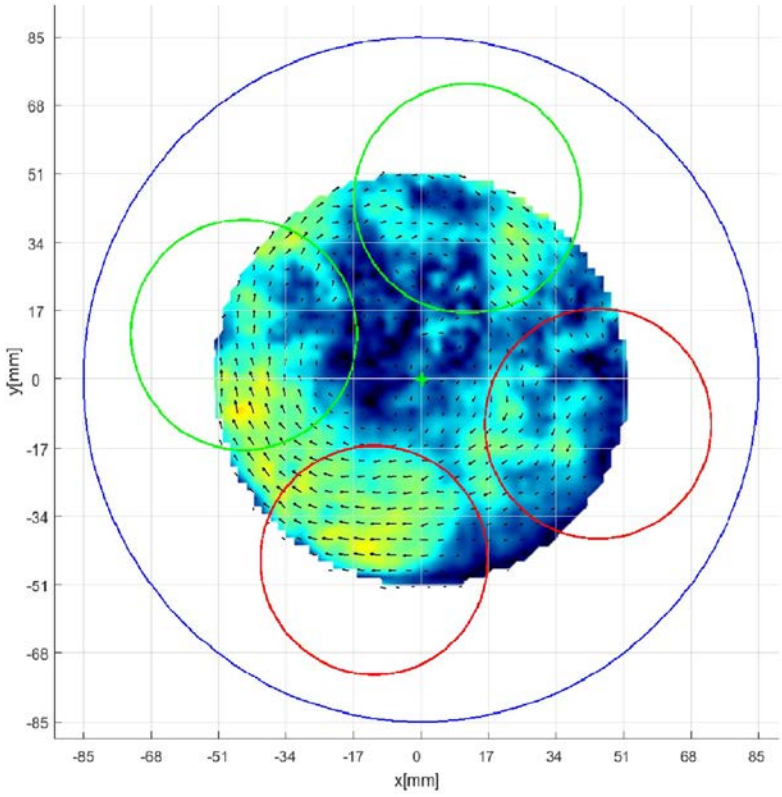

(b) $CAD = 0°$

Figure 92: Results scale, Titanium dioxide, plane $z = 20mm$ at $n = 600min - 1$, $\dot{m} = 210kg/h$ for different CAD.

References

[1] Ronald J Adrian and Jerry Westerweel. *Particle image velocimetry*. 30. Cambridge University Press, 2011.

[2] Terry Alger et al. *PIV in-cylinder flow measurements of swirl and the effect of combustion chamber design*. Tech. rep. SAE Technical Paper, 2004.

[3] Frederik Blumrich. "Optische korrelationsbasierte Messtechnik mittels zufälliger Punktemuster". In: (2009).

[4] J Bode et al. "Influence of three-dimensional in-cylinder flows on cycle-to-cycle variations in a fired stratified DISI engine measured by time-resolved dual-plane PIV". In: *Proceedings of the Combustion Institute* 36.3 (2017), pp. 3477–3485.

[5] CK Chan, WJD Annand, and JT Turner. "Measurement of velocity levels in a motored model of an internal combustion engine". In: *First International Conference on Laser Anemometry–Advances and Applications, Manchester, England*. 1985.

[6] Wook Choi et al. *In-cylinder flow field analysis of a single cylinder DI diesel engine using PIV and CFD*. Tech. rep. SAE Technical Paper, 2003.

[7] Cheng Tung Chong and Simone Hochgreb. "Measurements of laminar flame speeds of liquid fuels: Jet-A1, diesel, palm methyl esters and blends using particle imaging velocimetry (PIV)". In: *Proceedings of the Combustion Institute* 33.1 (2011), pp. 979–986.

[8] I Cosadia et al. "Cyclic variations of the swirling flow in a Diesel transparent engine". In: *Experiments in fluids* 41.1 (2006), p. 115.

[9] Romeo Danielis et al. "Le emissioni di CO2 delle auto elettriche e delle auto con motore a combustione interna. Un confronto per l'Italia tramite l'analisi del ciclo di vita". In: *Working papers SIET* (2016).

[10] J Dannemann et al. "Cycle resolved multi-planar flow measurements in a four-valve combustion engine". In: *Experiments in fluids* 50.4 (2011), pp. 961–976.

[11] Bart Degraeuwe et al. "Impact of passenger car NOX emissions on urban NO2 pollution â" Scenario analysis for 8 European cities". In: *Atmospheric Environment* 171 (2017), pp. 330–337. ISSN: 1352-2310. DOI: https://doi.org/10.1016/j.atmosenv.2017.10.040. URL: http://www.sciencedirect.com/science/article/pii/S1352231017307057.

[12] G. Fraidl. *AVL - Future Trends Gasoline Engines*. 2012.

[13] Frederic Moisy. *PIVMat 4.10: A PIV Post-processing and data analysis toolbox*. 2018.

[14] Suresh Gadekar, Akhilendra Pratap Singh, and Avinash Kumar Agarwal. *Tomographic PIV evaluation of in-cylinder flow evolution and effect of engine speed*. Tech. rep. SAE Technical Paper, 2016.

[15] D. Garcia. *A fast all-in-one method for automated post-processing of PIV data: Experiments in Fluids*. 2011.

[16] Jaal B Ghandhi et al. *Time resolved particle image velocimetry measurements in an internal combustion engine*. Tech. rep. SAE Technical Paper, 2005.

[17] T Hadad and R Gurka. "Effects of particle size, concentration and surface coating on turbulent flow properties obtained using PIV/PTV". In: *Experimental Thermal and Fluid Science* 45 (2013), pp. 203–212.

[18] A Henderson. *Guide to Laser Safety*. Vol. 1. Springer Science & Business Media, 1997.

[19] CW Hong and DG Chen. "Direct measurements of in-cylinder integral length scales of a transparent engine". In: *Experiments in fluids* 23.2 (1997), pp. 113–120.

[20] Tsuneaki Ishima et al. *Analysis on in-cylinder flow by means of LDA, PIV and numerical simulation under steady state flow condition*. Tech. rep. SAE Technical Paper, 2008.

[21] Kern Y Kang and Je H Baek. "Turbulence characteristics of tumble flow in a four-valve engine". In: *Experimental Thermal and Fluid Science* 18.3 (1998), pp. 231–243.

[22] Richard D Keane and Ronald J Adrian. "Optimization of particle image velocimeters". In: *ICALEO'89: Optical Methods in Flow and Particle Diagnostics*. Vol. 1404. International Society for Optics and Photonics. 1990, pp. 139–160.

[23] Addepalli S Krishna, JM Mallikarjuna, and Davinder Kumar. "Effect of engine parameters on in-cylinder flows in a two-stroke gasoline direct injection engine". In: *Applied Energy* 176 (2016), pp. 282–294.

[24] B Murali Krishna and JM Mallikarjuna. "Comparative study of in-cylinder tumble flows in an internal combustion engine using different piston shapes—an insight using particle image velocimetry". In: *Experiments in fluids* 48.5 (2010), pp. 863–874.

[25] LaVision GmbH. *Collimator Optics: Product-Manual for DaVis 7.x*. 2008. URL: `https://www.lavision.de/de/`.

[26] LaVision GmbH. *DaVis 8.4.0 Software*. 2017. URL: `https://www.lavision.de/en/products/davis-software/index.php`.

[27] LaVision GmbH. *FlowMaster: Product-Manual for DaVis 8.4*. 2017. URL: `https://www.lavision.de/en/products/davis-software/index.php`.

[28] LaVision GmbH. *ImagerProPlus & ImagerProX: Product-Manual for DaVis 7.2*. 2009. URL: `https://www.lavision.de/de/`.

[29] LaVision GmbH. *Particle Blaster 200: Product-Manual*. 2014. URL: `https://www.lavision.de/de/`.

[30] LaVision GmbH. *PIV seminar*. Göttingen, 2015.

[31] LaVision GmbH. *Sheet Optics (divergent): Product-Manual for DaVis 7.2*. 2009. URL: `https://www.lavision.de/de/`.

[32] LaVision GmbH. *Titanium Dioxide: seeding particles for PIV in combustion processes*. 2011. URL: `https://www.lavision.de/en/applications/fluid-mechanics/piv-system-components/seeding-particles/`.

[33] CH Lin et al. "Comparison of large eddy simulation predictions with particle image velocimetry data for the airflow in a generic cabin model". In: *HVAC&R Research* 12.S3 (2006), pp. 935–951.

[34] Litron Laser Ltd. "Litron PIV Products". In: (2015).

[35] Maximilian Schell. *Vorbereitung und Durchführung von optischen Messungen an einem Forschungsmotor*. 2013.

[36] A Melling. "Tracer particles and seeding for particle image velocimetry". In: *Measurement Science and Technology* 8.12 (1997), p. 1406.

[37] A Melling. "Tracer particles and seeding for particle image velocimetry". In: *Measurement Science and Technology* 8.12 (1997), p. 1406. URL: http://stacks.iop.org/0957-0233/8/i=12/a=005.

[38] Klaus Mollenhauer and Helmut Tschöke. *Handbook of Diesel Engines*. Berlin, Heidelberg: Springer Berlin Heidelberg, 2010. ISBN: 978-3-540-89082-9. DOI: 10.1007/978-3-540-89083-6.

[39] Franck Nicollet et al. "A PIV-Guided Large-Eddy Simulation of In-Cylinder Flows". In: *Oil & Gas Science and Technology–Revue d'IFP Energies nouvelles* 72.5 (2017), p. 28.

[40] E Nino, BF Gajdeczko, and Philip G Felton. *Two-color particle image velocimetry in an engine with combustion*. Tech. rep. SAE Technical Paper, 1993.

[41] L Prandtl. "Über Flüssigkeitsbewegung bei sehr kleiner Reibung (Heidelberg, 1904)". In: *Vier Abhandlungen zur Hydrodynamik und Aerodynamik, Göttingen* (1944).

[42] Jean Rabault et al. "A study using PIV of the intake flow in a diesel engine cylinder". In: *International Journal of Heat and Fluid Flow* 62 (2016), pp. 56–67.

[43] Markus Raffel et al. *Particle image velocimetry: a practical guide*. Springer, 2013.

[44] Gianfranco Rizzo and Raffaele Di Martino. "Aspetti dell'ingegneria contemporanea: l'evoluzione degli autoveicoli alternativi." In: ().

[45] Rodrigo Mancilla. *Entwicklung und Inbetriebnahme eines Prüfstandes für einen Einzylinder-Forschungsmotor*. 2014.

[46] Pentti Saarenrinne and Mika Piirto. "Turbulent kinetic energy dissipation rate estimation from PIV velocity vector fields". In: *Experiments in Fluids* 29.1 (2000), S300–S307.

[47] Victor Manuel Salazar and Sebastian Arnold Kaiser. *POD Analysis of the In-Cylinder Flow and Fuel Mole-Fraction in a Hydrogen-Fueled Internal Combustion Engine.* Tech. rep. Sandia National Laboratories (SNL-CA), Livermore, CA (United States), 2011.

[48] Fulvio Scarano et al. "On the use of helium-filled soap bubbles for large-scale tomographic PIV in wind tunnel experiments". In: *Experiments in Fluids* 56.2 (2015), p. 42.

[49] JJ Serrano-Aguilera et al. "Rheo-PIV of Aerosil® R816/polypropylene glycol suspensions". In: *Journal of Non-Newtonian Fluid Mechanics* 232 (2016), pp. 22–32.

[50] P Sweetland and Rolf D Reitz. *Particle image velocimetry measurements in the piston bowl of a DI diesel engine*. Tech. rep. SAE Technical Paper, 1994.

[51] Zachary J. Taylor et al. “Long-Duration Time-Resolved PIV to Study Unsteady Aerodynamics”. In: *IEEE Transactions on Instrumentation and Measurement* 59.12 (2010), pp. 3262–3269. ISSN: 0018-9456. DOI: 10.1109/TIM.2010.2047149.

[52] W. Thielicke. *The Flapping Flight of Birds - Analysis and Application*. 2014.

[53] W. &. Stamhuis E.J Thielicke. *PIVlab - Time-Resolved Digital Particle Image Velocimetry Tool for MATLAB (version: 1.41)*. 2014.

[54] William Thielicke and Eize J. Stamhuis. “PIVlab – Towards User-friendly, Affordable and Accurate Digital Particle Image Velocimetry in MATLAB”. In: *Journal of Open Research Software* 2 (2014), p. 1202. ISSN: 2049-9647. DOI: 10.5334/jors.bl.

[55] DP Towers and CE Towers. “Cyclic variability measurements of in-cylinder engine flows using high-speed particle image velocimetry”. In: *Measurement Science and Technology* 15.9 (2004), p. 1917.

[56] G Valentino et al. “Flow Field Characterization of the Intake Flow in a Diesel Engine by LDA and PIV”. In: *4th International Conference ICE99*. 1999, pp. 95–101.

[57] I Vincenti et al. “PIV study for the analysis of planar jets in cross-flow at low Reynolds number”. In: *ATTI 11th Convegno Nazionale AIVELA, Ancona* (2003).

[58] Vinzenz Markus Neubert. *Experimentelle Untersuchung der Brennraumströmung eines Zweiventil-Dieselmotors*. 2016.

[59] L.H. Weeks. *Automobile Biographies: An Account of the Lives and the Work of Those who Have Been Identified with the Invention and Development of Self-propelled Vehicles on the Common Roads ...* Monograph Press, 1904. URL: https://books.google.de/books?id=DnpAAAAAIAAJ.

[60] Kan Zha et al. *Characterization of Flow Asymmetry During the Compression Stroke Using Swirl-Plane PIV in a Light-Duty Optical Diesel Engine with the Re-entrant Piston Bowl Geometry.* Tech. rep. Sandia National Laboratories (SNL-CA), Livermore, CA (United States), 2015.